

Computational and experimental characterization of intra-aortic balloon pump support

Citation for published version (APA):

Schampaert, S. (2014). *Computational and experimental characterization of intra-aortic balloon pump support*. [Phd Thesis 1 (Research TU/e / Graduation TU/e), Biomedical Engineering]. Technische Universiteit Eindhoven. <https://doi.org/10.6100/IR776753>

DOI:

[10.6100/IR776753](https://doi.org/10.6100/IR776753)

Document status and date:

Published: 01/01/2014

Document Version:

Publisher's PDF, also known as Version of Record (includes final page, issue and volume numbers)

Please check the document version of this publication:

- A submitted manuscript is the version of the article upon submission and before peer-review. There can be important differences between the submitted version and the official published version of record. People interested in the research are advised to contact the author for the final version of the publication, or visit the DOI to the publisher's website.
- The final author version and the galley proof are versions of the publication after peer review.
- The final published version features the final layout of the paper including the volume, issue and page numbers.

[Link to publication](#)

General rights

Copyright and moral rights for the publications made accessible in the public portal are retained by the authors and/or other copyright owners and it is a condition of accessing publications that users recognise and abide by the legal requirements associated with these rights.

- Users may download and print one copy of any publication from the public portal for the purpose of private study or research.
- You may not further distribute the material or use it for any profit-making activity or commercial gain
- You may freely distribute the URL identifying the publication in the public portal.

If the publication is distributed under the terms of Article 25fa of the Dutch Copyright Act, indicated by the "Taverne" license above, please follow below link for the End User Agreement:

www.tue.nl/taverne

Take down policy

If you believe that this document breaches copyright please contact us at:

openaccess@tue.nl

providing details and we will investigate your claim.

**Computational and experimental
characterization of intra-aortic
balloon pump support**

A catalogue record is available from the Eindhoven University of Technology Library.

ISBN: 978-90-386-3666-5

Copyright © 2014 by S. Schampaert

All rights reserved. No part of this book may be reproduced, stored in a database or retrieval system, or published, in any form or in any way, electronically, mechanically, by print, photo print, microfilm or any other means without prior written permission by the author.

Printed by Gildeprint Drukkerijen, Enschede, The Netherlands

This research is supported by the Dutch Technology Foundation STW, which is part of the Netherlands Organization for Scientific Research (NWO) and partly funded by the Dutch Ministry of Economic Affairs (project number 11052).

Computational and experimental characterization of intra-aortic balloon pump support

PROEFSCHRIFT

ter verkrijging van de graad van doctor
aan de Technische Universiteit Eindhoven,
op gezag van de rector magnificus prof.dr.ir. C.J. van Duijn,
voor een commissie aangewezen door het College voor Promoties,
in het openbaar te verdedigen op
donderdag 16 oktober 2014 om 16.00 uur

door

Stéphanie Schampaert

geboren te Eindhoven

Dit proefschrift is goedgekeurd door de promotoren en de samenstelling van de promotiecommissie is als volgt:

Voorzitter: prof.dr. P.A.J. Hilbers

Promotor: prof.dr. N.H.J. Pijls

Co-Promotoren: dr.ir. M.C.M. Rutten

dr.ir. M. van 't Veer

Leden: dr. D. Perera (King's College London)

prof.dr. B. Meyns (Katholieke Universiteit Leuven)

prof.dr.ir. F.P.T. Baaijens

prof.dr.ir. F.N. van de Vosse

Wijk af, spring op, dans door

- *Loesje* -

Contents

Chapter 1: General introduction	11
1.1 The cardiac cycle	13
1.1.1 Coronary blood flow	13
1.1.2 Cardiac work	15
1.2 Cardiac support in cardiogenic shock	15
1.2.1 Pharmacologic support	16
1.2.2 Mechanical support	16
Intra-aortic balloon pump	16
1.3 Aim and outline of this thesis	20
Chapter 2: Modeling the interaction between intra-aortic balloon pump and cardiovascular system: the effect of timing	23
2.1 Introduction	25
2.2 Materials and methods	26
2.2.1 Cardiovascular system	26
Heart	26
Circulation	31
2.2.2 Intra-aortic balloon pump	33
2.2.3 Solution procedure	34
2.2.4 Simulations	35
2.2.5 <i>In vivo</i> validation	35
2.3 Results	36
2.4 Discussion	39
2.4.1 Cardiovascular system	39
2.4.2 Intra-aortic balloon pump	40
2.4.3 Strengths and limitations	41
2.4.4 Clinical application	41
2.5 Conclusion	43
Chapter 3: A mock circulation model for cardiovascular device evaluation	45
3.1 Introduction	47
3.2 Materials and methods	48
3.2.1 Control algorithms	48
Heart contraction model	48
Heart rate control model	49
Control strategy	50
3.2.2 Hardware implementation	51
Left and right ventricle	51
Systemic, pulmonary, and coronary circulation	52
3.2.3 Hemodynamic measurements	53

3.3 Results	54
3.3.1 Controller performance	54
3.3.2 Clinical scenarios	55
3.3.3 Cardiac function control	56
3.3.4 Frequency control	58
3.4 Discussion	58
3.4.1 Controller performance	59
3.4.2 Physiologic relevance	59
3.4.3 Limitations	60
3.4.4 Extended applications	61
3.5 Conclusion	62
Chapter 4: <i>In vitro</i> comparison of the support capabilities of intra-aortic balloon pump and Impella 2.5 LP	63
4.1 Introduction	65
4.2 Materials and methods	66
4.2.1 Model-controlled mock circulation	66
4.2.2 Simulations	67
4.3 Results	67
4.3.1 Healthy	67
Baseline	67
Mechanical circulatory support	68
4.3.2 Cardiogenic pre-shock	69
Baseline	69
Mechanical circulatory support	70
4.3.3 Cardiogenic shock	70
Baseline	70
Mechanical circulatory support	70
4.4 Discussion	71
4.5 Conclusion	74
Chapter 5: Autoregulation of coronary blood flow in the isolated beating pig heart	75
5.1 Introduction	77
5.2 Materials and methods	78
5.2.1 Isolation	78
5.2.2 Preparation	78
5.2.3 Instrumentation	79
5.2.4 Resuscitation	80
5.2.5 Hemodynamic interventions	80
5.3 Results	81
5.4 Discussion	84
5.5 Conclusion	87

Chapter 6: Intra-aortic balloon pump support in the isolated beating pig heart in non-ischemic and ischemic pump failure	89
6.1 Introduction	91
6.2 Materials and methods	92
6.2.1 Isolated beating pig heart model	92
6.2.2 Hemodynamic interventions	93
6.3 Results	93
6.3.1 Clinical scenarios of pump failure and ischemia	93
6.3.2 Intra-aortic balloon pump support	95
6.4 Discussion	96
6.4.1 Strengths and limitations of this study	99
6.5 Conclusion	100
Chapter 7: General discussion and conclusions	101
7.1 Research methods	103
7.1.1 Computational modeling	103
7.1.2 Experimental testing	105
Model-controlled mock circulation	105
Isolated beating pig heart	105
7.1.3 Clinical validation and future perspectives	106
7.2 Intra-aortic balloon pump support	107
7.3 Conclusion	109
References	111
Summary	125
Samenvatting	127
Gedicht	129
Dankwoord	131
Curriculum vitae	133
List of publications	135

Chapter 1

General introduction

1.1 The cardiac cycle

The function of the cardiovascular system is to transport blood with nutrients and waste products between different organs. The driving force that maintains the circulation inside this system is the rhythmic beating of the heart. The contraction of the heart is driven by periodic waves of electrical excitation that start in the sinus node. From there, excitation spreads through the right and left atria, triggering atrial contraction. Via the atrioventricular node the waves are then discharged down the bundle of His to the ventricular septum and myocardial walls, triggering ventricular contraction. This electro-mechanical process of excitation wave propagation through the heart and excitation-contraction coupling causes motion of the cardiac tissue and the pulsatile flow of blood in the circulation.

The temporal relationships between the latter processes are illustrated schematically in figure 1.1. Electrical excitation of the atria and ventricles, apparent as the P-wave and QRS-complex of the electrocardiogram (ECG), triggers their contraction. The initial part of ventricular contraction is isovolumetric, causing closure of the atrioventricular valves. When the left ventricular pressure exceeds aortic pressure, the aortic valve opens and ejection of blood into the aorta occurs. The T-wave of the ECG marks ventricular repolarization. As left ventricular pressure falls below aortic pressure, the aortic valve closes and ventricular pressure falls rapidly during an isovolumetric relaxation phase. When ventricular pressure drops below atrial pressure, the atrioventricular valves open and ventricular filling starts again.

1.1.1 Coronary blood flow

Due to the pulsatile pumping action of the heart, aortic pressure shows a peak systolic pressure, which is in part maintained during diastole, but gradually declines towards the end of diastole. It is the driving pressure for the systemic perfusion, including the perfusion of the heart itself via the coronary circulation.

The coronary circulation originates from the coronary ostia, located just distal from the aortic valve leaflets. The major vessels of the coronary circulation are the left main coronary artery, which bifurcates into the left anterior descending and the left circumflex coronary artery, and the right coronary artery. These main arteries branch through smaller arteries and arterioles into a network of capillaries, where the exchange of nutrients and waste products takes place through the thin capillary wall. After passing the capillary bed, the blood is collected in the coronary veins for transport back to the right atrium via the coronary sinus.

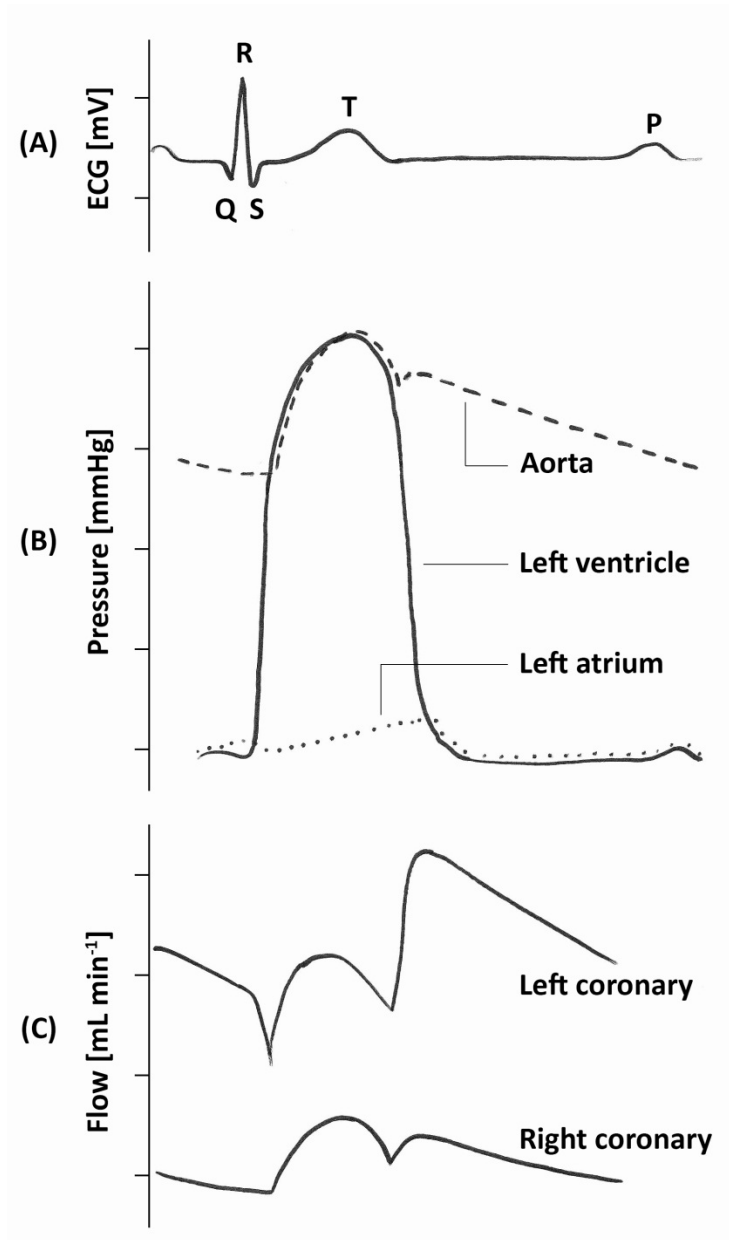


Figure 1.1: Schematic diagram of electrical and mechanical events in the cardiac cycle. (A) ECG, (B) Pressure signals in the left heart, (C) Coronary blood flow produced by the aortic pressure pulse.

As the branches of the coronary arteries are embedded in the cardiac muscle, strong compression of the left ventricular muscle (and to a lesser extent of the right) around the intramuscular vessels occurs during ventricular contraction. Therefore, coronary blood flow, although primarily driven by aortic pressure, shows a reduced systolic arterial flow component relative to diastolic flow, despite presence of a higher systolic driving pressure.

Resting coronary blood flow in the human heart averages between 200 and 300 mL min⁻¹ (Guyton *et al.*, 2006). It is controlled by the process of autoregulation, in which the arteriolar vessels are the primary site of vascular resistance and regulate their vascular tone by means of vasodilation or vasoconstriction in order to maintain a balance between blood flow and myocardial demand. During hyperemia, however, the arteriolar vascular tone is decreased and the capillaries constitute the lowest resistance to blood flow. In that case, coronary blood flow is directly related to the diastolic perfusion pressure.

1.1.2 Cardiac work

Besides being the driving force for coronary perfusion, aortic pressure is also the load the heart must eject blood against (afterload). It determines the velocity of fiber shortening, which affects the rate of volume ejection and consequently the amount of blood left within the ventricle at the end of systole. Furthermore, by affecting intraventricular wall tension during systole, it is a major determinant of the external mechanical work the heart has to perform. Together with the mechanical potential energy, it closely relates mechanical performance to cardiac energy metabolism in terms of oxygen consumption and heat production (Westerhof *et al.*, 2000).

1.2 Cardiac support in cardiogenic shock

When the heart is unable to pump effectively, primarily due to failure of the ventricles, the profound depression of myocardial contractility may be the underlying pathophysiologic mechanism of cardiogenic shock. Cardiogenic shock is a state of end-organ hypoperfusion due to cardiac failure, which complicates approximately 5 to 8 % of all ST-elevation myocardial infarction cases. The clinical symptoms of cardiogenic shock will be revealed as persistent systemic hypotension (systolic arterial pressure < 90 mmHg) with severe reduction in cardiac index (< 2.2 L min⁻¹ m⁻²) despite adequate left ventricular filling pressure (left ventricular end diastolic pressure > 15 mmHg) (Khalid *et al.*, 2008; Reynolds *et al.*, 2008). Despite compensatory mechanisms, such as peripheral vasoconstriction and redistribution of flow to the vital organs, this results in a malicious cycle of ongoing reduction in contractility as the insufficient pump force of the heart also affects coronary blood flow and thereby cardiac function itself. As this vicious circle of cardiac deterioration will continue, the survival rate of cardiogenic shock is often less than 15 % (Guyton *et al.*, 2006).

Basically, two therapeutic therapies to support the endangered circulation in cardiogenic (pre-)shock states exist: pharmacologic inotropic support and mechanical support.

1.2.1 Pharmacologic support

Positive inotropic agents, like (nor)epinephrine or dobutamine, enhance the strength of myocardial contraction by increasing the level of calcium in the cytoplasm of the cardiac muscle cell. This enhancement in force generation is independent of preload (i.e., sarcomere length). Furthermore, the increase in ventricular inotropy goes along with an increased velocity of fiber shortening that increases the rate of ventricular pressure development. This makes pharmacologic inotropic agents support the failing heart by reducing end systolic volume, while increasing stroke volume and ejection fraction, and consequently correcting the hypotension. Although positive inotropic drugs have proven to be able to support the endangered circulation in the short term, prolonged use should be carefully regulated as an improved cardiac function also leads to increased myocardial oxygen consumption. Therefore, in the presence of myocardial ischemia, e.g., due to coronary artery obstruction (myocardial infarction), only short-term benefits of inotropic drugs can be expected.

1.2.2 Mechanical support

The intention of mechanical circulatory support is to support the endangered circulation mechanically by restoring a normal blood flow, while simultaneously unloading the ventricle. Support devices available today range from short-term, minimally invasive assist devices, such as the intra-aortic balloon pump (IABP) and relatively new transvalvular assist devices, to long-term left ventricular assist devices, which require open-chest surgery for implantation.

Intra-aortic balloon pump

Historical overview

Precise understanding of the cardiac cycle was the foundation of the development of the IABP. After proving that coronary pressure and flow could be manipulated during the cardiac cycle (Kantrowitz *et al.*, 1953), Kantrowitz *et al.* (1958) translated this concept into a surgical procedure by wrapping the hemidiaphragm around the distal thoracic aorta, while stimulating the phrenic nerve synchronous with the cardiac cycle. Although the phrenic nerve failed to stand up against long-term stimulation, the changed pressure configuration of the aortic pressure waveform were promising. Using this obtained knowledge, Moulopoulos *et al.* (1962) developed the first experimental prototype of the IABP: a distensible balloon condom, tied around the

end of a polyethylene catheter that contained multiple side holes through which balloon inflation and deflation occurred.

In 1968, Kantrowitz *et al.* first introduced this IABP in a clinical setting of cardiogenic shock, quickly followed by an extended series of 16 patients treated with balloon counterpulsation (Kantrowitz *et al.*, 1968). In this series, 44 % of the patients were long-term survivors of cardiogenic shock, representing a substantial improvement over the 85 to 95 % mortality from cardiogenic shock typical of that decade (Griffith *et al.*, 1954). However, as the balloon catheter needed to be inserted surgically by exposure of the femoral artery, important vascular and local wound complications had been reported in 5 to 36 % of the treated patients (Alpert *et al.*, 1976; Bregman *et al.*, 1971).

With the development of percutaneous and prefolded balloon catheters (Subramanian *et al.*, 1980; Bregman *et al.*, 1980), the IABP became a minimally invasive cardiac assist device (Figure 1.2). Today, the IABP consists of two major components: a double-lumen catheter with a 25 - 50 cc polyurethane balloon attached at its distal end, and a pump console, which shuttles helium through the main lumen of the catheter. A fiber-optic pressure sensor is located at the tip of the catheter to monitor aortic pressure, which in turn can be used as trigger signal for balloon actuation. The catheter is usually inserted through a percutaneous femoral approach and positioned, under fluoroscopic guidance, in the descending aorta, distal to the left subclavian artery and proximal to the renal artery branches.

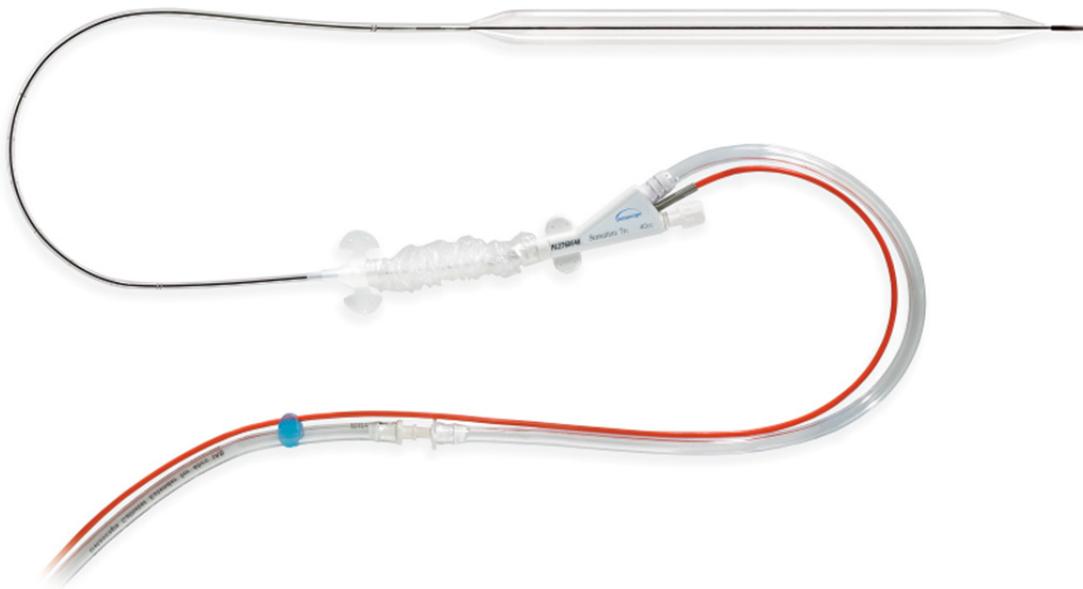


Figure 1.2: The IABP as known today: a catheter-mounted polyurethane balloon with a fiber-optic pressure sensor located at the tip of the catheter (*printed with permission from Maquet Getinge Group, Rastatt, Germany*).

Basic principle

Meeting the characteristics of the heart and the coronary circulation, the IABP attempts to create a more favorable balance between myocardial oxygen supply and myocardial oxygen consumption by the physiologic principle of counterpulsation. By rapid inflation and deflation of the catheter-mounted polyurethane balloon, synchronous with the cardiac cycle, the IABP changes the configuration of the aortic pressure waveform (Figure 1.3).

Rapid inflation of the balloon, upon onset of diastole, results in a proximal and distal displacement of blood, proportional to the volume of the balloon, within the aorta. The secondary diastolic blood pressure augmentation increases the intrinsic windkessel effect, whereby the extra potential energy stored in the aorta is converted to kinetic energy with the elastic recoil of the vessel (Krishna *et al.*, 2009). As this aortic pressure peak is in phase with the natural coronary flow peak, the induced diastolic blood pressure augmentation has the potential to be an increased driving force for coronary perfusion, and thus to increase coronary blood flow.

By rapid deflation of the balloon in early systole, the IABP also induces a systolic reduction in afterload, theoretically reducing the energy consumption of the heart as this lowers the resistance to left ventricular ejection. Consequently, volume ejection rate is expected to increase secondary to the fiber shortening velocity in the heart.

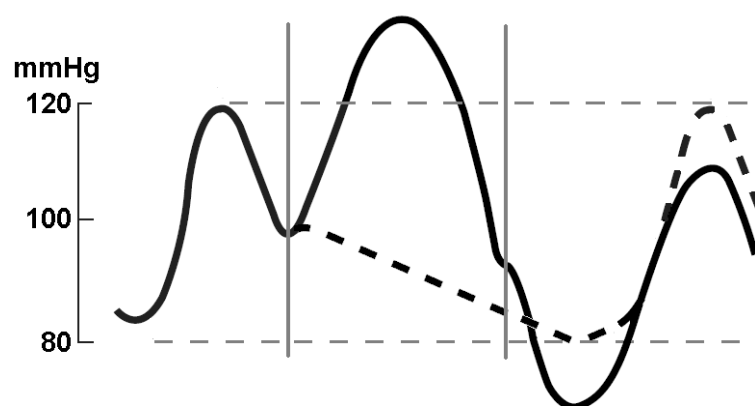


Figure 1.3: Aortic pressure curve without (dotted) and with (solid) IABP support. The vertical lines represent inflation (left) and deflation (right) of the catheter-mounted polyurethane balloon.

Physiologic studies

Although the IABP is expected to create clinical improvement in terms of coronary perfusion and myocardial oxygen consumption, the measured effects reported in literature are inconsistent and ambiguous among patients and animal experiments.

The extreme divergence reported in literature is clearly reflected in the coronary blood flow change measured with the IABP *in situ*: results range from a 100 % increase (Zehetgruber *et al.*, 1997), to no change (Leinbach *et al.*, 1971) or even a 10 % decrease (Williams *et al.*, 1982). On top of this, controversy exists whether the augmented blood pressure is capable of increasing coronary blood flow in the presence of coronary artery disease and coronary autoregulation (Kern *et al.*, 1993; Kimura *et al.*; 1996; Takeuchi *et al.*, 2004; Yoshitani *et al.*, 2007). A severe coronary artery stenosis might prevent adequate transmission of the augmented diastolic aortic pressure through the stenosis, failing to increase the diastolic inflow to the myocardium and time-average flow rate (Powell *et al.*, 1970). Moreover, once coronary autoregulation is restored, coronary blood flow is not proportional to diastolic aortic pressure anymore, but is regulated by a flow regulatory mechanism.

The magnitude of effects induced by the IABP are also expected to be influenced by a large number of patient-specific factors as well as factors attributing to the mechanics of the assist device itself, such as timing settings (Kern *et al.*, 1999) and balloon volume, as the amount of blood displaced by the balloon is proportional to its volume. Patient-specific factors involved include heart rate, because of the time required for complete inflation and deflation of the balloon, systemic vascular resistance and aortic compliance, as they both might prevent (lateral) distribution of pressure, and cardiac performance, determining the corresponding baseline hemodynamics (Powell *et al.*, 1970; Kern *et al.*, 1993, Zehetgruber *et al.*, 1997).

Randomized studies

Besides the highly variable registry data, only a few randomized clinical trials have been reported, all lacking to reach their primary efficacy end points: IABP-SHOCK II (Thiele *et al.*, 2012), Balloon pump-assisted Coronary Intervention (BCIS-1) (Perera *et al.*, 2010), Counterpulsation Reduces Infarct Size Pre-percutaneous coronary intervention Acute Myocardial Infarction (CRISP-AMI) (Patel *et al.*, 2011).

The IABP-SHOCK II trial (Thiele *et al.*, 2012) enrolled 600 patients with acute myocardial infarction (with or without ST-segment elevation) with cardiogenic shock, who were randomized in a 1:1 ratio to IABP support or no IABP support. There was no difference in 30-day all-cause mortality, the primary study end point of this trial, between the IABP and control group.

In the BCIS-1 trial (Perera *et al.*, 2010), 301 patients with severe ischemic cardiomyopathy were randomly assigned to receive elective IABP support before

primary coronary intervention or to undergo primary coronary intervention alone. No difference in frequency of major adverse cardiac and cerebrovascular events at hospital discharge between the group with and without IABP support was observed, and also the difference in mortality at 6 months failed to reach significance. Although longer-term follow up showed significantly fewer deaths in the IABP group compared to the control group, the mechanism of benefit remains unclear.

The CRISP-AMI study (Patel *et al.*, 2011) examined the role of the IABP in anterior ST-segment elevation acute coronary syndrome without cardiogenic shock. No difference in the infarct size was found between the IABP (161 patients) and control group (176 patients).

Its safety profile and ease of use resulted in a strong recommendation in the guidelines of the American College of Cardiology, the American Heart Association, and the European Society of Cardiology for many years. However, due to mostly negative results from these randomized trials (Thiele *et al.*, 2012; Perera *et al.*, 2010; Patel *et al.*, 2011), the guidelines have recently downgraded the recommendation for IABP use (O’Gara *et al.*, 2013; Steg *et al.*, 2012; Wijns *et al.*, 2010). Although these randomized trials suggest that routine IABP insertion indeed will not ameliorate the risk of major adverse complications associated with percutaneous coronary intervention in the context of left ventricular impairment, there is a signal that a subset of this heterogeneous cohort might benefit from IABP support, indicating that selective application of IABP support could be a more promising strategy.

1.3 Aim and outline of this thesis

Because of the large number of interaction factors involved, attributing either to the mechanics of the assist device or to the cardiovascular system, the exact physiologic effects of IABP support are still not fully understood, and its use has been based upon presumptions rather than upon clear scientific data. Therefore, advanced models that behave in a physiologic manner are required for characterizing IABP support under well-controlled hemodynamic conditions. By computational modeling, *in vitro* and *ex vivo* testing, and performing clinical measurements, the goal of this research was to provide an accurate description of the physiologic effects of IABP therapy on both cardiac and coronary hemodynamics, in order to predict clinical settings in which its use would be most effective.

In **chapter 2**, a computational model is presented that couples a 0-dimensional lumped parameter model to an elaborate heart contraction model and a representative IABP model. In this model, the dynamic interaction between IABP and cardiovascular system, and how alterations of specific IABP parameters (i.e., timing)

affect this coupling, is tested. For validation purposes, data are collected from patients undergoing IABP therapy after percutaneous coronary intervention or after/as a bridge to cardiac surgery.

To address the need for hydraulic systems that behave in a physiologic manner for testing cardiovascular devices under well-controlled circumstances, an integrated mock circulation system is developed in **chapter 3**. This model is controlled by an elaborate heart contraction model, a realistic frequency control model, and a relatively simple lead-lag controller. Implemented in a servo-pump driven mock loop of the systemic, pulmonary, and coronary circulation, the system's behavior is tested in response to changes in left ventricular contractile states, loading conditions, and heart rate.

Despite the long record of supporting patients after myocardial infarction or cardiac surgery, the relatively new transvalvular assist devices challenge the position of the IABP. In **chapter 4**, the support capabilities of the IABP and the Impella 2.5 left percutaneous (a transvalvular rotary blood pump) are compared in the *in vitro* set-up under identical circumstances.

When using the isolated beating pig heart model for further testing and validating of cardiovascular devices, knowledge about the state of physiologic regulatory processes is mandatory. In **chapter 5**, the autoregulation of coronary blood flow in the working isolated beating pig heart is studied in response to brief occlusions of the coronary artery, to step-wise changes in left ventricular loading conditions and contractile states, and to pharmacologic vasodilating stimuli.

Informed on the (absent) state of autoregulation mechanisms in the isolated beating pig heart, the influence of persisting ischemia on IABP efficacy is investigated in **chapter 6**. By gradually creating severe global myocardial ischemia superimposed upon different contractile states, the clinical condition of a large myocardial infarction with different degrees of pump failure is mimicked and the effect of IABP support investigated.

In **chapter 7**, the main findings of this thesis are discussed and put in broader perspective. General conclusions are drawn and recommendations for further research are provided.

Chapter 2

Modeling the interaction between intra-aortic balloon pump and cardiovascular system: the effect of timing

The contents of this chapter are based on:

Schampaert S., Rutten M.C.M., Van 't Veer M., Van Nunen L.X., Tonino P.A.L., Pijls N.H.J., Van de Vosse F.N.; Modeling the interaction between the intra-aortic balloon pump and the cardiovascular system: the effect of timing; *American Society of Artificial Internal Organs Journal*, 59(1): 30-36, 2013.

Abstract

Because of the large number of interaction factors involved, the effects of the intra-aortic balloon pump (IABP) have not been investigated deeply. To enhance its clinical efficiency and to better define indications for use, advanced models are required to test the interaction between the IABP and the cardiovascular system. A patient with mild blood pressure depression and a lowered cardiac output is modeled in a lumped parameter computational model, developed with physiologically representative elements for relevant components of circulation and device. IABP support is applied, and the moments of balloon inflation and deflation are varied around their conventional timing modes. For validation purposes, timing is adapted within acceptable ranges in ten patients undergoing IABP therapy for typical clinical indications. In both model and patients, the IABP induces a diastolic blood pressure augmentation as well as a systolic reduction in afterload. The support capabilities of the IABP benefit the most when the balloon is deflated simultaneously with ventricular contraction, whereas inflation before onset of diastole unconditionally interferes with ejection. The physiologic response makes the model an excellent tool for testing the interaction between the IABP and the cardiovascular system, and how alterations of specific IABP parameters (i.e., timing) affect this coupling.

2.1 Introduction

The intra-aortic balloon pump (IABP) has a long record of supporting patients after acute myocardial infarction or cardiac surgery (Kantrowitz *et al.*, 1968). However, because of the large number of interaction factors involved, attributing either to the mechanics of the assist device or to the cardiovascular system, the effects of the IABP are still not fully understood, and its use has been based upon presumptions instead of clear scientific data. For example, IABP balloon inflation and deflation timing have traditionally been set to ensure complete balloon deflation during left ventricular ejection, because minimal clinical improvement or deterioration of systemic hemodynamics were expected otherwise (Smith *et al.*, 1991; Kantrowitz *et al.*, 1992). However, recent findings suggest that systemic hemodynamics and myocardial efficiency may be improved by later balloon deflation approaching left ventricular ejection in comparison to conventional IABP timing (Kern *et al.*, 1999). Thus, despite changes in acute cardiac care, the IABP has maintained its position herein, but indications for use may be redefined and its clinical efficiency might be enhanced.

Therefore, advanced models are required for testing the effects of the IABP under well-controlled circumstances. Several computational models have been developed for the evaluation of the IABP (Sun, 1991; Abdolrazaghi *et al.*, 2010; Kuklinski *et al.*, 1984), but all with important limitations. Previously developed models generally lack physiologic meaning, because used model elements do not correspond to measurable quantities. Furthermore, the mechanical interaction between pump and cardiovascular system is often eliminated by simply prescribing the variation in artery radius (Abdolrazaghi *et al.*, 2010) or driving heart contraction by the commonly used time-varying elastance model (Suga *et al.*, 1973), while Vandenberghe *et al.* (2006) showed that this model insufficiently describes left ventricular function when applied to an assisted left ventricle.

To enhance its clinical efficiency and to better define indications for use, the aim of this study is to test the dynamic interaction between the IABP and the cardiovascular system, and how alteration of specific IABP parameters (i.e., timing) affects this coupling. To this purpose, we have developed a lumped parameter computational model with representative elements for relevant components of both circulation and IABP, rendering an elaborate device model with elements corresponding to measurable quantities with physiologic meaning. For validation purposes, data are collected from patients undergoing IABP therapy after percutaneous coronary intervention or after/as a bridge to cardiac surgery.

2.2 Materials and methods

2.2.1 Cardiovascular system

The model of the cardiovascular system consists of two integrated parts: the heart and the circulation.

Heart

The left and right ventricle are modeled using the single fiber model by Arts *et al.* (1991) and Bovendeerd *et al.* (2006), describing ventricular wall mechanics, myocardial constitutive properties and intramyocardial pressure. Parameter values of the ventricular models are based on experimental data and derived from the work of Bovendeerd *et al.* (2006) (Table 2.1).

Ventricular wall mechanics

The model of the ventricular wall mechanics describes how ventricular pressure and volume are related to the local tissue state, i.e., fiber stress and strain, and radial wall stress and strain. The left ventricle is modeled as a thick-walled sphere, consisting of a set of nested thin shells. However, since the assumption of a thick-walled sphere does not hold for the right ventricle, radial wall stresses are neglected for the right ventricular wall mechanics. Muscle fiber stress and strain are assumed to be homogeneously distributed and the dimensionless ratio of muscle fiber stress to ventricular pressure depends on the dimensionless ratio of cavity volume to wall volume. Left and right ventricular pressure are respectively given by:

$$p_{LV} = \frac{1}{3}(\sigma_f - 2\bar{\sigma}_{m,r})\ln\left(1 + \frac{V_w}{V_{LV}}\right) \quad (2.1)$$

$$p_{RV} = \frac{1}{3}(\sigma_f)\ln\left(1 + \frac{V_w}{V_{RV}}\right) \quad (2.2)$$

Here, σ_f is the fiber stress, $\bar{\sigma}_{m,r}$ is the radial wall stress at the outer surface of the wall of the shell $r = \bar{r}$ that contains the ventricular cavity volume and one third of the wall volume. V_w represents the wall volume of the corresponding ventricle, and V_{LV} and V_{RV} are the cavity volumes of the left and right ventricle, respectively. σ_f is composed of an active (σ_a) and a passive ($\sigma_{m,f}$) component:

$$\sigma_f = \sigma_a + \sigma_{m,f} \quad (2.3)$$

Table 2.1: Model parameters for left and right ventricle.

Parameter	Left ventricle	Right ventricle
V_w	200	100
V_0	60	95
σ_{f0}	0.9	0.9
σ_{r0}	0.2	0.2
c_f	12	12
c_r	9	9
σ_{ar}	55	55
c	1	1
l_{s0}	1.9	1.9
$l_{s,a0}$	1.5	1.5
$l_{s,ar}$	2.0	2.0
v_0	10	10
c_v	0	0
t_{\max}	$0.5 \cdot t_{\text{cycle}}$	$0.5 \cdot t_{\text{cycle}}$

V_w , wall volume [mL]; V_0 , cavity volume at zero transmural pressure [mL]; σ_{f0} , passive fiber stress [kPa]; σ_{r0} , passive radial stress [kPa]; c_f , fitting constant for passive stress along fiber direction [-]; c_r , fitting constant for passive transverse stress [-]; σ_{ar} , active fiber stress in reference state [kPa]; c , contractility [-]; l_{s0} , sarcomere length at zero transmural pressure [μm]; $l_{s,a0}$, sarcomere length below which active stress becomes zero [μm]; $l_{s,ar}$, sarcomere length in reference state [μm]; v_0 , unloaded sarcomere shortening velocity [$\mu\text{m s}^{-1}$]; c_v , constant governing shape of stress-velocity relation [-]; t_{\max} , twitch duration; t_{cycle} , cardiac cycle duration [s].

The relation between ventricular volume and tissue strain at $r = \bar{r}$, which relates wall mechanics to cavity mechanics, is given by:

$$\lambda_f = \left(\frac{V_{LV} + \frac{1}{3}V_w}{V_{LV0} + \frac{1}{3}V_w} \right)^{\frac{1}{3}} \quad (2.4)$$

Here, λ_f is the fiber stretch ratio, V_{LV0} is the cavity volume at zero transmural pressure, with a corresponding sarcomere length l_{s0} . Under the assumption of incompressibility of the myocardial tissue, the radial stretch ratio λ_r at the same location equals:

$$\lambda_r = \lambda_f^{-2} \quad (2.5)$$

Myocardial constitutive properties

Muscle contraction is modeled with a Hill-type model (Hill, 1938), which allows flexibility in the deformation history of the heart during the cardiac cycle, and enables, in contrast to variable elastance models, to mimic the contractile properties of the heart under mechanical support conditions. Active and passive fiber stresses are modeled by constitutive laws for fiber and radial stress, in which active fiber stress depends on contractility (c), sarcomere length (l_s) (Kentish *et al.*, 1986), time elapsed since activation (t_a) (Korakianitis *et al.*, 2006), and sarcomere shortening velocity (v_s) as:

$$\sigma_a(c, l_s, t_a, v_s) = c \sigma_{ar} f(l_s) g(t_a) h(v_s) \quad (2.6)$$

With:

$$f(l_s) = \begin{cases} 0 & l_s \leq l_{s,a0} \\ \frac{l_s - l_{s,a0}}{l_{s,ar} - l_{s,a0}} & l_s > l_{s,a0} \end{cases} \quad (2.7)$$

$$g(t_a) = \begin{cases} 0 & t_a < 0 \\ \sin^2\left(\pi \frac{t_a}{t_{\max}}\right) & 0 \leq t_a \leq t_{\max} \\ 0 & t_a > t_{\max} \end{cases} \quad (2.8)$$

$$h(v_s) = \frac{1 - (v_s/v_0)}{1 + c_v (v_s/v_0)} \quad (2.9)$$

Here, $l_{s,a0}$ denotes the sarcomere length below which active stress becomes zero, and $l_{s,ar}$ and σ_{ar} represent the sarcomere length and active fiber stress in the

reference state. t_{\max} corresponds to the twitch duration (which depends on cardiac cycle time t_{cycle}), and v_0 is the unloaded sarcomere shortening velocity, which governs the shape of stress-velocity relation. At baseline level, left ventricular contractility $c = 1$, while c may be lowered for pathologic case studies. Passive fiber stresses along fiber and in radial direction are modeled as:

$$\sigma_{m,f}(\lambda_f) = \begin{cases} \sigma_{f0}(e^{c_f(\lambda_f-1)} - 1) & \lambda_f \geq 1 \\ 0 & \lambda_f < 1 \end{cases} \quad (2.10)$$

$$\sigma_{m,r}(\lambda_r) = \begin{cases} \sigma_{r0}(e^{c_r(\lambda_r-1)} - 1) & \lambda_r \geq 1 \\ 0 & \lambda_r < 1 \end{cases} \quad (2.11)$$

Here, it is assumed that no stress can be transmitted in compression.

Intramyocardial pressure

The intramyocardial pressure p_{im} is modeled to be linearly dependent on the transmural position in the wall of the left ventricle. p_{im} is equal to p_{LV} at the endocardial surface and zero at the epicardial surface. Again, the shell with $r = \bar{r}$ is considered representative:

$$\bar{p}_{im} = p_{im}(\bar{r}) = \bar{\sigma}_{m,r} + \frac{r_0 - \bar{r}}{r_0 - r_i} p_{LV} \quad (2.12)$$

Here, r_i is the radius of the cavity volume and r_0 is the radius of the cavity and wall volume together. The intramyocardial pressure acts on the myocardial capacitance ($C_{\text{myo},c}$) and thereby creates a connection between the model of the left ventricular wall mechanics and the coronary circulation.

Table 2.2: Parameter values of the circulation model, comprising a systemic, pulmonary, and coronary circulation.

Parameter	R [Pa s m^{-3}]	L [$\text{Pa s}^2 \text{m}^{-3}$]	C [$\text{m}^3 \text{Pa}^{-1}$]	V_0 [m^3]
<i>Aorta</i> ,1	$5.0 \cdot 10^6$	$5.6 \cdot 10^4$	$9.9 \cdot 10^{-9}$	$125 \cdot 10^{-6}$
<i>Aorta</i> ,2	$9.9 \cdot 10^6$	$5.6 \cdot 10^4$	$4.7 \cdot 10^{-9}$	$125 \cdot 10^{-6}$
<i>Aorta</i> ,3	$9.9 \cdot 10^6$	$5.6 \cdot 10^4$	$2.0 \cdot 10^{-9}$	$125 \cdot 10^{-6}$
<i>Aorta</i> ,4	$9.9 \cdot 10^6$	$5.6 \cdot 10^4$	$2.0 \cdot 10^{-9}$	$125 \cdot 10^{-6}$
<i>p,head</i>	$6.4 \cdot 10^8$	-	-	-
<i>p,abdomen</i>	$5.6 \cdot 10^8$	-	-	-
<i>p,kidney</i>	$5.2 \cdot 10^8$	-	-	-
<i>p,leg</i>	$6.4 \cdot 10^8$	-	-	-
<i>vcs</i>	$1.0 \cdot 10^5$	$1.7 \cdot 10^4$	$2.3 \cdot 10^{-7}$	$75 \cdot 10^{-5}$
<i>vci</i> ,1	$1.0 \cdot 10^5$	$1.7 \cdot 10^4$	$2.3 \cdot 10^{-7}$	$75 \cdot 10^{-5}$
<i>vci</i> ,2	$1.0 \cdot 10^5$	$1.7 \cdot 10^4$	$2.3 \cdot 10^{-7}$	$75 \cdot 10^{-5}$
<i>vci</i> ,3	$1.0 \cdot 10^5$	$1.7 \cdot 10^4$	$2.3 \cdot 10^{-7}$	$75 \cdot 10^{-5}$
<i>art,pul</i>	$1.9 \cdot 10^6$	$1.3 \cdot 10^4$	$3.0 \cdot 10^{-8}$	$700 \cdot 10^{-6}$
<i>p,pul</i>	$1.8 \cdot 10^7$	-	-	-
<i>ven,pul</i>	$4.0 \cdot 10^4$	$9.4 \cdot 10^5$	$4.0 \cdot 10^{-7}$	$70 \cdot 10^{-5}$
<i>cor,art</i>	$1.0 \cdot 10^9$	$1.0 \cdot 10^7$	$3.0 \cdot 10^{-11}$	$6 \cdot 10^{-6}$
<i>myo,endo</i>	$2.4 \cdot 10^9$	-	$1.4 \cdot 10^{-8}$	$7 \cdot 10^{-6}$
<i>myo,epi</i>	$3.5 \cdot 10^9$	-	-	-
<i>cor,ven</i>	$7.0 \cdot 10^8$	$1.0 \cdot 10^7$	$7.0 \cdot 10^{-10}$	$10 \cdot 10^{-6}$

aorta , aorta; *p,head* , head periphery; *p,abdomen* , abdomen periphery; *p,kidney* , kidney periphery; *p,leg* , leg periphery; *vcs* , vena cava superior; *vci* , vena cave inferior; *art,pul* , pulmonary artery; *p,pul* , pulmonary periphery; *ven,pul* , pulmonary vein; *cor,art* , coronary artery; *myo,endo* , subendocardial myocardium; *myo,epi* , subepicardial myocardium; *cor,ven* , coronary vein.

Circulation

The systemic, pulmonary, and coronary circulation are modeled on the basis of the elements of a lumped parameter mathematical model (Figure 2.1). Heart valves have been modeled as ideal diodes, and vessels are modeled with constant resistances (R), inertances (L) and compliances (C) (Table 2.2). The pressure drop across each of these components is given by:

$$\Delta p_R = Rq \quad (2.13)$$

$$\Delta p_L = L \frac{dq}{dt} \quad (2.14)$$

$$\Delta p_C = \frac{V - V_0}{C} \quad (2.15)$$

Here, q is the flow through a resistance or inertance, V is the volume in a capacitance, and V_0 is the volume in a capacitance at zero pressure.

The intramyocardial pressure (Bovendeerd *et al.*, 2006), that acts on the myocardial capacitance, makes the connection between the model of the left ventricular mechanics and the coronary circulation model of Geven *et al.* (2004), which comprises a coronary epicardial artery, an intramyocardial pressure dependent myocardial perfusion resistance, and a venous outlet.

The values for the elements of the lumped parameter model are determined iteratively and result in representative pressure and flow signals (Table 2.2). A total blood volume of 5 L is chosen to be representative.

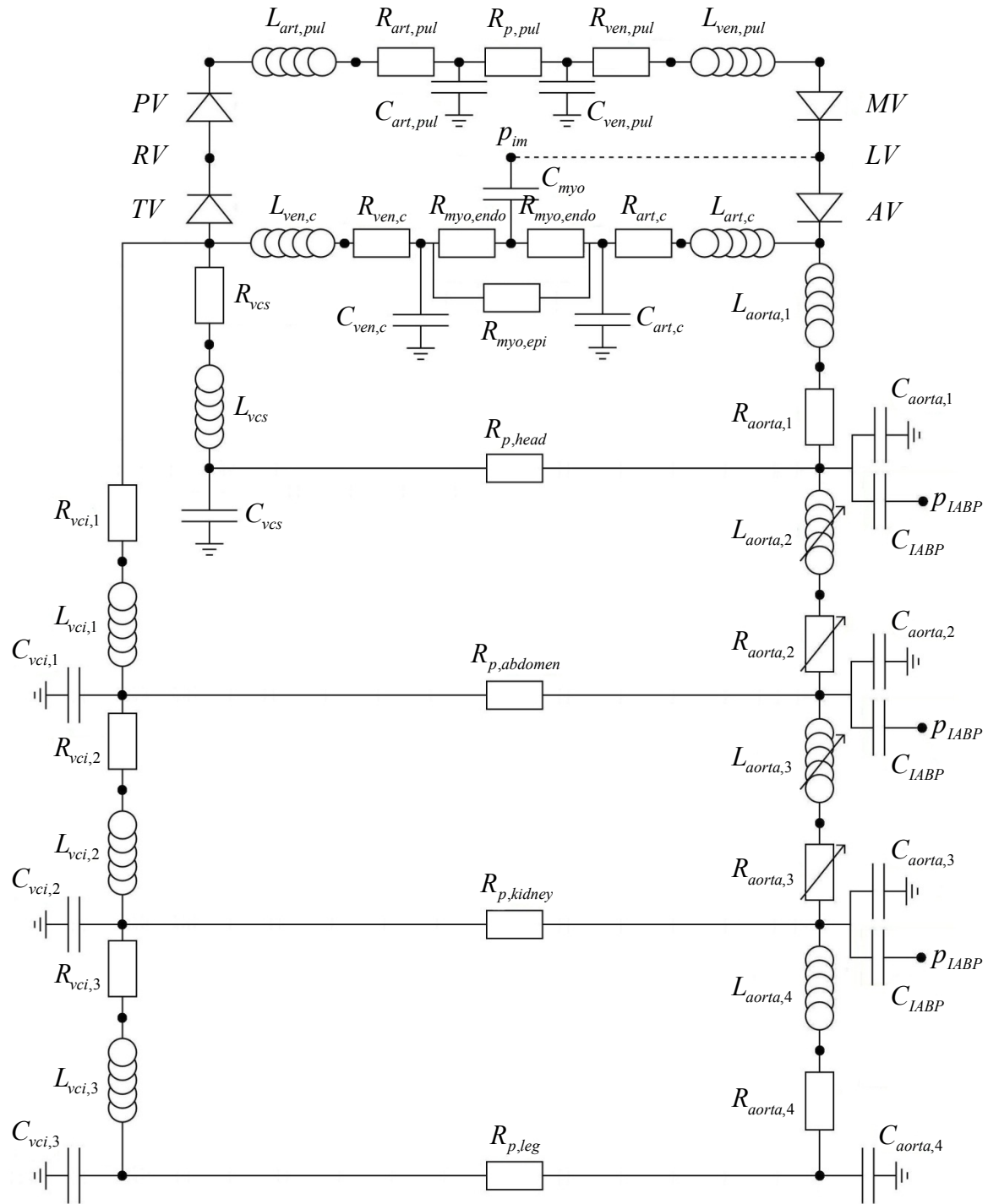


Figure 2.1: Lumped parameter computational model of the systemic, pulmonary, and coronary circulation represented by an electrical circuit. LV and RV are the left and right ventricle, and AV , MV , PV , and TV are the aortic, mitral, pulmonary, and tricuspid valve. L_{aorta} and $L_{art,pul}$ are the inertia of the blood in aortic and pulmonary artery elements. R_{aorta} , $R_{art,pul}$, C_{aorta} , and $C_{art,pul}$ are the resistance and compliance of the aortic and pulmonary artery elements. $R_{p,head}$, $R_{p,abdomen}$, $R_{p,kidney}$, $R_{p,leg}$, and $R_{p,pul}$ are the peripheral resistance of the

systemic and pulmonary circulation. R_{vci} , R_{vcs} , $R_{ven,pul}$, C_{vci} , C_{vcs} , and $C_{ven,pul}$ are the resistance and compliance of the systemic and pulmonary veins. L_{vci} , L_{vcs} , and $L_{ven,pul}$ are the inertia of the blood in the veins. $R_{art,c}$, $R_{myo,endo}$, $R_{myo,epi}$, and $R_{ven,c}$ represent the coronary arterial, intramyocardial, and venous resistance, and $C_{art,c}$, C_{myo} , and $C_{ven,c}$ are the coronary arterial, intramyocardial, and venous compliance. $L_{art,c}$ and $L_{ven,c}$ are the inertia of the blood in the coronary circulation, and p_{im} is the intramyocardial pressure. The IABP is numerically modeled by additional compliances (C_{IABP}) and time-varying components (λ) of the relevant aortic segments. The prescribed balloon pressure (p_{IABP}) acts on the balloon compliance.

2.2.2 Intra-aortic balloon pump

The IABP is described as a cylinder-shaped collapsible tube with a fixed length and a cross-sectional area concentric with the vessel at any moment in time. This concept is implemented into the circulation model by additional compliances (C_{IABP}) and time-varying components (resistances and inertances) of relevant aortic segments (Figure 2.1). The prescribed balloon pressure (p_{IABP}), which varies linearly between -200 and 200 mmHg during transition of phases (typically 80 ms) (Sun, 1991), induces a time-varying pressure drop across the balloon compliances, rendering an instantaneous volume change (set to 40 cc, here) within the system.

Fluid inductance and resistance of the relevant aortic segments are expected to be significantly modified by this induced volume change. As the circular cross-section of the IABP is assumed to have a finite volume when fully deflated, the instantaneous geometry and the relative position of the cylinder-shaped collapsible tube in the descending aorta are described by a concentric cylinder model. For a laminar flow through a concentric annulus, the resistance of an aortic segment including a balloon (R_{IABP}) can be approximated by:

$$R_{IABP} \approx R_{aorta} \left[1 - \xi^4 - \frac{(1 - \xi^2)^2}{\ln(\xi)} \right]^{-1} \quad (2.16)$$

Here, R_{aorta} is the resistance of an aortic segment without a balloon, and $\xi = \frac{r_{IABP}}{r_{aorta}}$ is the ratio between the radius of the balloon (r_{IABP}) and the radius of the aorta (r_{aorta}).

The cross-sectional area of the aorta depends linearly on the pressure inside the vessel segment. Assuming a uniform velocity profile in a concentric annulus, the inertance of an aortic segment including a balloon (L_{IABP}) can be approximated by:

$$L_{IABP} \approx L_{aorta} \frac{1}{1 - \xi^2} \quad (2.17)$$

Here, L_{aorta} is the inertance of an aortic segment without a balloon, and ξ is the ratio between the radius of the balloon and the aorta as defined before.

2.2.3 Solution procedure

The lumped parameter model was analyzed using DIScrete Computation (DISCO) (Schreurs, 2012), a discrete system computation system in which finite element procedures are used to generate and solve a set of differential equations for various initial and boundary conditions.

Assembling and applying nodal equilibrium in a finite number of points resulted in a set of second-order linear differential equations, which describe the system behavior:

$$\underline{A}\ddot{p} + \underline{B}\dot{p} + \underline{C}p = f_e \quad (2.18)$$

Here, the linear properties are denoted with the constant matrices \underline{A} , \underline{B} , and \underline{C} . The nodal point pressures and flows are in columns \tilde{p} and \tilde{f} , respectively. Temporal discretization, with time step Δt , is performed using the Euler implicit integration scheme ($\theta = 1$), such that the system of differential equations is satisfied on time $t + \theta\Delta t$. Difference formulas for $\ddot{\tilde{p}}_{t+\Delta t}$ and $\dot{\tilde{p}}_{t+\Delta t}$ are substituted into the differential equations:

$$\ddot{\tilde{p}}_{t+\Delta t} = \frac{1}{\Delta t} \{ \dot{\tilde{p}}_{t+\Delta t} - \dot{\tilde{p}}_t \} \quad (2.19)$$

$$\dot{\tilde{p}}_{t+\Delta t} = \frac{1}{\Delta t} \{ \tilde{p}_{t+\Delta t} - \tilde{p}_t \} \quad (2.20)$$

$\tilde{p}_{t+\Delta t}$ was solved from the resulting set of algebraic equations:

$$\left[\frac{1}{\Delta t^2} \underline{A} + \frac{1}{\Delta t} \underline{B} + \underline{C} \right] \tilde{p}_{t+\Delta t} = \tilde{f}_{t+\Delta t} + \left[\frac{1}{\Delta t^2} \underline{A} + \frac{1}{\Delta t} \underline{B} \right] \tilde{p}_t + \left[\frac{1}{\Delta t} \underline{A} \right] \dot{\tilde{p}}_t \quad (2.21)$$

2.2.4 Simulations

With the model, a number of simulations is performed. First, we consider a near-physiologic representation of the circulation with model heart dimensions and contractility properties set to normal values. A clinical scenario meeting the hemodynamic criteria for IABP support is subsequently modeled by decreasing left ventricular contractility (c) to 0.7, while keeping the lumped parameter impedances constant. IABP support is applied, and the enhancement of coronary flow and blood pressure is tested with the pump operating at its generally in-hospital used settings (inflation upon onset of diastole, deflation in early systole). Finally, the moments of balloon inflation and deflation are varied around their conventional timing modes, while the percent changes of several performance indices (mean aortic pressure, cardiac output, coronary flow, cardiac stroke work) with respect to baseline are calculated.

2.2.5 *In vivo* validation

For validation purposes, data are collected from ten patients (65 ± 13 years) undergoing IABP therapy for typical clinical indications after percutaneous coronary intervention ($n = 7$) or after/as a bridge to cardiac surgery ($n = 3$). Clinical data are shown in table 2.3. In all patients, a 40 or 50 cc polyurethane balloon mounted with a 7 Fr catheter (Maquet Getinge Group, Rastatt, Germany) is inserted through a percutaneous femoral approach and positioned, under fluoroscopic guidance, in the descending thoracic aorta, distal to the left subclavian artery and proximal to the renal artery branches. The catheter-mounted balloon is connected to a CS300 IABP System (Maquet Getinge Group, Rastatt, Germany), which is triggered by the electrocardiogram.

When patients' condition permits, the pump is switched off for a short period of time (± 30 s) and baseline aortic pressure signal is recorded by the pressure sensor located at the tip of the balloon. Subsequently, IABP therapy is applied using the manual operation mode, and the moments of balloon inflation and deflation are step-wise varied around their conventional timing settings, while the percent change of mean aortic pressure with respect to baseline is calculated.

Table 2.3: Clinical data of ten patients undergoing IABP therapy.

Patient	Age	Sex	Balloon size	Condition/ Indication
1	66	Male	40	CS, CABG
2	48	Male	40	OHCA, IS
3	41	Male	40	AMI, CS
4	53	Male	40	CS
5	73	Male	40	CABG
6	68	Male	50	AMI, CS
7	82	Male	40	CS
8	77	Female	50	IS, SCAD
9	64	Male	50	AMI, CS
10	74	Male	50	IS, CABG

Age [years]; Balloon size [cm³].

CS, cardiogenic shock; CABG, coronary artery bypass grafting; OHCA, out-of-hospital cardiac arrest; IS, ischemia; AMI, anterior myocardial infarction; SCAD, spontaneous coronary artery dissection.

2.3 Results

With the model heart dimensions and contractility properties set to normal values, simulated pressure and flow signals are physiologically correct (Figure 2.2), and hemodynamic parameters are in agreement with reference values found in literature (Table 2.4). Aortic pressure shows a peak systolic pressure, which gradually declines towards the end of diastole. Coronary flow, which is primarily driven by aortic pressure, shows a reduced systolic arterial flow component relative to diastolic flow, despite having a higher systolic driving pressure. Scaling active fiber stress with 0.7 results in a lowered cardiac output and a mild blood pressure depression, meeting the hemodynamic criteria for IABP support.

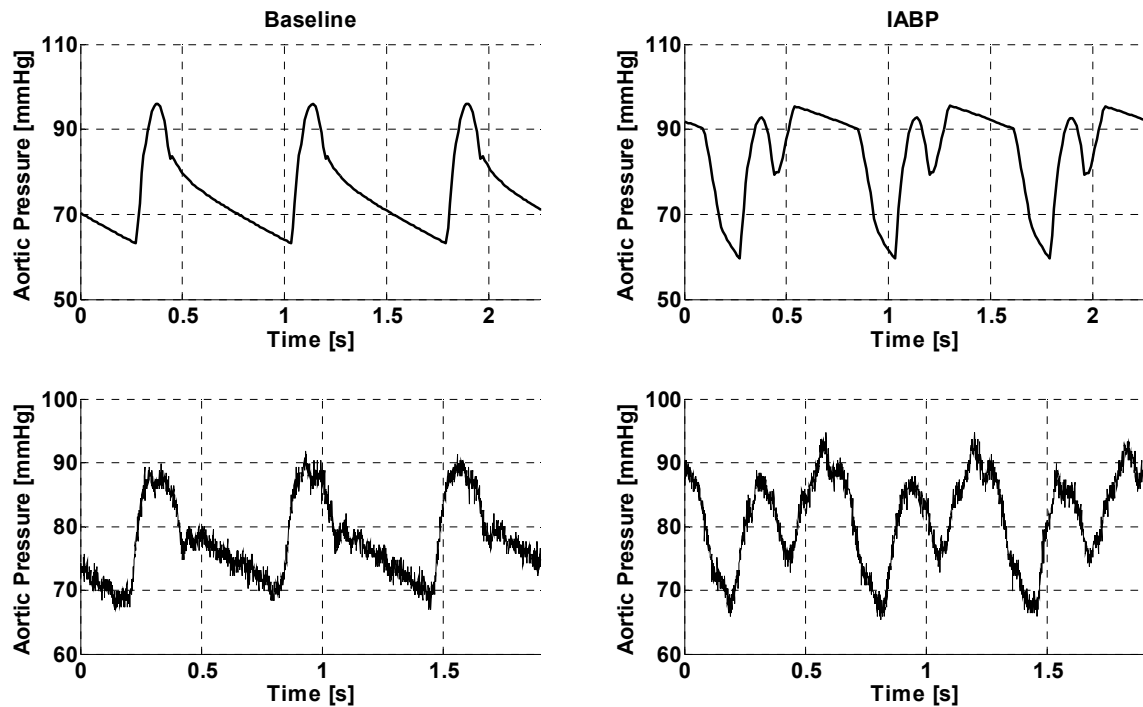


Figure 2.2: Top row: Pressure registrations of the lumped parameter model at baseline and IABP supported conditions ($c = 0.7$). Bottom row: *In vivo* human signals at baseline and during standard in-hospital IABP support.

The system's response to IABP support indicates a proper implementation of a counterpulsating balloon (Figure 2.2, Table 2.4). With the IABP attached and operating in its conventional timing mode, pressure signals obtained from the numerical simulations closely resemble *in vivo* human signals (Table 2.5). In both model and patients, rapid deflation of the catheter-mounted polyurethane balloon briefly creates a vacuum at the end of diastole, reflected by a reduced afterload. In the model, this results in a cardiac output increase, whereas the area within the pressure-volume loop, which is a measure for the delivered cardiac stroke work, remains at baseline level. Rapid inflation of the balloon, immediately after ejection, induces a diastolic blood pressure augmentation, which significantly enhances mean aortic pressure and appears to be an increased driving force for coronary perfusion.

Table 2.4: Reference values and simulation results for pressure and flow at relevant sites in the circulation.

Parameter	Reference	Model		
		$c = 1.0$		$c = 0.7$
		Baseline	Baseline	IABP
HR	60 – 80	80	80	80
$P_{ao,sys}$	90 – 140	120	96	96
$P_{ao,dia}$	60 – 90	80	63	60
$P_{ao,mean}$	70 – 105	95	75	85
CO	5.0 – 7.6	5.2	4.1	4.4
Q_{cor}	200 – 300	262	207	237
SW	6000 – 8000	7306	4528	4676

HR , heart rate [min^{-1}]; $P_{ao,sys}$, peak systolic aortic pressure [mmHg]; $P_{ao,dia}$, end diastolic aortic pressure [mmHg]; $P_{ao,mean}$, mean aortic pressure [mmHg]; CO , cardiac output [L min^{-1}]; Q_{cor} , coronary flow [mL min^{-1}]; SW , cardiac stroke work [mmHg mL].

In both model and patients (Figure 2.3, Figure 2.4), the percent change of several important hemodynamic parameters with respect to baseline show the same trend for variation in timing. All evaluated parameters (mean aortic pressure, cardiac output, coronary blood flow, cardiac stroke work) benefit the most when balloon inflation starts at the end of ejection, just before aortic valve closure. However, it is remarkable that in the two patients with low heart rates (patients 8 and 10, having a heart rate of 56 min^{-1} and 60 min^{-1} respectively, and consequently a relatively short ejection phase with respect to the complete heart cycle) slightly later deflation (after aortic valve closure) seems to produce maximum systemic hemodynamic advantages. Earlier inflation, and further elongation of the inflated balloon state, unconditionally interferes with left ventricular ejection, whereas for late inflation, the blood flow augmentation is suboptimal. When the balloon is deflated at the start of left ventricular contraction (R-peak), a brief vacuum is created just before ejection. The lower resistance to ejection consequently results in a maximum cardiac output increase, probably caused by suction of blood out of the ventricle by the created vacuum. Early deflation of the balloon leads to an inflated balloon state for a shorter period of time, resulting in a sub-optimal blood flow augmentation to the organs and a limited afterload reduction, because of the smaller decline in aortic pressure.

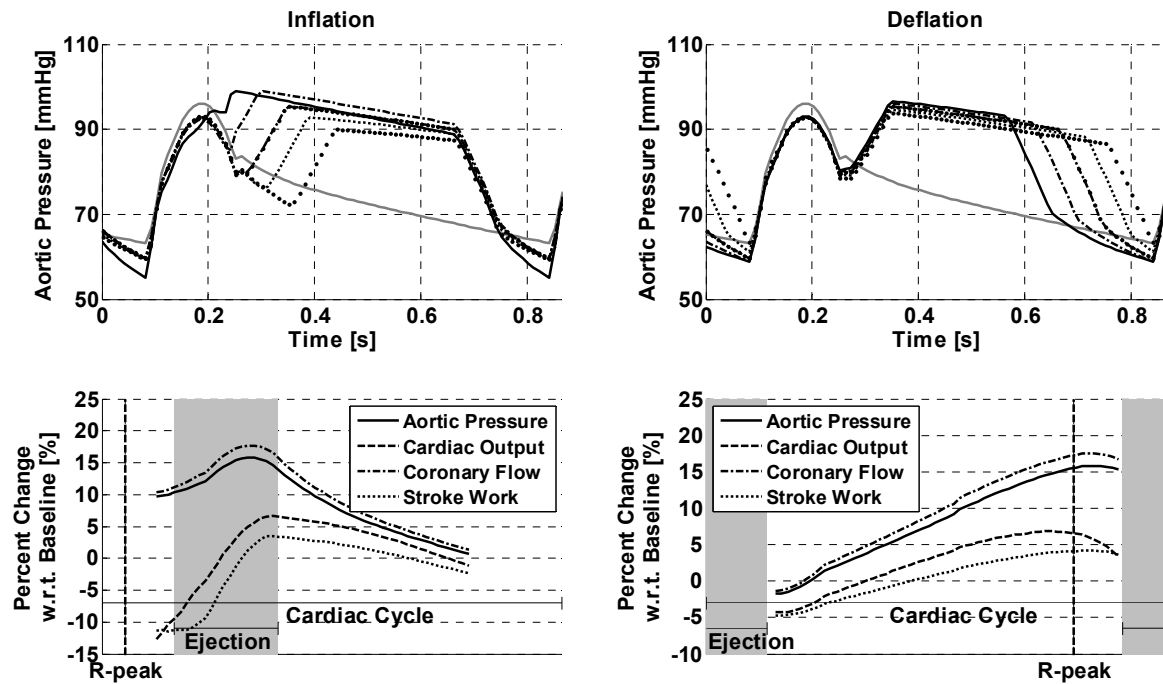


Figure 2.3: Top row: Simulated aortic pressure waveforms for unassisted (grey) and assisted cardiac cycles (black). The start of balloon inflation (left) and deflation (right) are varied around their conventional timing modes, and postpone from the solid curves towards the dotted curves. Bottom row: Simulated percent changes of several hemodynamic performance indexes (mean aortic pressure, cardiac output, coronary blood flow, and cardiac stroke work) for variation in balloon inflation (left) and deflation (right) compared to baseline. On the horizontal axis one cardiac cycle was plotted. The R-peak is represented by a dotted vertical line, and the grey area represents the left ventricular ejection phase.

2.4 Discussion

In this study, a realistic numerical model is presented, capable of simulating the interaction between the IABP and the cardiovascular system, and providing new insight as how alterations of timing affect this coupling.

2.4.1 Cardiovascular system

The main requirements for the model of the cardiovascular system are to generate physiologic pressure and flow signals through physiologically representative elements, and left and right ventricular contraction being the only input for the model. The presented model consists of two integrated systems: the heart and the circulation. Both ventricles are regulated by a heart model, in which muscle contraction is calculated separately from the total deformation of the ventricles. This allows flexibility in the deformation history of the heart during the cardiac cycle, and

enables to mimic the contractile properties of the heart under mechanical support conditions. Incorporated in a lumped parameter model, the circulation features a complete systemic, pulmonary, and coronary vascular bed, which is essential as an assist device interacts with the complete circulation (Cox *et al.*, 2009). The final values (resembling the estimation closely) are determined iteratively and set to render systemic, pulmonary, and coronary pressure and flow waveforms in agreement with physiology.

Table 2.5: *In vivo* measured hemodynamic data on heart rate and blood pressure.

Patient	HR	Baseline			IABP			
		$P_{ao,sys}$	$P_{ao,dia}$	$P_{ao,mean}$	$P_{ao,sys}$	$P_{ao,dia}$	$P_{ao,mean}$	$P_{ao,aug}$
1	96	89	69	78	86	67	81	91
2	127	97	61	78	95	62	80	86
3	106	85	70	72	81	60	73	80
4	103	111	79	93	104	83	93	96
5	87	134	65	89	107	68	93	122
6	97	95	65	78	87	68	83	101
7	96	123	58	86	119	48	89	109
8	56	137	66	94	114	55	103	145
9	100	133	76	98	125	83	116	156
10	60	113	63	82	103	57	82	115
Mean	93	112	67	85	102	65	89	110
± SD	± 21	± 20	± 6	± 9	± 15*	± 11	± 13**	± 25

HR , heart rate [min^{-1}]; $P_{ao,sys}$, peak systolic aortic pressure [mmHg]; $P_{ao,dia}$, end diastolic aortic pressure [mmHg]; $P_{ao,mean}$, mean aortic pressure [mmHg]; $P_{ao,aug}$, augmented aortic pressure [mmHg].

* Paired t-test: $p < 0.01$ vs. Baseline; ** Paired t-test: $p < 0.05$ vs. Baseline.

2.4.2 Intra-aortic balloon pump

The IABP is considered to be a cylinder-shaped collapsible tube with a fixed length. The circular cross-section of the balloon, related to the change in shape induced by the transmural pressure, is assumed to be concentric with the vessel at any moment in time, which enables description of the instantaneous geometry and the relative position of the IABP in the descending aorta by a concentric cylinder model. Incorporated into the circulation model by additional compliances and time-varying components (resistances and inertances) of relevant aortic segments, this renders an

elaborate IABP model with physiologically representative elements, corresponding to measurable quantities and physiologic meaning.

2.4.3 Strengths and limitations

Important advantages of numerical evaluation of the interaction between the IABP and the cardiovascular system are the simplicity with which mechanical support can be applied and the ability of the model to create identical circumstances. This allows evaluation of the influence of one specific parameter on the coupling between circulation and device. In this paper, we thoroughly describe the effect of timing, but additional model simulations show an increased blood pressure and afterload reduction for increasing balloon volume. In addition, the model confirms that IABP support is influenced by a large number of patient-specific factors, and that it might be reserved for patients in deep cardiogenic shock, having a stiff aorta and a heart rate not exceeding 140 min^{-1} , because of the time required for complete inflation and deflation of the balloon. The extended number of patient-specific factors influencing the support capabilities of the IABP might be an explanation for the differences in percent changes of mean aortic pressure between model and patients, but also between the individual patients.

Although the model is capable of simulating the interaction between the IABP and the cardiovascular system, and generates pressure and flow curves in agreement with *in vivo* data, the presence of feedback mechanisms is limited. At the moment the model does include cardiac function control, but it lacks mechanisms to regulate blood pressure and heart rate. In addition, both ventricles are passively filled and a linear relation between the transmural pressure and the cross-sectional area of the aorta is assumed, while due to the complex non-linear, anisotropic and viscoelastic properties of the arterial wall, this relation can be rather complicated.

2.4.4 Clinical application

Every interventional cardiologist has witnessed cases of patients with cardiogenic (pre-)shock or anterior wall myocardial infarction with prompt relief of chest pain, ST-segment resolution, and hemodynamic improvement after IABP insertion, along with cases where the IABP had no or only minimal effect. Reasons for these varying observations are unclear. Mathematical modeling of the interaction between the IABP and the cardiovascular system provides a better understanding of the pump's performance and helps to represent blood flow and pressure in systemic arteries before and after inserting the pump. Consequently, the numerical model is a valuable tool for training and research purposes, while supporting medical specialists in a better understanding of the indications for use.

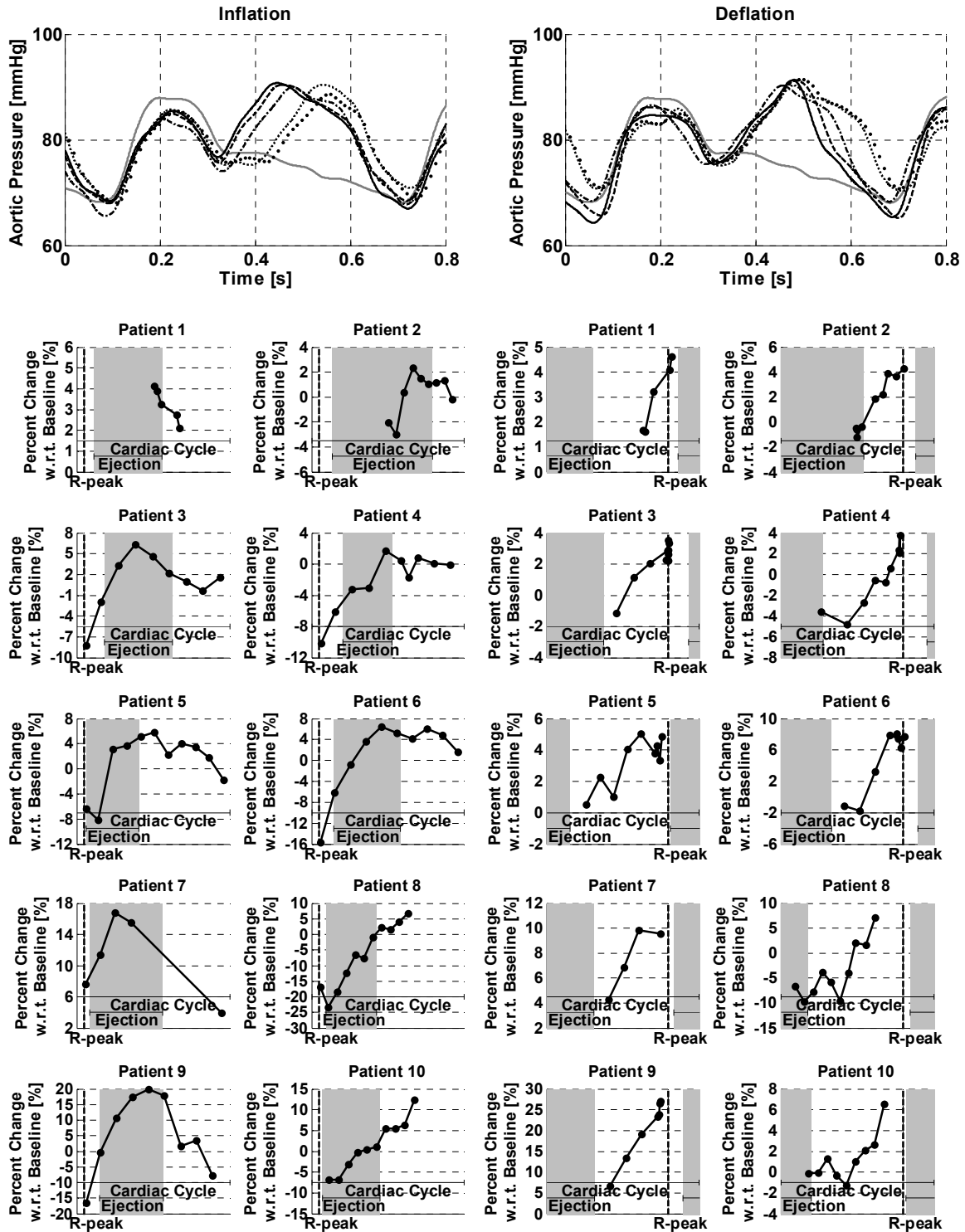


Figure 2.4: Top row: *In vivo* measured aortic pressure waveforms for unassisted (grey) and assisted cardiac cycles (black). The start of balloon inflation (left) and deflation (right) are varied around their conventional timing modes, and postpone from the solid curves towards the dotted curves. Bottom rows: Percent changes of mean aortic pressure for variation in balloon inflation (left) and deflation (right) with respect to baseline for the ten individual patients. On the horizontal axis one cardiac cycle was plotted. The R-peak is represented by a dotted vertical line, and the grey area represents the left ventricular ejection phase.

2.5 Conclusion

The presented lumped parameter computational model enables evaluation of the interaction between the IABP and the cardiovascular system, and provides new insight as to how alterations of timing parameters affect this coupling. Operating in its generally in-hospital settings, the IABP induces a diastolic blood flow augmentation to the coronary circulation, as well as a systolic reduction in afterload. The support capabilities of the IABP benefit the most when the balloon is deflated simultaneously with the start of contraction, while inflation before onset of diastole unconditionally interferes with ejection.

Chapter 3

A mock circulation model for cardiovascular device evaluation

The contents of this chapter are based on:

Schampaert S., Pennings K.A.M.A., Van de Molengraft M.J.G., Pijls N.H.J., Van de Vosse F.N., Rutten M.C.M.; A mock circulation model for cardiovascular device evaluation; *Physiological Measurement*, 35: 687-702, 2014.

Abstract

The aim of this study is to develop an integrated mock circulation system that functions in a physiologic manner for testing cardiovascular devices under well-controlled circumstances. The presented model is a hydraulic servo-motor operated mock loop, including a systemic, pulmonary, and coronary circulation. The system is controlled by an elaborate heart contraction model, a realistic frequency control model, and a relatively simple lead-lag controller. The behavior of the presented system was tested in response to changes in left ventricular contractile states, loading conditions, and heart rate. For validation purposes, generated hemodynamic parameters and responses were compared to literature. The generated pressure and flow signals closely mimic human pressure and flow under both physiologic and pathologic conditions. In addition, the system's response to changes in preload, afterload, and heart rate indicate a proper implementation of the incorporated feedback mechanisms (frequency and cardiac function control). Therefore, the presented mock circulation allows for generic in vitro testing of cardiovascular devices under well-controlled circumstances.

3.1 Introduction

Mock circulation systems have been used widely for *in vitro* testing and validating of cardiovascular devices such as heart valves, stent grafts, and ventricular assist devices. These systems vary from relatively simple pulse duplicators (Cornhill, 1977; Warnock *et al.*, 2005), to extended hybrid models (Ochsner *et al.*, 2013; Fresiello *et al.*, 2013) and other feedback controlled systems incorporating the contractile behavior of the heart (Pantalos *et al.*, 2004; Ferrari *et al.*, 2002; Timms *et al.*, 2005; Timms *et al.*, 2010; Reul *et al.*, 1975). The latter type is of importance for the application to ventricular assist devices, since the strong interaction between these devices and the ventricle cannot be modeled properly without the appropriate response of the heart and circulation (Cox *et al.*, 2009).

The most commonly used heart contraction mechanism in such mock loops (Baloa *et al.*, 2001; Colacino *et al.*, 2008; Fresiello *et al.*, 2013) is driven by the time-varying elastance model of Suga *et al.* (1973). This model describes the left ventricle as a compliant chamber with time-varying elastic material properties. However, Vandenberghe *et al.* (2006) showed that the time-varying elastance model insufficiently describes left ventricular function when applied to a diseased or assisted left ventricle. To overcome this insufficiency, a more elaborate model is needed, in which muscle contraction and total deformation of the ventricle are calculated separately. This allows for more flexibility in the deformation history of the heart during the cardiac cycle, and enables mimicking the contractile properties of the heart under diseased and mechanical circulatory support conditions.

In all but one reported mock loops (Fresiello *et al.*, 2013), heart rate has a preset value, typically 75 min^{-1} . Heart rate changes, however, have a more profound effect on cardiac output than changes in e.g., the contractile behavior of the heart muscle. Therefore, in our model, we aimed to have a varying heart rate to accommodate the blood demand of the body. Three important mechanisms controlling heart rate *in vivo* are renal blood volume regulation, systemic vasoconstriction/-relaxation, and the baroreflex response (Guyton *et al.*, 2006). Typical response times for these mechanisms are hours, minutes, and seconds, respectively. For short-term analyses, the baroreflex pressure control mechanism is the most important, because of its fast response and impact on cardiac output.

Because circulatory assist devices are most frequently used to support left ventricular failure, the right ventricle and the pulmonary circulation are often neglected in previously developed mock circulation systems (Pantalos *et al.*, 2004; Kolyva *et al.*, 2012), or the right ventricle is simply synchronized with the left ventricle (Ferrari *et al.*, 2002). Also the coronary circulation is often driven by prescribed aortic pressure and resistance (Segers *et al.*, 1999; Matthys *et al.*, 2001).

However, neglecting the right-sided circulation leads to a non-physiologically strong coupling between left ventricular preload and afterload, while prescribing aortic pressure and resistance is a restriction on the value of the coronary flow model in mimicking physiologic conditions (Geven *et al.*, 2004). Since an assist device interacts with the complete circulation, it is essential to use a circulatory model having a systemic, pulmonary, and coronary circulation (Timms *et al.*, 2010; Cox *et al.*, 2009). To address the need for mock circulations that function in a physiologic manner for testing cardiovascular devices (i.e., ventricular assist devices) under well-controlled circumstances (Pantalos *et al.*, 2004), an integrated mock circulation system was developed, featuring a systemic, pulmonary, and coronary circulation, an elaborate heart contraction model, a realistic frequency control model, and a relatively simple lead-lag controller. The dynamic behavior of the presented system was tested in response to changes in contractile states, loading conditions, and heart rate. For model validation, generated hemodynamic parameters were compared to reference values found in literature (Table 3.1).

3.2 Materials and methods

The main consideration of the developed integrated mock circulation system is the physiologic basis of both the pressure and flow signals in the systemic, pulmonary, and coronary circulation, together with the dynamic response of important feedback mechanisms (frequency and cardiac function control). These modeling conditions were met by implementing control algorithms in a servo-pump driven mock circulation loop.

3.2.1 Control algorithms

The integrated mock circulation system is controlled by an elaborate heart contraction model (Bovendeerd *et al.*, 2006), a realistic frequency control model (Van Roon *et al.*, 2004), and a relatively simple lead-lag controller (Van de Molengraft *et al.*, 1994).

Heart contraction model

The left and right ventricle are modeled using the single fiber model by Bovendeerd *et al.* (2006), including ventricular wall mechanics and myocardial constitutive properties. This model is extensively described in **chapter 2**.

The model of ventricular wall mechanics describes how ventricular pressure and volume are related to local tissue properties, i.e., fiber stress and strain, and radial wall stress and strain. Both ventricles are modeled as thick-walled spheres, consisting

of a set of nested thin shells. Muscle fiber stress and strain are assumed to be homogeneously distributed and the dimensionless ratio of muscle fiber stress to ventricular pressure depends on the dimensionless ratio of cavity volume to wall volume. Muscle contraction is modeled with a Hill-type model (Hill, 1938), which allows flexibility in the deformation history of the heart during the cardiac cycle, and enables, in contrast to variable elastance models, to mimic the contractile properties of the heart under mechanical support conditions. Active and passive fiber stress are modeled by constitutive laws for fiber and radial stress, in which active fiber stress depends on contractility c , sarcomere length (Kentish et al., 1986), time elapsed since activation (Korakianitis et al., 2006), and sarcomere shortening velocity.

Heart rate control model

The baroreflex model used here is based on work of Van Roon *et al.* (2004). They proposed a baroreflex-controlled heart rate which was both vagally and sympathetically controlled and dependent on systemic arterial pressure only. The static relationship between baroreceptor activity and blood pressure is reflected by a sigmoid function, which is used together with a first-order system and a parallel gain to transform the changes in blood pressure into dimensionless values of baroreceptor activity (B_b), which in turn is transformed to autonomic vagal (F_{vag}) and sympathetic frequencies (F_{sym}):

$$F_{vag} = K_{vag} G_v B_b + D_{vag} \quad (3.1)$$

$$F_{sym} = K_{sym} G_s B_b + D_{sym} \quad (3.2)$$

Here, K_{sym} and K_{vag} are conversion factors, G_v and G_s are extra gain factors, and D_{sym} and D_{vag} denervation levels. The heart rate of the baroreflex ($f_{h,b}$) is obtained by a non-linear combination of F_{vag} and F_{sym} :

$$f_{h,b} = f_{h,d} \left(1 - \frac{F_{vag}}{F_{vag} + c_{F,vag}} \right) \left(1 + \frac{F_{sym}}{c_{F,sym}} \right) \quad (3.3)$$

Here, $f_{h,d}$ is the heart rate of a denervated heart and $c_{F,vag}$ and $c_{F,sym}$ are fitting constants. The dynamic responses of vagal and sympathetic activation are described by a time delay and a first-order system, and have a characteristic time in the order of 20 s.

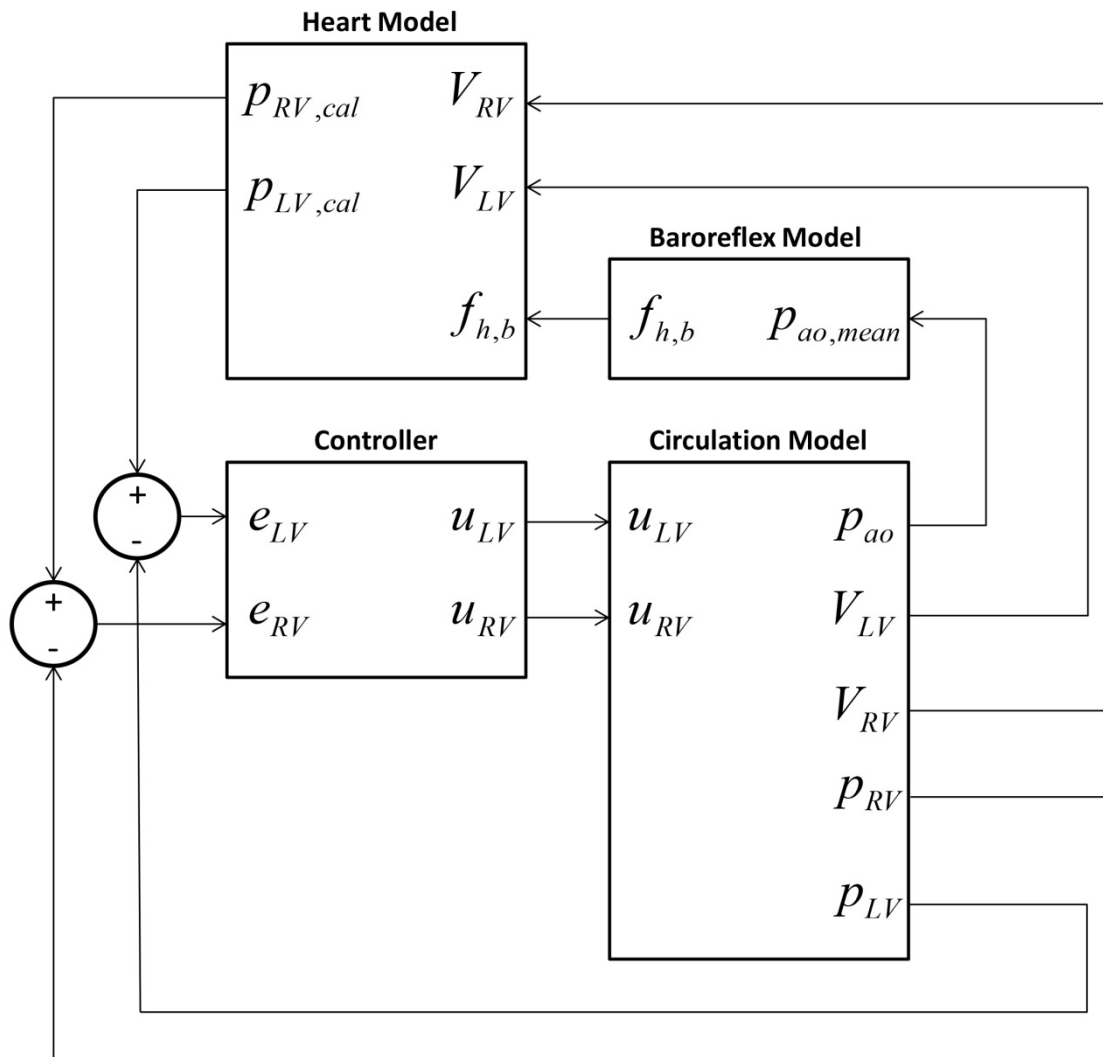


Figure 3.1: Block diagram of the schematic control loop, summarizing the most important hardware (circulation model) and control algorithms (heart model, baroreflex model, controller), including their inputs and outputs.

Control strategy

The closed-loop model consists of the circulation model, the heart model (including cardiac function control), the baroreflex model, and a controller (Figure 3.1). The circulation model generates signals for the actual left (p_{LV}) and right ventricular pressure (p_{RV}), aortic pressure (p_{ao}) and left (V_{LV}) and right ventricular volume (V_{RV}). It also keeps track of the time. The ventricular volumes and average aortic pressure ($p_{ao,mean}$) are fed into the heart model and baroreflex model to generate the required ventricular pressures ($p_{LV,cal}$, $p_{RV,cal}$) and heart frequency ($f_{h,b}$), which is updated on a per-beat basis at the start of each contraction. This way, each contraction cycle is

conducted with constant frequency within one heartbeat. The controller set-point is the difference between actual and instantaneously required ventricular pressures (e_{LV}, e_{RV}). For the design of the servo-controller, manual loop shaping of the open loop frequency response function of the system was used (Van de Molengraft *et al.*, 1994; Franklin *et al.*, 2002). The controller consists of three components: an integral action is used for disturbance rejection at low frequencies, a lead compensator is used for phase advance in the resonance frequency region, and a second-order low-pass filter takes care of measurement noise reduction at high frequencies.

3.2.2 Hardware implementation

The servo-pump driven mock circulation loop (Figure 3.2), in which the control algorithms are implemented, is based on work of Vaes *et al.* (2007). It consists of two servo-motor operated piston pumps acting as left and right ventricle, and a systemic, pulmonary, and coronary vascular bed. Water is used as circulating fluid.

Left and right ventricle

The piston pumps each have a variable stroke volume (maximum of 180 mL) and are driven by a linear actuator (ETB32, Parker Hannifin, The Netherlands). Three-leaflet flexible polyurethane valves (LifeTec Group, Eindhoven, The Netherlands), connected to the ventricular chambers, determined blood flow direction. Aortic, pulmonary, and mitral valve flow were measured by electromagnetic flow meters (MDL 1401, Skalar Medical, Delft, The Netherlands) positioned upstream of the related valves. Cardiac output was subsequently computed by integration of aortic flow. Left and right ventricular volume were computed from the recorded time series of the position of the two piston pumps, controlled by the heart model of Bovendeerd *et al.* (2006), in which ventricular pressure, assessed by P10EZ pressure sensors (Beckton Dickinson, Sint-Niklaas, Belgium), functioned as input parameter. The control algorithm was implemented in Matlab/Simulink real-time workshop (Matlab R2006a, Mathworks, Natick, Massachusetts, U.S.A.), running on a 64-bit Linux system featuring a low-latency kernel (Fedora 9 x86-64, kernel 2.6.18-2.0003.rt6). The interface with the mock loop is a multi-IO acquisition system having sufficient quadrature encoder readouts, analog inputs and outputs and digital I/O (PCI-6602 counter board, PCI-6040 multi I/O board, and PCI-6713 analog output, all by National Instruments, Austin, Texas, U.S.A.). The control loop is operated at an update rate of 1024 min^{-1} .

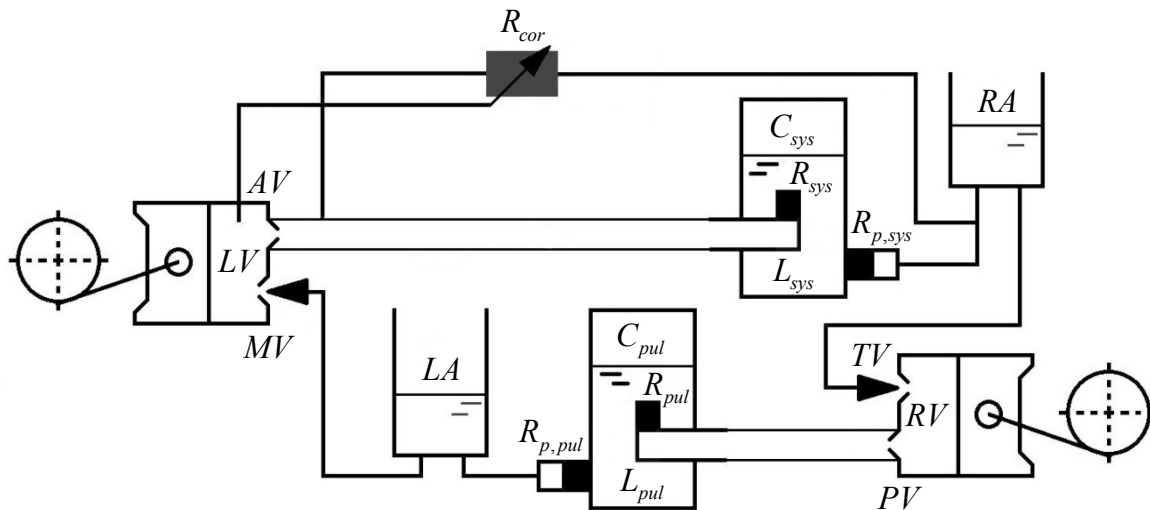


Figure 3.2: Schematic representation of the *in vitro* mock circulation model including a systemic, pulmonary, and coronary vascular bed. The left ventricle (LV) pumps water through the aortic valve (AV) into the aorta. Proximally, it features a coronary flow model, modeled by a left ventricular pressure dependent resistance (R_{cor}). The rest of the systemic impedance was modeled by the systemic windkessel components, representing systemic arterial resistance (R_{sys}), systemic arterial inertance (L_{sys}), systemic arterial compliance (C_{sys}), and peripheral resistance ($R_{p,sys}$). The systemic windkessel model is connected to a compliance chamber representing a passive right atrium (RA), which functions as preload for right ventricular filling (RV) through the tricuspid valve (TV). The pumping actions of the right ventricle generate a flow through the pulmonary valve (PV) into the pulmonary windkessel components, representing pulmonary arterial resistance (R_{pul}), pulmonary arterial inertance (L_{pul}), pulmonary arterial compliance (C_{pul}), and peripheral resistance ($R_{p,pul}$), and consequently into a compliance chamber representing the left atrium (LA). The generated preload is the driving factor for passive left ventricular filling through the mitral valve (MV).

Systemic, pulmonary, and coronary circulation

The aorta was modeled by a straight polyurethane tube (25 mm diameter, 0.1 mm wall thickness, and 450 mm length) (LifeTec Group, Eindhoven, The Netherlands). In order to resist high pressures, the wall thickness was chosen to be relatively high and consequently showed relatively low compliance properties. Aortic pressure was assessed by a P10EZ pressure sensor (Beckton Dickinson, Sint-Niklaas, Belgium), with a pressure range from -50 mmHg to 300 mmHg. Proximally, it featured a physiologically correct coronary flow model (Geven *et al.*, 2004), comprising a coronary epicardial artery, a compressible myocardium, and a venous outlet. The myocardium was modeled as a resistive circuit consisting of two parallel rigid tubes,

representing the subepicardial and subendocardial myocardium. The variable resistance and volume of the subendocardial myocardium were represented by a collapsible, silicone rubber tube through the left ventricle as a part of the subendocardial branch. The silicone rubber tube collapsed under higher levels of left ventricular pressure, thus changing both compliance and resistance of the myocardial vascular bed model. A single rigid tube connected the venous myocardial outlet to the compliance chamber, representing the right atrium, and had no additional resistance. An ultrasonic flow probe (T410, Transonic Europe, Maastricht, The Netherlands) registered the flow rate through the coronary artery branching off the aorta. Systemic and pulmonary impedances, characterizing the circulation behavior, were modeled by standard four-element windkessels, positioned distal from the aorta and pulmonary valve, respectively. The four-element windkessels featured manually operated needle valves for the systemic, pulmonary, and peripheral resistances. The capacitance is an air chamber with a maximum volume of 4 L. After leaving the afterload, the circulating liquid enters an open cylindrical container (height of 500 mm; cross-sectional area of 5542 and 6708 mm²), which functioned as left and right ventricular preload vessels, respectively.

3.2.3 Hemodynamic measurements

Before the start of each experiment, the water level in the mock loop was equalized and the pressure and flow sensors were set to zero. The entire circuit was primed to a pressure level of 7 mmHg. Initially, the systemic and pulmonary windkessel models were tuned such that both impedances, characterizing the circulation behavior, rendered physiologically representative pressure and flow signals. After appropriate input conditions for the coronary circulation were created, coronary resistances were fine-tuned considering coronary pressure and flow patterns and magnitudes. Data were recorded simultaneously with a sampling rate of 1024 s⁻¹ per acquisition channel.

After testing the performance of the controller, the ability of the model to simulate different clinical scenarios (both physiologic and pathologic) was evaluated. As pathologic scenario, we chose to model left ventricular dilated cardiomyopathy (DCM), as this is the most common indication for long-term mechanical circulatory support. We simulated this clinical scenario by changing left ventricular contractility, wall volume, and cavity volume at zero pressure with respect to physiologic baseline parameters. Furthermore, we adapted systemic arterial and peripheral resistance in agreement with compensation mechanisms present in the human body. For model validation, the signals acquired in the experimental model were compared qualitatively and quantitatively to pressure and flow registrations as reported in literature in order to prove the system's physiologic behavior (Table 3.1). However,

as heart failure presents itself in many different stages and forms, hemodynamic reference values for DCM patients are highly variable. In general, however, DCM is characterized by an increased left ventricular volume (both in systole and diastole) and a decreased left ventricular ejection fraction, which together result in a decreased cardiac output and a lowered perfusion pressure. Finally, the system's response to variation in preload, afterload, and heart rate was tested by adjusting the priming level of the flow circuit, the systemic peripheral resistance, and switching on the baroreflex function.

3.3 Results

3.3.1 Controller performance

The performance of the controller was determined by taking the root mean square of the relative error of the left ventricular pressure set-point and actual signal with the mock circulation operating at normal blood pressure and cardiac output (Figure 3.3). The controller was capable of keeping the pressure error below 15 mmHg, only when the heart valves open and close the error got as high as 30 mmHg. The relative root mean square error, calculated for 10 consecutive periods, for the bare system was 17 %.

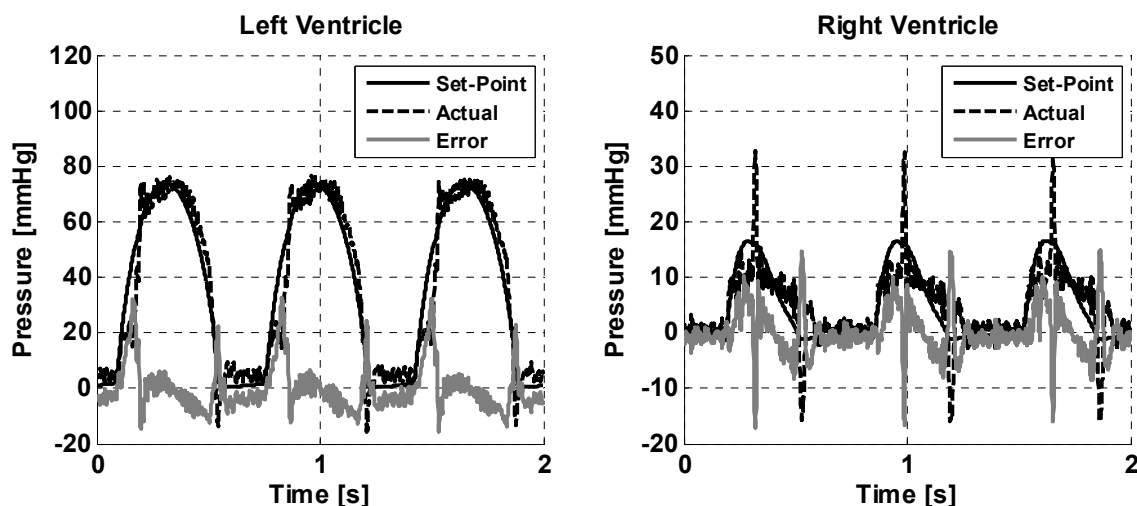


Figure 3.3: Actual (dotted) and required (solid) left (left) and right ventricular pressures (right) of the bare system. The error (grey) is defined as the difference between the actual and required pressure.

3.3.2 Clinical scenarios

Despite small reflection waves, nearly physiologic pressure and flow signals were measured when the model heart dimensions and contractility properties ($c = 1$) were set to normal values, and heart rate was kept constant at a frequency of 80 min^{-1} (Figure 3.4). Under these conditions, the heart generated a cardiac output of 6.5 L min^{-1} . Aortic pressure showed a peak systolic pressure of 124 mmHg, which gradually declined from the start of diastole (81 mmHg) towards the end of it (72 mmHg). Mean aortic pressure amounted 91 mmHg. Coronary flow (129 mL min^{-1}) showed a reduced systolic arterial flow component relative to diastolic flow, despite having a higher systolic driving pressure. Modeling transversal stresses in the left ventricular wall in diastole caused a moderate suction capacity at the start of left ventricular filling. All evaluated hemodynamic parameters were in agreement with physiologic values found in literature (Table 3.1).

Table 3.1: Comparison of physiologic (Guyton *et al.*, 2006; Fuster *et al.*, 2001) and pathologic reference (George *et al.*, 2013; Birks *et al.*, 2006; Sato *et al.*, 1993) and simulated values of hemodynamic parameters.

Parameter	Healthy		DCM	
	Reference	Simulation	Reference	Simulation
EF	58	66	10 - 34	34
SV	70	82	-	57
HR	75	80	59 - 93	80
CO	5.25	6.5	2.9 - 4.5	4.5
V_{ED}	120	124	175 - 269	166
V_{ES}	50	42	99 - 197	110
$p_{ao,sys}$	120	124	-	83
$p_{ao,dia}$	80	72	-	38
$p_{ao,mean}$	100	91	55 - 75	55

EF , ejection fraction [%]; SV , stroke volume [mL]; HR , heart rate [min^{-1}]; CO , cardiac output [L min^{-1}]; V_{ED} , end diastolic volume [mL]; V_{ES} , end systolic volume [mL]; $p_{ao,sys}$, systolic aortic pressure [mmHg]; $p_{ao,dia}$, diastolic aortic pressure [mmHg]; $p_{ao,mean}$, mean aortic pressure [mmHg].

By lowering left ventricular contractility ($c = 0.7$) and increasing left ventricular wall volume, left ventricular cavity volume at zero pressure, systemic arterial resistance, and systemic peripheral resistance, in agreement with the compensation mechanisms of the human body, a clinical scenario of (early-stage) DCM was simulated. In correspondence to patient data (George *et al.*, 2013; Birks *et al.*, 2006; Sato *et al.*, 1993), the less efficient pumping function (ejection fraction of only 34 %) of the enlarged heart resulted in a lowered cardiac output (4.5 L min^{-1}), and thereby a lowered perfusion pressure of the coronary circulation (55 mmHg on average) (Figure 3.4, Table 3.1). Nevertheless, hemodynamic reference values for end-stage DCM patients were even slightly worse compared to the model simulations.

3.3.3 Cardiac function control

The system's response to changes in preload and afterload, shown in figure 3.5, are in agreement with physiology (Iaizzo *et al.*, 2005). When preload was step-wise increased from 6 to 10 mmHg, left ventricular end diastolic volume increased from approximately 113 to 128 mL. The implemented relation between ventricular volume and tissue strain, caused the active fiber stress to increase, mimicking more forceful cardiac muscle contraction. Without changing the settings of the circulation system (windkessels), the increased active fiber stress resulted in a higher cardiac output, which in turn resulted in a secondary increase in mean arterial pressure (from 84 to 91 mmHg). Hence, the pressure-volume loops shifted from left to right with increasing preload.

When the afterload was increased from 61 to 86 mmHg on average, the modeled velocity of fiber shortening decreased, resulting in a decreased active fiber stress. Consequently, stroke volume reduced (from 102 to 83 mL) and more blood was left within the ventricle at the end of systole (left ventricular end systolic volume increased from approximately 16 to 36 mL). Hence, the isovolumetric relaxation part of the pressure-volume loops shifted from left to right with increasing afterload.

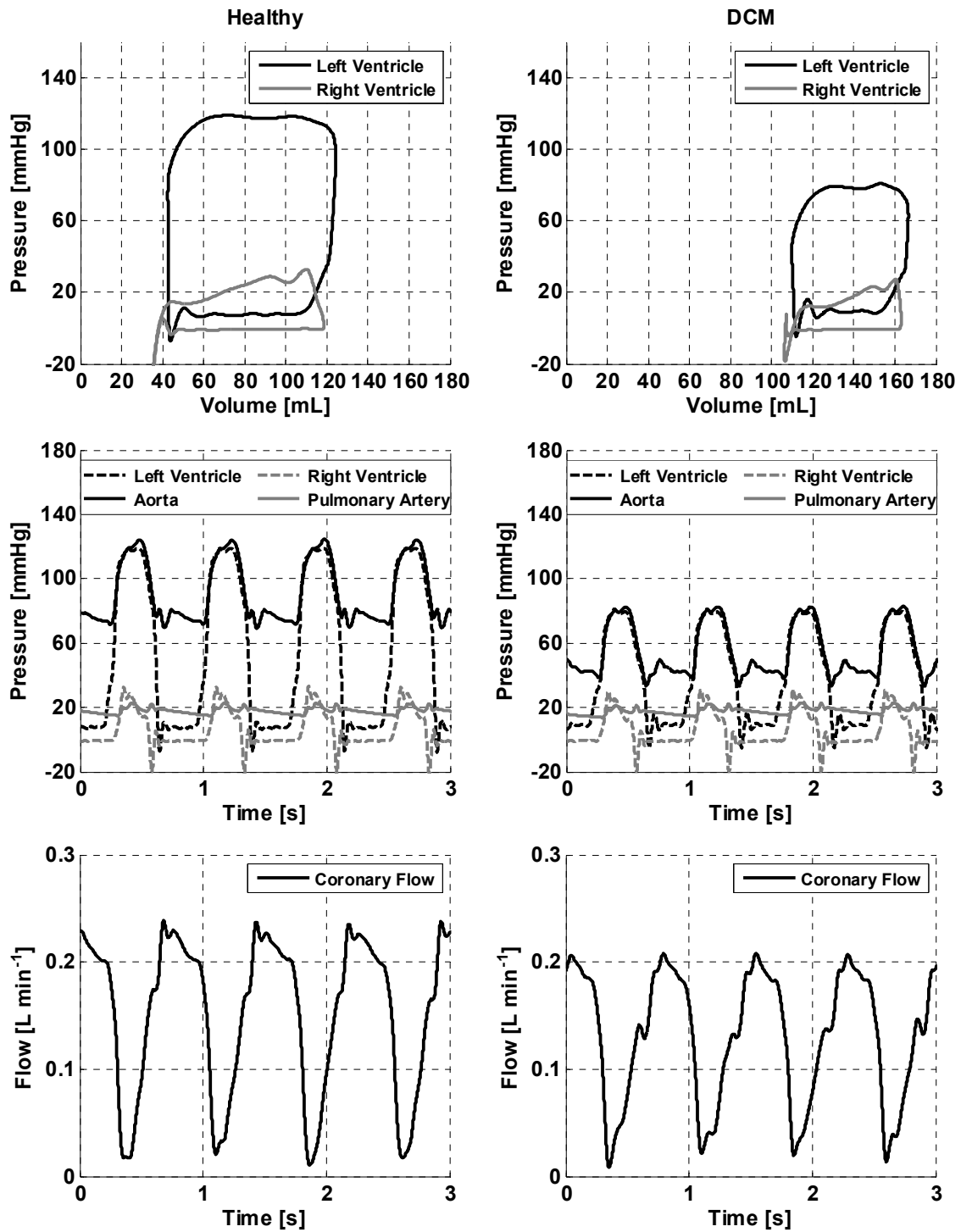


Figure 3.4: Measured pressure-volume loops (averaged over ten consecutive cycles) (top row), pressures (center row), and coronary flow (bottom row) for physiologic (left) and left ventricular DCM conditions (right).

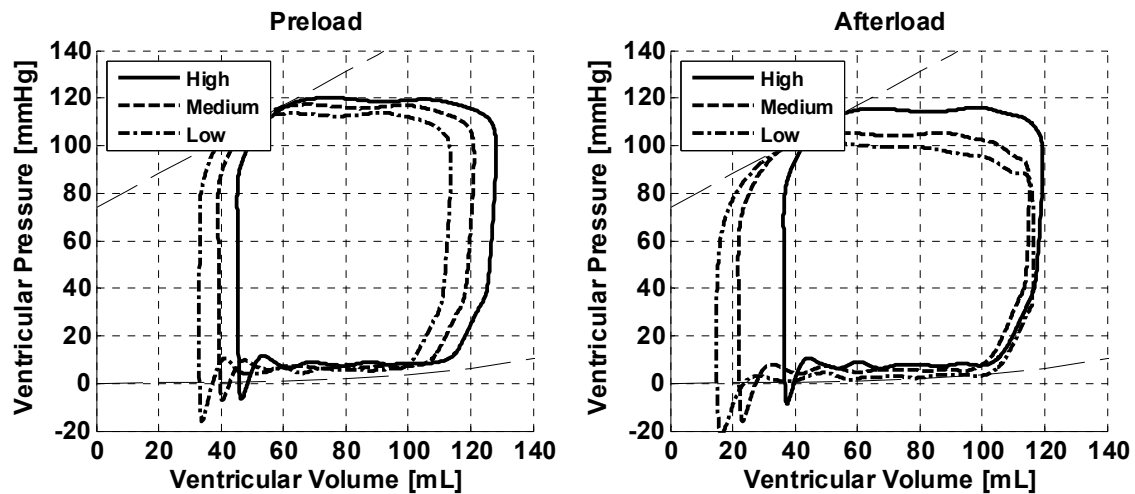


Figure 3.5: Left ventricular pressure-volume loops (averaged over ten consecutive cycles) for preload variation (left) and afterload variation (right). The loads increase from the solid loops towards the dash-dotted loops.

3.3.4 Frequency control

When the heart rate was reduced step-wise from 120 min^{-1} to 80 min^{-1} , the shape of the pressure-volume loop changed from a small filling volume (72 mL), low stroke volume (43 mL), and corresponding low systolic pressure (97 mmHg) to a larger filling volume (124 mL) and stroke volume (82 mL), with higher systolic pressure (119 mmHg) (Figure 3.6). This was caused by the increased ventricular filling time, which increased end diastolic volume and consequently ventricular contraction.

The frequency response of the baroreflex function (Figure 3.6) indicates a fully functional implementation of this incorporated feedback mechanism. When mean systemic pressure was step-wise decreased, the negative feedback loop reflexively causes heart rate to increase and stabilize. Likewise, an increase in aortic pressure activated the baroreflex, causing heart rate to decrease.

3.4 Discussion

The aim of this study was to develop an integrated mock circulation system that functions in a nearly physiologic manner, featuring an advanced ventricular contraction model with baroreflex control. The resulting model is a hydraulic circulatory system, with physiologically representative elements, regarding geometry and function, based on concepts from physiologic models from literature.

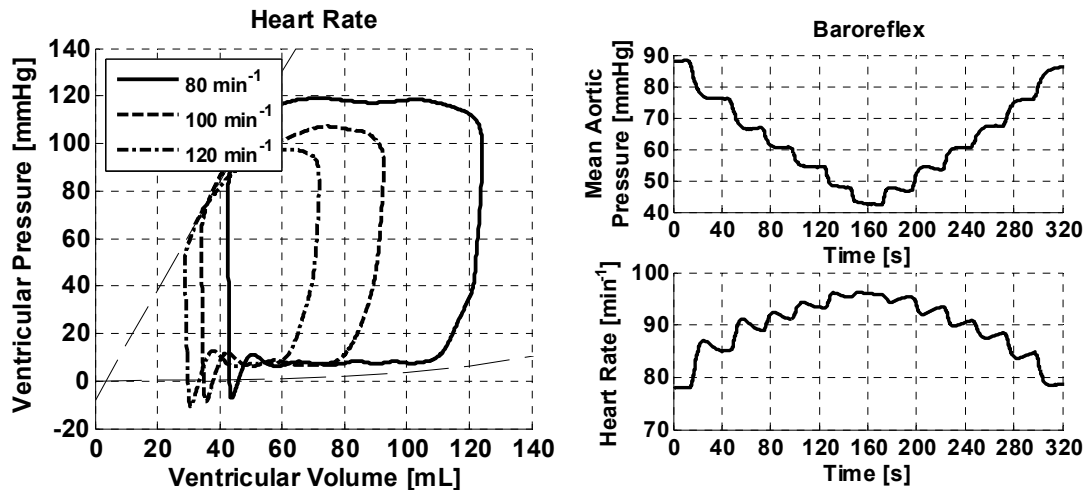


Figure 3.6: Left ventricular pressure-volume loops (averaged over ten consecutive cycles) for frequency variation (left). The frequency increases from the solid loop towards the dotted loop. Realization of the baroreflex function (right), which depends on mean aortic pressure.

3.4.1 Controller performance

The model, together with the controller, was shown to be stable. The average tracking error was 17 %. As the highest tracking errors occurred when the cardiac valves in the model opened or closed, inducing steep pressure rises or -drops, this was considered acceptable. A further contributor to the error was a relatively high frequency disturbance generated by the linear actuator. The frequency of this disturbance was outside the bandwidth of the controller and therefore not rejected. Colacino *et al.* (2007) have used a similar controller, in combination with a time-varying elastance heart model and realized a good tracking performance as well.

3.4.2 Physiologic relevance

With the aorta modeled as a straight tube having human aortic dimensions and compliance properties, and four-element windkessels (including needle valves) representing systemic and pulmonary impedances, the model-controlled mock circulation was capable of generating pressure and flow curves that closely mimicked systemic and pulmonary flow and pressure. In addition, the coronary flow model of Geven *et al.* (2004) proved to be still capable of producing physiologic representative coronary flow signals when interacting with an elaborate heart contraction model (Bovendeerd *et al.*, 2006).

The system's response to changes in preload, afterload, and heart rate indicates a solid implementation of the incorporated feedback mechanisms (frequency and cardiac function control). As active fiber stress is scaled in time according to the

calculated heart rate (Equation 2.8), the duration of left ventricular contraction is shorter for increasing heart rate, leading to a decreased ability of the heart to contract (reflected in the decreased slope of the end systolic pressure-volume relation). How this phenomenon affects the shape of the pressure-volume loops, however, depends very much on the filling of the ventricle. With a low preload (as shown in the results), the driving force to accelerate the liquid into the ventricle is low, so ventricular filling is slow. In combination with a high frequency, when the ventricular filling phase is short, this leads to partial filling of the ventricle, and therefore lower systemic pressure and cardiac output. Consequently, the ventricular filling rate decreases with frequency. At higher preloads, this phenomenon is less pronounced as ventricular filling is faster. Consequently, the ventricle is adequately filled at both low and high frequencies (data not shown).

3.4.3 Limitations

The mock circulation developed in this study functions in a nearly physiologic manner, but allows only for generic testing of cardiovascular devices. More refined phantoms (Biglino *et al.*, 2013) might be employed instead of the tube modeling the aorta, allowing more patient-specific *in vitro* modeling. Furthermore, by introducing animal samples in mock circulations, varying from sole valve samples (Erasmí *et al.*, 2005; Jimenez *et al.*, 2006) up to complete hearts (De Hart *et al.*, 2011; Richards *et al.*, 2009; Leopaldi *et al.*, 2012, Leopaldi *et al.*, 2013), the samples can be investigated in their truly morphologic and physiologic way, while allowing excellent control of the hemodynamic condition. Nevertheless, for initial phase testing of cardiovascular devices, mock circulation models are indispensable.

The autoregulation within the mock circulatory system as presented in this study was limited to heart function and frequency. The heart model featured the Frank-Starling mechanism and thereby included cardiac function control. Blood pressure autoregulation was driven by the baroreflex model of Van Roon *et al.* (2004) only. Peripheral resistance was assumed to be constant. Exercise or other vasorelaxing activities were not modeled. Furthermore, although the venous blood volume plays an important role in maintaining blood pressure, especially in congestive heart failure patients, the effect of it was not incorporated in the control model, since this parameter was easily changed manually and the response time was sufficiently long to do so.

In our model, the preload levels are just the hydrostatic pressures inside the preload compliances, and they generate the driving forces for ventricular filling. However, due to the absence of an active atrium, ventricular filling is reduced. The atrial contraction in early systole (atrial kick) accounts for approximately 20 % of the ventricular filling under normal circumstances (Balboa *et al.*, 2001). In our model, the

filling is completely passive, although transversal stresses in the left ventricular wall in diastole generate a moderate suction capacity during ventricular filling phase. Although blood or xanthan gum solutions are also feasible circulating fluids for the mock loop, in this study, water, which viscosity is roughly three times as low as blood's, was used as a medium instead. In the main vessels of the circulation, viscosity effects are of little importance compared to other hemodynamic forces. Only in the coronary circulation they may play a role. However, since Geven *et al.* (2004) showed that the deviation in characteristic impedance of the coronary circulation is acceptable, the influence of viscosity was neglected there as well.

3.4.4 Extended applications

The main objective of developing an integrated mock circulation system with physiologically representative elements for relevant components of the circulation was to create a tool for performance testing and validating novel cardiovascular devices (i.e., ventricular assist devices). With a left ventricular assist device (HeartAssist 5, Reliant Heart Inc., Houston, Texas, U.S.A.) connected between the left ventricular piston pump and the aorta, bypassing the aortic valve, the system was subjected to a major systemic pressure disturbance. Working (at different pump speeds, ranging from 7500 to 11500 min^{-1}) in parallel with the model heart, the assist device reduced left ventricular end diastolic and end systolic volume. Furthermore, isovolumetric phases were absent, showing oblique upward and downward lines (Figure 3.7).

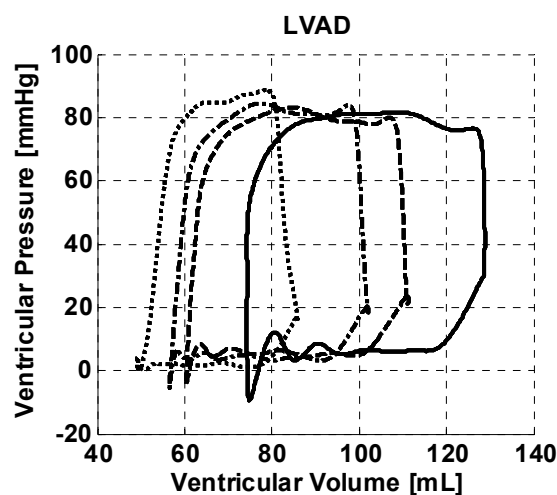


Figure 3.7: Left ventricular pressure-volume loops (averaged over ten consecutive cycles) without (solid curves) and with the left ventricular assist device (LVAD) attached and operating in different pump speeds, which increase from the dashed towards the dotted curves.

3.5 Conclusion

The presented mock circulation features a heart contraction model with baroreflex control, capable of mimicking the contractile properties of the heart under diseased and mechanical circulatory support conditions. Incorporated in a mock circulation loop, this model, together with a relatively simple lead-lag controller, proved to be capable of mimicking left ventricular function, and enables realistic evaluation of cardiovascular devices in phantom studies.

Chapter 4

***In vitro* comparison of support capabilities of intra-aortic balloon pump and Impella 2.5 LP**

The contents of this chapter are based on:

Schampaert S., Van 't Veer M., Van de Vosse F.N., Pijls N.H.J., De Mol B.A.J.M., Rutten M.C.M.; *In vitro* comparison of support capabilities of intra-aortic balloon pump and Impella 2.5 left percutaneous; *Artificial Organs*, 35(9): 983-901, 2011.

Abstract

The Impella 2.5 left percutaneous (LP), a relatively new transvalvular assist device, challenges the position of the intra-aortic balloon pump (IABP), which has a long record of supporting patients after myocardial infarction or cardiac surgery. However, while more costly and more demanding in management, the advantages of the Impella 2.5 LP are yet to be established. Different clinical scenarios, ranging from healthy to cardiogenic shock, were simulated in a model-controlled mock circulation, featuring a systemic, pulmonary, and coronary circulation, an elaborate heart contraction model, and a realistic heart rate control model. In this system, the enhancement of coronary flow and blood pressure was tested with both assist devices supporting the circulation in turn. Hemodynamic differences between the IABP and the Impella 2.5 LP are small. In our laboratory model, both systems approximately yielded a 10 % cardiac output increase and a 10 % coronary flow increase. However, as the Impella 2.5 LP provided significantly better left ventricular unloading, the circulatory support capabilities are slightly in favor of the Impella 2.5 LP. The support capabilities of both the IABP and the Impella 2.5 LP strongly depend on the simulated hemodynamic condition. Maximum hemodynamic benefits are achieved when mechanical circulatory support is applied in a simulated scenario of deep cardiogenic shock.

4.1 Introduction

The primary and principal idea behind mechanical circulatory support is to enhance the endangered circulation in cardiogenic shock or cardiogenic pre-shock states. Two assist devices available today, offering only minimally invasive mechanical circulatory support, are the intra-aortic balloon pump (IABP) (Maquet Getinge Group, Rastatt, Germany) and the Impella 2.5 left percutaneous (LP) (Abiomed Cardiovascular Inc., Danvers, Massachusetts, U.S.A.).

The IABP, first introduced in the clinical settings of cardiogenic shock in 1968 (Kantrowitz *et al.*, 1968), has a long record of supporting patients after myocardial infarction or cardiac surgery. The intra-aortic balloon pump is a catheter-mounted polyurethane balloon, which is usually inserted through a percutaneous femoral approach and positioned in the descending thoracic aorta, distal to the left subclavian artery and proximal to the renal artery branches. Aimed effects of counterpulsation are achieved by rapid inflation, upon onset of diastole, and deflation, in early systole, of the balloon and include a diastolic blood flow augmentation in the coronary and systemic circulation as well as a systolic reduction in resistance to left ventricular ejection (Scheidt *et al.*, 1973). Also a reduction in peak left ventricular wall stress and reduced myocardial oxygen consumption are expected when applied in the acute phase of myocardial infarction. These effects, aside from hemodynamic stabilization, might result in reduction of infarct size (Kern *et al.*, 1993; Sjauw *et al.*, 2007).

The Impella 2.5 LP is a novel catheter-mounted micro-axial rotary blood pump, designed for short-term mechanical circulatory support. The Impella 2.5 LP is inserted percutaneously through the femoral artery and positioned across the aortic valve into the left ventricle. The rotary pump is able to produce an output up to 2.5 L min^{-1} by continuously expelling aspirated blood from the left ventricle into the ascending aorta (Raess *et al.*, 2009). The Impella 2.5 LP is a minimally invasive assist device designed to directly unload the ventricle (Remmelink *et al.*, 2007), to reduce myocardial workload and oxygen consumption and to increase cardiac output, coronary flow and end-organ perfusion (Meyns *et al.*, 2003; Henriques *et al.*, 2006).

In current practice, IABP therapy is still the most accessible and most frequently used method of mechanical cardiac assistance in the catheterization laboratory, but the relatively new transvalvular assist devices challenge this position. However, while more costly and more demanding in management, the advantages of the Impella 2.5 LP are yet to be established. So far, the support capabilities of the IABP and other rotary blood pumps have been investigated but mainly in small observational studies and in animal experiments with conflicting results and variable magnitude of the results (Ntalianis *et al.*, 2008; Azevedo *et al.*, 2005; Haston *et al.*, 1979; Remmelink *et*

al., 2010). Although some studies confirmed the blood flow augmentation in the coronary and systemic circulation during IABP support (Kolyva *et al.*, 2010; Jung *et al.*, 2009), the Impella 2.5 LP was found to provide superior hemodynamic assistance (Seyfarth *et al.*, 2008). However, data on survival were ambiguous, and early survival did not improve (Stone *et al.*, 1997; Cheng *et al.*, 2009). External influences of a considerable number of parameters on pump performance and lack of well-defined indications for use might explain these conflicting results. Therefore, Pantalos *et al.* (2004) stated the need for a mock circulation that behaves in a physiologic manner for testing cardiac devices under well-controlled hemodynamic conditions. Several mock circulatory systems have been developed for the evaluation of mechanical assist devices, often neglecting the right ventricle and the pulmonary circulation (Vandenbergh *et al.*, 2004; Kolyva *et al.*, 2012). In 2002, Ferrari *et al.* (2002) developed a mock circulatory system including both left and right ventricle, and the systemic and pulmonary circulation. However, left ventricular control was based on the often used time-varying elastance concept of Suga *et al.* (1973), while VandenBerghe *et al.* (2006) showed that the time-varying elastance theory fails to accurately simulate left ventricular function during mechanical circulatory support. Also Timms *et al.* (2005) included both ventricles in their mock loop, but although their mock loop did respond to preload by increasing stroke volume, it was not based on a ventricular model.

The aim of this study is to evaluate the hemodynamic benefits of the 40 cc IABP and the Impella 2.5 LP in a physiologic *in vitro* model of the systemic, pulmonary and coronary circulation, and compare their circulatory support capabilities under identical circumstances in terms of cardiac output, coronary flow, cardiac stroke work, and arterial blood pressure.

4.2 Materials and methods

4.2.1 Model-controlled mock circulation

The servo-pump driven mock circulation, based on work of Vaes *et al.* (2007), is extensively described in **chapter 3** (Schampaert *et al.*, 2014). It consists of two servo-motor operated piston pumps acting as left and right ventricle, and a systemic, pulmonary, and coronary circulation (Geven *et al.*, 2004). For this study, the systemic circulation was divided into an upper and a lower part by extending the aorta by a proximal side branch, mimicking the brachycephalic arteries. The system was controlled by an elaborate heart contraction model (Bovendeerd *et al.*, 2006), a realistic frequency control model (Van Roon *et al.*, 2004), and a relatively simple lead-lag controller (Van de Molengraft *et al.*, 1994).

4.2.2 Simulations

Before the start of each experiment, the water level in the mock loop was equalized and the pressure and flow sensors were set to zero. The compliance chambers were primed to a predetermined level of 7 mmHg.

A near-physiologic representation of the circulation was simulated when the model heart dimensions and contractility properties were set to normal values, and the resistances of the windkessel models were adjusted such that systemic and pulmonary impedances, which characterize the circulation behavior, rendered for physiologic mean and pulse pressure patterns. Heart rate was kept constant at a frequency of 80 min^{-1} . Clinical scenarios of cardiogenic pre-shock and cardiogenic shock, sufficing the hemodynamic criteria of cardiogenic shock, were modeled by decreasing left ventricular contractility (c) to 0.7 and 0.4 respectively, while keeping the windkessel impedances constant.

The enhancement of coronary flow and blood pressure was tested with both the IABP and the Impella 2.5 LP operating at their generally in-hospital used settings, while again the impedances of the mock circulation remained unchanged. A 40 cc IABP was inserted through an artificial side branch off the aorta resembling a percutaneous approach and positioned distal to the branch mimicking the brachycephalic arteries and proximal to the remaining part of the systemic impedance. IABP support was applied with an assist rate of 1:1, for which the system was triggered by a mock loop generated electrocardiogram signal, indicating the start of the ventricular contraction. The balloon was inflated immediately after the end of ejection and deflation was completed just before aortic valve opening. Subsequently, the Impella 2.5 LP was also inserted through the artificial side branch, and positioned across the aortic valve. The rotary blood pump was operating at performance level P7, corresponding to a rotational pump speed of 47.000 min^{-1} .

4.3 Results

The model-controlled mock circulation was capable of generating flow patterns and pressure curves that closely mimicked aortic and coronary *in vivo* flow and pressure under both physiologic and pathologic conditions.

4.3.1 Healthy

Baseline

Despite small reflection waves, close to physiologic pressure and flow signals were measured when the model heart dimensions and contractility properties were set to normal (Table 4.1, Figure 4.1). The servo-motor operated piston pumps, acting as left

and right ventricle, generated a cardiac output of 4.5 L min^{-1} . Aortic pressure ranged from 71 to 118 mmHg with a mean of 88 mmHg. The area within the pressure-volume curve, which is a measure for the delivered cardiac stroke work, amounted $6.4 \cdot 10^3 \text{ mmHg mL}$. Coronary flow showed a reduced systolic arterial flow component relative to diastolic flow with a mean of 162 mL min^{-1} , in concordance with a normal blood flow pattern in the left coronary artery. Reproducibility of baseline hemodynamics was confirmed by a coefficient of variation of less than 5 % for all evaluated hemodynamic parameters.

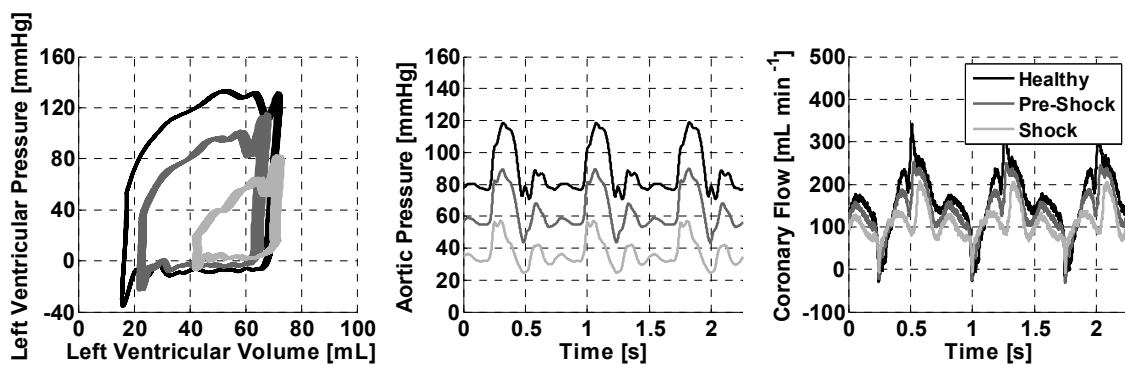


Figure 4.1: Data registrations of the model-controlled mock circulation experiments in healthy condition ($C = 1$), cardiogenic pre-shock ($C = 0.7$) and cardiogenic shock ($C = 0.4$). Pressure-volume loops (left), aortic pressure (center), coronary flow (right).

Mechanical circulatory support

Mechanical support with IABP or Impella 2.5 LP only produced minor benefits for the healthy circulation (Table 4.1, Figure 4.2).

Balloon inflation during IABP support induced a small diastolic blood pressure augmentation, resulting in a coronary flow increase of 5 %. A reduction in end diastolic aortic pressure was achieved by rapid deflation of the balloon. This resulted in a cardiac output increase of approximately 10 %, while cardiac stroke work remained at baseline level. Pulsatility, defined as the difference between maximum and minimum aortic pressure, was slightly enhanced with the IABP.

The Impella 2.5 LP provided little support to the healthy circulation by continuously expelling aspirated blood from the left ventricle into the ascending aorta. Consequently, pulsatility lowered and a decrease in left ventricular work was observed. Cardiac output and coronary flow increased both by roughly 5 % when mechanical support with the Impella 2.5 LP was applied on healthy hemodynamics.

Table 4.1: Important hemodynamic parameters measured in the model-controlled mock circulation experiments in healthy condition ($c = 1.0$), cardiogenic pre-shock ($c = 0.7$) and cardiogenic shock ($c = 0.4$) supported with IABP and Impella 2.5 LP.

Hemodynamic condition	Parameter	Baseline	IABP	Impella 2.5 LP
Healthy	CO	4.5	5.0	4.7
	Q_{cor}	162	171	168
	SW	$6.4 \cdot 10^3$	$7.2 \cdot 10^3$	$6.1 \cdot 10^3$
	$P_{ao,mean}$	88	99	93
	PI	48	54	45
Cardiogenic pre-shock	CO	3.6	3.9	4.0
	Q_{cor}	139	151	149
	SW	$3.6 \cdot 10^3$	$4.1 \cdot 10^3$	$3.3 \cdot 10^3$
	$P_{ao,mean}$	63	74	71
	PI	48	61	38
Cardiogenic shock	CO	2.4	2.9	3.0
	Q_{cor}	109	125	124
	SW	$1.3 \cdot 10^3$	$1.7 \cdot 10^3$	$1.2 \cdot 10^3$
	$P_{ao,mean}$	37	48	49
	PI	33	70	25

CO , cardiac output [$L \min^{-1}$]; Q_{cor} , coronary blood flow [$mL \min^{-1}$]; SW , cardiac stroke work [$mmHg \text{ mL}$]; $P_{ao,mean}$, mean aortic pressure [$mmHg$]; PI , pulsatility index [$mmHg$].

4.3.2 Cardiogenic pre-shock

Baseline

A clinical scenario of cardiogenic pre-shock, with a mildly depressed blood pressure of 63 mmHg on average (90/42 mmHg), was modeled in the mock circulation by lowering left ventricular contractility (c) to 0.7 (Table 4.1, Figure 4.1). Stroke volume decreased and, with the heart beating at a constant frequency of $80 \min^{-1}$, a lowered cardiac output of $3.6 L \min^{-1}$ was generated. Cardiac stroke work decreased to $3.6 \cdot 10^3 mmHg \text{ mL}$, but also coronary flow was reduced to $139 mL \min^{-1}$.

Mechanical circulatory support

More pronounced advantages were observed when mechanical circulatory support was applied to a simulated scenario of cardiogenic pre-shock compared to healthy condition (Table 4.1, Figure 4.2).

IABP support induced a diastolic blood pressure augmentation, which was an increased driving force for coronary perfusion, reflected by a coronary flow increase of roughly 10 %. The reduced end diastolic aortic pressure resulted in a 10 % cardiac output increase, but also went along with a small increase in cardiac stroke work.

The transvalvular assist device effectively unloaded the left ventricle, which was confirmed by a significant decrease in cardiac stroke work compared to baseline level. Continuously aspirating blood from the left ventricle into the aorta resulted in a pulsatility decrease, while a cardiac output and coronary flow increase of approximately 10 % was achieved.

4.3.3 Cardiogenic shock

Baseline

By decreasing left ventricular contractility (c) even further to 0.4, a clinical scenario of cardiogenic shock was simulated sufficing the hemodynamic criteria of cardiogenic shock (Table 4.1, Figure 4.1). Blood pressure ranged from 57 to 24 mmHg with a mean of 37 mmHg. For the generation of a cardiac output of 2.4 L min^{-1} , the heart had to deliver a cardiac stroke work of $1.3 \cdot 10^3 \text{ mmHg mL}$. Coronary flow was reduced to 109 mL min^{-1} .

Mechanical circulatory support

In a clinical scenario of cardiogenic shock, mechanical assistance was able to increase important hemodynamic parameters significantly (Table 4.1, Figure 4.2).

The IABP-induced diastolic blood pressure augmentation resulted in an increase in coronary perfusion of 15 %. An even more significant cardiac output increase of 0.5 L min^{-1} was generated by the supported heart, while cardiac stroke work remained at baseline level.

The Impella 2.5 LP effectively supported the circulation in cardiogenic shock, since important hemodynamic parameters, like cardiac output and coronary flow, increased more than 15 %, while the transvalvular assist device significantly lowered left ventricle work.

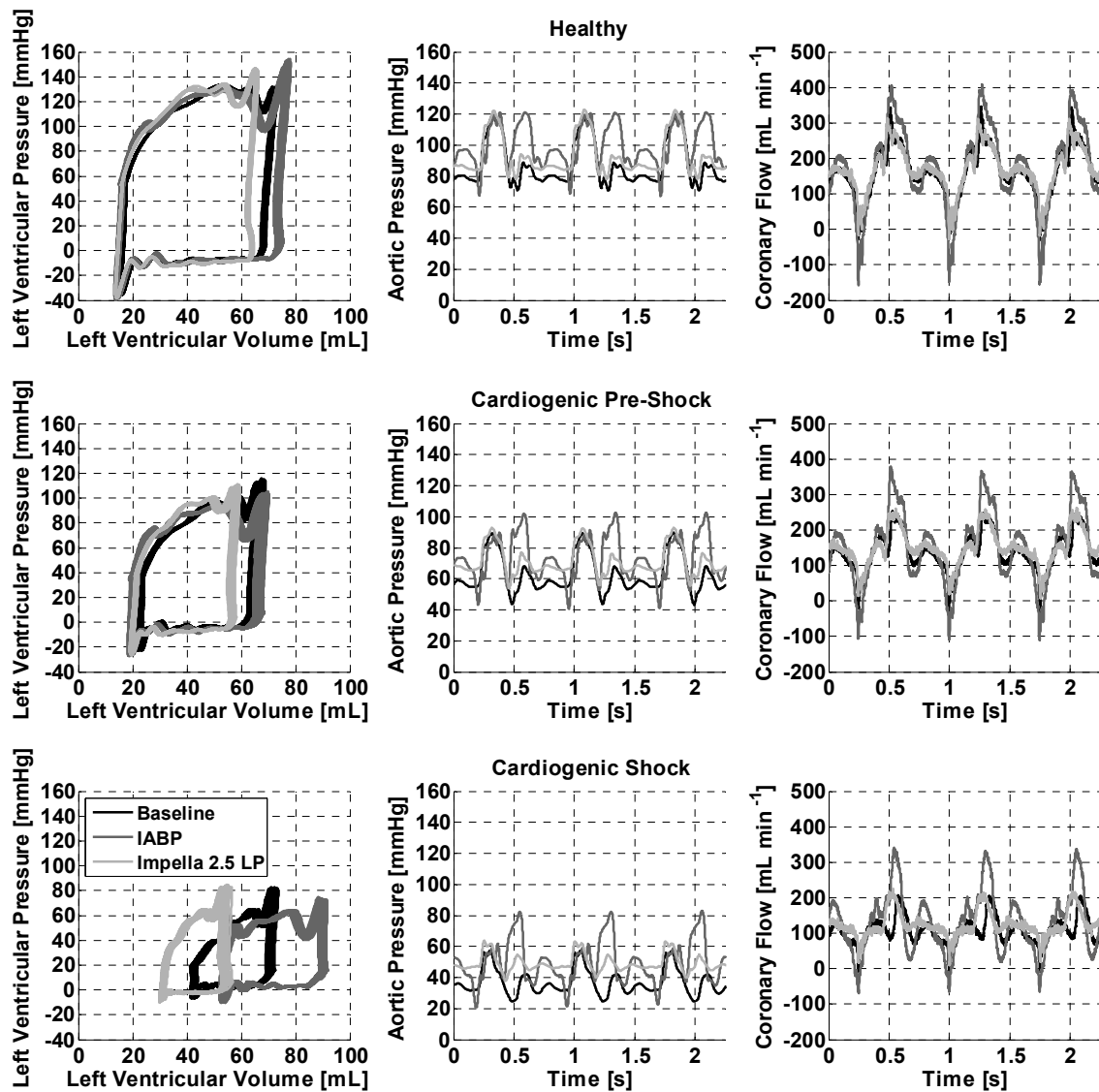


Figure 4.2: Data registrations of the model-controlled mock circulation experiments in healthy condition (upper row), cardiogenic pre-shock (center row) and cardiogenic shock (bottom row) supported with IABP and Impella 2.5 LP. Pressure-volume loops (left), aortic pressure (center), coronary flow (right).

4.4 Discussion

The aim of this study was to evaluate the benefits of the 40 cc IABP and the Impella 2.5 LP, and compare their circulatory support capabilities in terms of cardiac output, coronary flow, cardiac stroke work, and arterial blood pressure. Both devices were tested under identical circumstances in a model-controlled mock circulation featuring the systemic, pulmonary, and coronary circulation.

Henriques *et al.* (2006) reviewed the current status, capabilities, limitations, and future perspectives of the currently available percutaneous treatment options for mechanical cardiac assistance in acute myocardial infarction, and found immediate and superior circulatory support of the Impella 2.5 LP compared to the IABP. However, since this finding was based on the variable results of small observational studies and animal experiments (Ntalianis *et al.*, 2008; Azevedo *et al.*, 2005; Haston *et al.*, 1979; Remmelink *et al.*, 2010), Pantalos *et al.* (2004) stated the need for a mock circulation for testing cardiac devices. The major advantages of *in vitro* evaluation in a mock circulation, compared to experimental or randomized evaluation in human or animals are the costs, the simplicity with which mechanical support can be applied, and the ability of a model to create identical circumstances. In this study, the model-controlled mock circulation featured the systemic, pulmonary, and coronary circulation. The ventricular wall mechanics were based on the model of Bovendeerd *et al.* (2006), and the coronary flow model, thoroughly validated under baseline and hyperemic conditions by Geven *et al.* (2004), comprised a variable resistance, which was operated by the ventricular pressure. Vessels were modeled with flexible tubes and three windkessel models characterized the circulation behavior. The values of the windkessel elements were set to render physiologic systemic, pulmonary, and cerebral pressure waveforms and were left unchanged. Compliance chambers functioned as preload for passive ventricular filling. This rendered the pressure and flow signals of the *in vitro* experiments to be in agreement with physiologic data. Decreasing left ventricular contractility was an effective method to model a clinical scenario of cardiogenic pre-shock and cardiogenic shock, since it directly resulted in a blood pressure depression and a lowered cardiac output. Mechanical support was easily applied, and our laboratory model showed small hemodynamic differences between the IABP and the Impella 2.5 LP. The support capabilities were slightly in favor of the Impella 2.5 LP as it provided significantly better ventricular unloading. The unloading effect may result in reduced peak left ventricular wall stress and myocardial oxygen consumption. The combination of improved coronary perfusion and reduced workload of the left ventricle may accelerate myocardial recovery, restore left ventricular function and reduce final infarct size. Therefore, the Impella 2.5 LP might provide superior support for infarct patients.

A randomized patient study of Zehutgruber *et al.* (1997) showed a larger coronary flow increase in patients with a compromised hemodynamic state and a significantly attenuated increase in patients with normal baseline hemodynamics. In addition, Van 't Hof *et al.* (1999) stated that the use of intra-aortic balloon pumping should be reserved for patients with severe hemodynamic compromise. The model-controlled mock loop experiments performed in this study also showed that the effect of the

IABP and the Impella 2.5 LP strongly depended on the simulated hemodynamic condition. In a clinical scenario of cardiogenic shock, important hemodynamic parameters, like cardiac output, coronary flow, and arterial blood pressure, increased up to more than 15 %, while less pronounced advantages were observed when mechanical support was applied on normal baseline hemodynamics. Both the IABP and the Impella 2.5 LP were capable to support the endangered circulation, but their support capabilities were insufficient to replace the complete pump function of the native heart.

The autoregulation of the model-controlled mock circulation was limited. The heart model featured the Frank-Starling mechanism and thereby included cardiac function control, but mechanisms to regulate blood pressure were lacking. In humans, local metabolic vascular control appears to be the dominant factor in coronary autoregulation. Since this phenomenon was not included in the *in vitro* model, attention is needed for the interpretation of the coronary flow increase resulting from mechanical support. Furthermore, heart rate was kept constant at a relatively low heart rate of 80 min^{-1} , while an increase in heart rate is expected in a clinical scenario of cardiogenic pre-shock or cardiogenic shock. An increase in heart rate may influence the performance of the IABP, because of the inadequate time required for complete inflation and deflation of the balloon. Therefore, by further increasing patients' heart rate, the Impella 2.5 LP is expected to produce more hemodynamic benefits compared to the IABP. The performance of the IABP might also be influenced by the posture of the patient (Khir *et al.*, 2005), while gravity forces play a less important part during support with the Impella 2.5 LP. Lowering the characteristic resistance allowed compensation for the relatively low compliance properties of the flexible tube mimicking the aorta by the arterial compliance chamber, but also caused a relatively rapid decrease in aortic pressure. Furthermore, the aorta was modeled by a cylindrical tube with a constant diameter of 25 mm and was surrounded by water. In physiology the aorta tapers and is surrounded by tissue and other organs. All these factors may interfere with the ability of the aortic wall to expand and consequently may influence the performance of the IABP (Papaioannou *et al.*, 2002). Water was used as a medium instead of blood in the model-controlled mock circulation. Despite that the viscosity of blood is roughly three times as high for blood as for water, no huge influence of this phenomenon on the support capabilities of both the IABP and the Impella 2.5 LP is expected.

4.5 Conclusion

Hemodynamic differences between the IABP and the Impella 2.5 LP are small. In our laboratory model, both systems approximately yield a 10 % cardiac output increase and a 10 % coronary flow increase. However, since the Impella 2.5 LP provides significantly better left ventricular unloading, the hemodynamic differences are slightly in favor of the Impella 2.5 LP. In contrast, pulsatility is enhanced with the IABP and lowered with the Impella 2.5 LP supporting the heart.

The benefits of mechanical support strongly depend on the simulated hemodynamic condition. In our laboratory model, important hemodynamic parameters increased up to more than 15 % in case of a clinical scenario of deep cardiogenic shock, while less pronounced advantages were observed in case of a mild blood pressure depression and a slightly lowered cardiac output.

The model-controlled mock circulation is a useful tool for the evaluation of different mechanical assist devices, since the hemodynamic conditions can be controlled accurately and consequently good comparison opportunities are created.

Chapter 5

Autoregulation of coronary blood flow in the isolated beating pig heart

The contents of this chapter are based on:

Schampaert S., Van 't Veer M., Rutten M.C.M., Van Tuijl S., De Hart J., Van de Vosse F.N., Pijls N.H.J.; Autoregulation of coronary blood flow in the isolated beating pig heart; *Artificial Organs*, 37(8): 724-730, 2013.

Abstract

The isolated beating pig heart model is an accessible platform to investigate the coronary circulation in its truly morphologic and physiologic state, while its use is beneficial from a time, cost, and ethical perspective. However, whether the coronary autoregulation is still intact is not known. Here, we study the autoregulation of coronary blood flow in the working isolated pig heart in response to brief occlusions of the coronary artery, to step-wise changes in left ventricular loading conditions and contractile states, and to pharmacologic vasodilating stimuli. Six slaughterhouse pig hearts (473 ± 40 g) were isolated, prepared, and connected to an external circulatory system. Through coronary reperfusion and controlled cardiac loading, physiologic cardiac performance was achieved. After release of a coronary occlusion, coronary blood flow rose rapidly to an equal (maximum) level as the flow during control beats, independent of the duration of occlusion. Moreover, a linear relation was found between coronary blood flow and coronary driving pressure for a wide variation of preload, afterload, and contractility. In addition, intracoronary administration of papaverine did not yield a transient increase in blood flow indicating the presence of maximum coronary hyperemia. Together, this indicates that the coronary circulation in the isolated beating pig heart is in a permanent state of maximum hyperemia. This makes the model excellently suitable for testing and validating cardiovascular devices (i.e., heart valves, stent grafts, ventricular assist devices) under well-controlled circumstances, whereas it decreases the necessity of scarifying large mammals for performing classical animal experiments.

5.1 Introduction

In performing coronary physiology research, the need for appropriate models becomes stronger for efficacy and ethical reasons. Mock circulatory systems of the coronary circulation (Segers *et al.*, 1999; Matthys *et al.*, 2001; Geven *et al.*, 2004) are able to create well-controlled hemodynamic conditions, but lack specific anatomical structures and features. On the other hand, the large number of interacting physiologic parameters involved in experimental animal studies often leads to results which show considerable variability and are difficult to interpret. Furthermore, experimental research in large mammals raises increasing ethical objections. As an intermediate between *in vitro* and *in vivo* testing, experiments carried out using the model of the isolated beating pig heart (De Hart *et al.*, 2011; De Weger *et al.*, 2010) (LifeTec Group, Eindhoven, The Netherlands) forms an accessible platform to investigate the coronary circulation in its truly morphologic and close to physiologic state, while allowing excellent control of the individual hemodynamic parameters. Moreover, the isolated pig hearts are not categorized as animal experiments as these organs are slaughterhouse by-products. This so-called *ex vivo* testing is therefore less demanding in management and reduces ethical objections (Modersohn *et al.*, 2011), because sacrificing large animals for experimental research is avoided.

For that purpose, however, knowledge about the state of physiologic regulatory processes like in intact animals is mandatory. Although the isolated pig heart has proven to be capable of generating flow patterns and pressure curves that closely mimic *in vivo* flow and pressure (De Hart *et al.*, 2011), it is not known whether physiologic feedback mechanisms regulating coronary blood flow are still intact. In the *in vivo* coronary circulation, blood flow through the coronary system is regulated almost entirely by vasodilator substances released from the endothelium and myocytes in response to cardiac muscle's need for nutrition, causing local arterial and arteriolar vasodilatation. Consequently, a close to linear relation between metabolic demand and myocardial blood flow is maintained (Abe *et al.*, 1984). Although this mechanism works equally well in the intact as in the denervated heart (Guyton *et al.*, 2006), the presence of coronary autoregulation in isolated hearts varies among different species (Pohl *et al.*, 1994; Bünger *et al.*, 1975; Weisfeldt *et al.*, 1970), and has never been investigated for the isolated beating pig heart. In clinical practice, most important intracoronary techniques (like measurement of coronary or fractional flow reserve) to assess severity of atherosclerosis in the coronary arteries and for making decisions on stenting or bypass surgery require the presence of maximum hyperemia, which is usually obtained by pharmacologic agents, administered either intravenously or directly intracoronary (Tonino *et al.*, 2009; Botman *et al.*, 2007). Therefore, when using the isolated beating pig heart model for

further experiments on coronary blood flow and intracoronary diagnostic or interventional techniques, it is important to be informed the on presence or absence of autoregulation mechanisms and the presence or absence of a maximum hyperemic state.

Therefore, the purpose of this study was to study the coronary autoregulation of the isolated beating pig heart in response to brief occlusions of the coronary artery (Olivecrona, 2007), to step-wise changes in loading conditions and contractile states (Hoffman *et al.*, 1990), and to pharmacologic vasodilating stimuli.

5.2 Materials and methods

The hearts used in this study ($n = 6$) were obtained from Dutch landrace hybrid pigs that were slaughtered for human consumption. The protocols of the slaughterhouse and laboratory were developed in accordance with EC regulations 1069/2009 regarding the use of slaughterhouse animal material for diagnosis and research, supervised by the Dutch Government (Dutch Ministry of Agriculture, Nature, and Food Quality) and approved by the associated legal authorities of animal welfare (Food and Consumer Product Safety Authority).

5.2.1 Isolation

Following regular slaughter protocols, the pigs were first electrocuted, causing immediate unconsciousness and brain death. Electrocution was followed by exsanguination by cutting the jugular vein, carotid artery, and trachea. Immediately after death occurred, the thorax of the pigs was opened by a parasternal incision to isolate the heart (heart weight 473 ± 40 g). The pulmonary artery was cut just before the bifurcation, while the aorta was cut at the level of the first supra-aortic vessels. The isolated heart was immediately cooled and cannulated for administration of 1 L of cold cardioplegic solution (4 °C Modified St. Thomas 2 added with 5000 IU of Heparin) to the coronary arteries, such that warm ischemic time never exceeded 5 minutes. In addition, 5 L of fresh blood (heparinized with 5000 IU/L) was collected from subsequently slaughtered pigs.

5.2.2 Preparation

Preparations of the heart were carried out in the laboratory under cold and cardioplegic conditions by hourly administration of 1 L of modified St. Thomas 2 solution until resuscitation of the heart. After discarding the pericardial sack, a 24 mm cannula was inserted into the aorta and fixed at a distance of approximately 40 mm distal to the valve annulus, making sure not to impair aortic valve function. The

pulmonary veins were removed to the level of the left atrium and were ligated. A 27 mm cannula was inserted into the left atrium and secured with a purse string suture allowing sufficient atrial filling after resuscitation. Similarly, a 19 mm cannula was inserted into the pulmonary artery, whereas the inferior and superior vena cava were ligated to close the right atrium. The coronary ostia were left intact in order to enable natural perfusion of the myocardium.

5.2.3 Instrumentation

After preparation, the isolated pig heart was fixed in supine position and mounted in an external circulation platform (LifeTec Group, Eindhoven, The Netherlands) (De Hart *et al.*, 2011). In the circulation loop, a centrifugal pump (Sarns 9000 Perfusion System, 3M, Saint Paul, Minnesota, U.S.A.) pumped blood from a venous reservoir, through an arterial blood filter (AFFINITY Arterial 38 μm blood filter, Medtronic, Minneapolis, Minnesota, U.S.A.) and a combined oxygenator-heat exchanger (AFFINITY NT Oxygenator, Medtronic, Minneapolis, Minnesota, U.S.A.) into a preload model. The preload model controlled the left atrial filling pressure by means of a Starling resistance overflow from the preload model back into the venous reservoir. The afterload module consists of a compliant polyurethane tube having human aortic dimensions and compliance characteristics. The remaining systemic impedance was modeled by a standard four-element windkessel model, positioned distal to the aorta. The four-element windkessel model featured manually operated needle valves for the systemic resistances and an air chamber as capacitance. From this afterload module, the blood was returned to the venous reservoir. The venous coronary blood, which exits at the coronary sinus, was returned from the right atrium to the right ventricle, which ejected it through the pulmonary valve back into the venous reservoir.

Total coronary flow was measured with an ultrasound flow probe (LifeTec Group, Eindhoven, The Netherlands) around the pulmonary artery line, as the right ventricle was only subjected to a volume loading, resulting from ventricular filling with coronary venous blood. An ultrasonic flow probe (Transonic Europe, Maastricht, The Netherlands) and an occluder were placed around the left circumflex (LCx) artery. The aortic, left atrial, and right atrial pressures were monitored with P10EZ pressure sensors (Beckton Dickinson, Sint-Niklaas, Belgium). The atrial pressure sensors were mounted to the atrial cannulas at a distance of 10 mm from the atria. Aortic pressure and pulsatile aortic flow (MA28PAX, Transonic Systems Inc., Ithaca, New York, U.S.A.) were measured 50 and 100 mm distal from the aortic valve annulus, respectively. Left ventricular pressure was assessed with a P10EZ pressure sensor (Beckton Dickinson, Sint-Niklaas, Belgium) into the ventricle trans-apically via a cannula. Data were recorded at a sampling rate of 1000 min^{-1} , using a data acquisition board (PCI

6221, National Instruments) and dedicated software (LabVIEW 7.1, National Instruments, Austin, Texas, U.S.A.).

In summary, in this beating heart model, afterload, preload, and contractility can be varied independently as well as heart rate and myocardial oxygen supply. All these parameters can be measured continuously and in addition total coronary blood flow, cardiac output, and myocardial oxygen consumption are monitored continuously.

5.2.4 Resuscitation

Blood, 38 °C and oxygenated with a 20 % O₂, 5 % CO₂, 75 % N₂ gas mixture, was supplied from the perfusion loop retrograde into the aortic-cannula, with the aortic and left atrial lines cross clamped. After reinstating coronary perfusion, the heart showed spontaneous contractions and gradually regained sinus rhythm. In some cases, defibrillation with 10 - 30 J was required to restore the hearts' rhythm.

After successful resuscitation and stabilization, the preload-container to the left atrium was gradually opened and the aortic cross clamp removed to load the heart. The heart started to eject in a 2-chamber working heart mode, in which the left heart was subjected to a physiologic preload and afterload, while the right ventricle was only subjected to volume loading, resulting from ventricular filling with coronary venous blood. Subsequently, the systemic windkessel model was tuned such that its impedance, characterizing the circulation, created physiologically representative pressure and flow signals. Thus, appropriate input conditions for the coronary circulation were created.

5.2.5 Hemodynamic interventions

To investigate the presence of reactive hyperemia, the manifestation of local blood flow regulation in the heart (Figure 5.1), LCx coronary artery blood flow was studied before, during, and after a 5, 10, 20, and 30 seconds occlusion separated from each other by three minutes of reperfusion (Reimer *et al.*, 1986). By subsequently changing the impedances of the systemic and pulmonary windkessel models, and administration of positive (10 mg dobutamine) and negative inotropic agents (1 mg propranolol or 2.5 mg metoprolol), the isolated beating pig heart was subjected to a wide variation of preload, afterload, and contractility. Finally, in three hearts intracoronary administration of a 15 mg bolus of papaverine was performed, a vasodilator which induced hyperemic response has thoroughly been described *in vivo* and is independent of an intact endothelium (De Bruyne *et al.*, 2003; McGeoch *et al.*, 2008; McGinn *et al.*, 1990). Hemodynamic parameters were continuously monitored and after performing the hemodynamic interventions, the heart was arrested with a potassium chloride injection into the aortic cannula after cross clamping the aorta.

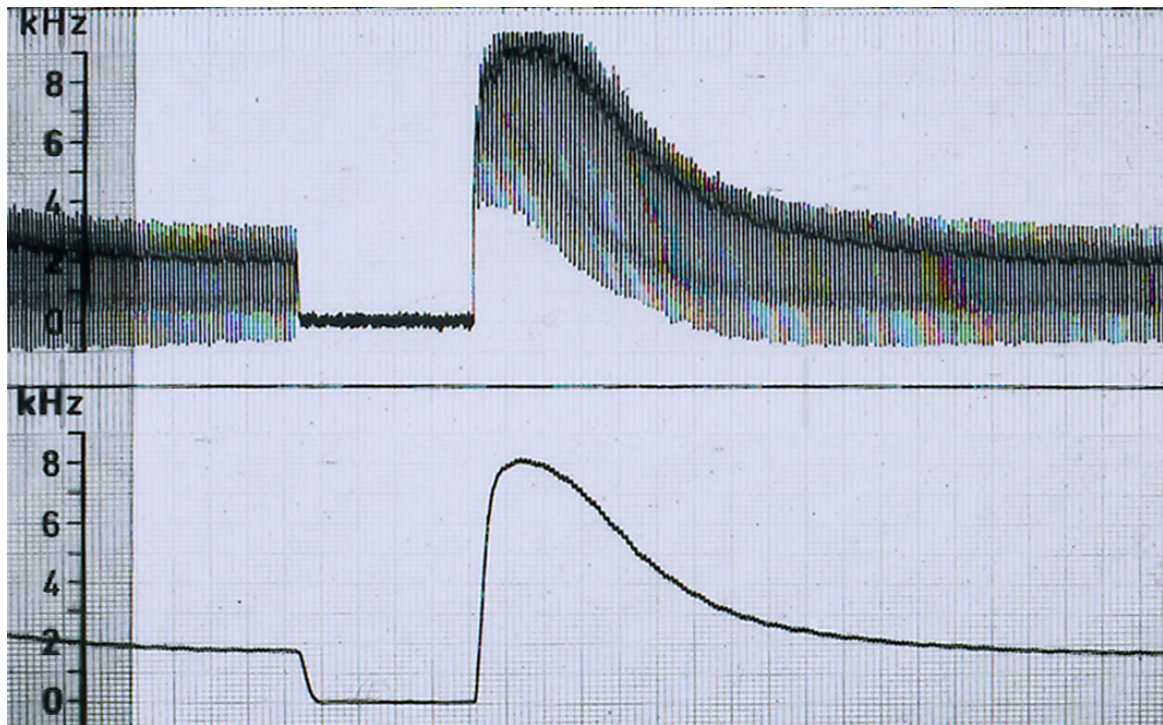


Figure 5.1: Pulsatile (upper) and mean (lower) coronary artery flow associated with a 20-second occlusion in the *in vivo* dog heart. Reactive hyperemia was clearly visible after release of the occlusion (courtesy of N.H.J. Pijls).

5.3 Results

The isolated beating pig heart was capable of generating flow patterns and pressure curves that closely mimic aortic and coronary *in vivo* flow and pressure (Table 5.1). LCx coronary artery blood flow was studied before, during and after a 5, 10, 20, and 30 seconds occlusion. Representative time series are shown in figure 5.2. During control beats, blood flow through the LCx artery amounted $278 \pm 72 \text{ mL min}^{-1}$, which was in all hearts approximately one-third of total coronary flow, as measured by an ultrasound flow probe around the pulmonary artery, as the right ventricle was only subjected to a volume loading, resulting from ventricular filling with coronary venous blood. In analogy to intact animals and humans, it showed a reduced systolic arterial flow component, despite having a systolic driving pressure. Inflation of the occluder, placed around the LCx artery, immediately blocked myocardial blood supply and consequently induced a brief period of ischemia. After release of the occlusion, coronary blood flow rose rapidly to an equal level as the flow during control beats (peak to basal ratio of approximately one), independent of the duration of occlusion, thereby showing absence of reactive hyperemia, and suggesting presence of maximum hyperemia.

Table 5.1: Baseline hemodynamic parameters recorded during steady state periodic working left heart mode.

Heart	Baseline					
	HR	$P_{ao,sys}$	$P_{ao,dia}$	$P_{ao,mean}$	CO	Q_{cor}
1	71 ± 5.3	110 ± 2.3	70 ± 0.1	83 ± 0.2	3.0 ± 0.1	1.0 ± 0.01
2	109 ± 11	121 ± 0.4	80 ± 0.3	99 ± 0.3	8.2 ± 0.1	1.4 ± 0.02
3	121 ± 1.0	93 ± 2.2	79 ± 1.7	86 ± 2.1	2.0 ± 0.1	0.7 ± 0.03
4	78 ± 9.8	109 ± 0.3	79 ± 1.9	91 ± 1.6	3.8 ± 0.0	1.1 ± 0.02
5	101 ± 9.6	106 ± 3.7	68 ± 1.5	85 ± 2.1	3.1 ± 0.1	0.7 ± 0.07
6	123 ± 4.1	103 ± 6.4	72 ± 7.6	84 ± 6.7	3.2 ± 0.5	0.7 ± 0.05

HR , heart rate [min^{-1}]; $P_{ao,sys}$, systolic aortic pressure [mmHg]; $P_{ao,dia}$, diastolic aortic pressure [mmHg]; $P_{ao,mean}$, mean aortic pressure [mmHg]; CO , cardiac output [L min^{-1}]; Q_{cor} , coronary flow [L min^{-1}].

By changing the impedances of the systemic and pulmonary windkessel models, and administration of positive (10 mg dobutamine) and negative inotropic agents (1 mg propranolol or 2.5 mg metoprolol), the isolated beating pig heart was subjected to a wide variation of preload, afterload, and contractility (Table 5.2). We calculated coronary pressure as the difference between mean aortic pressure and right atrial pressure, and compared it to total coronary blood flow (Hoffman *et al.*, 1990). In the physiologic pressure range, a linear relationship ($R^2 = 0.94 \pm 0.03$, $p < 0.001$) was found in all hearts with a positive non-zero intercept (Figure 5.3, Table 5.3), which existence was already confirmed in other organisms (Bellamy, 1978; Spaan *et al.*, 2006). Zero flow pressure intercepts were estimated by extrapolation and found to vary between 10 and 32 mmHg. Coronary resistance, calculated as the ratio of the difference between perfusion pressure and zero flow pressure to actual flow rate (Bellamy, 1978), was constant but varied among the different hearts between 44 and 83 mmHg min L^{-1} . The linear relation between perfusion pressure and blood flow also indicates absence of autoregulation and presence of a permanent maximum hyperemic state.

Table 5.2: The range in which preload, afterload, and contractility were primarily varied.

Heart	Variation range		
	$p_{la,mean}$	$p_{ao,mean}$	dp/dt_{max}
1	10 - 30	48 - 100	1380 - 2490
2	11 - 25	61 - 102	1500 - 2940
3	16 - 32	58 - 85	1380 - 1530
4	13 - 33	59 - 95	870 - 3360
5	16 - 36	68 - 94	960 - 2340
6	-	61 - 91	-

$p_{la,mean}$, mean left atrial pressure [mmHg]; $p_{ao,mean}$, mean aortic pressure [mmHg]; dp/dt_{max} , maximum rate of left ventricular pressure change [mmHg s⁻¹].

Finally, to ensure that this constant state of coronary resistance is a maximum hyperemic state, in three hearts intracoronary administration of a 15 mg bolus of papaverine was performed. We compared blood flow in the LCx artery before and after its administration. In all hearts, papaverine did not yield a transient increase in LCx arterial blood flow anymore. Blood flow after stabilization expressed as a percent of coronary blood flow at rest before administration was $98 \pm 7\%$.

Table 5.3: Regression and correlation analysis between coronary driving pressure and coronary blood flow.

Heart	Weight	n	Regression		Correlation	
			p_{zf}	R_{cor}	R ²	p-value
1	475	34	14	53	0.96	< 0.001
2	530	34	16	53	0.98	< 0.001
3	476	24	11	83	0.94	< 0.001
4	405	26	10	56	0.91	< 0.001
5	485	25	32	67	0.95	< 0.001
6	469	16	21	44	0.91	< 0.001

Weight, heart weight [g]; n, number of data points [-]; p_{zf} , zero flow pressure [mmHg]; R_{cor} , coronary resistance calculated as the ratio of the difference between perfusion pressure and zero flow pressure to the flow rate [mmHg min L⁻¹], R², coefficient of determination [-]; p-value, probability [-].

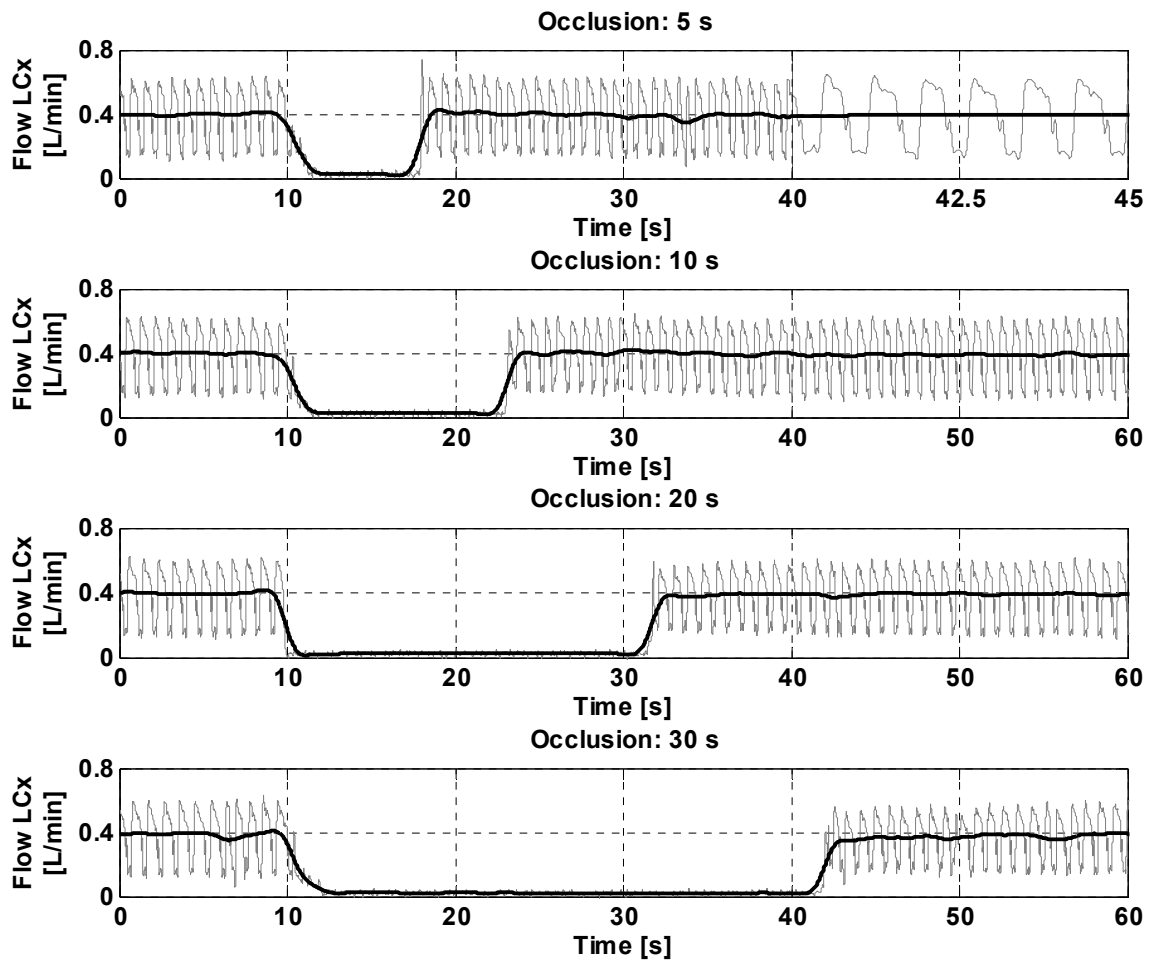


Figure 5.2: Left circumflex coronary artery flow associated with a 5, 10, 20, and 30 seconds occlusion. The grey trace is pulsatile flow, the black trace is mean flow (window = 1 s). At onset of a sudden occlusion of the LCx artery ($t \approx 10$ s), coronary blood flow was immediately blocked ($\approx 0 \text{ mL min}^{-1}$). After release of the occlusion ($t \approx 15$ s, $t \approx 20$ s, $t \approx 30$ s, $t \approx 40$ s, respectively), coronary blood flow rose rapidly to an equal (maximum) level as the flow during control beats. This phenomenon was found to be independent of the duration of occlusion. Note the physiologic flow pattern in the LCx artery.

5.4 Discussion

In this study, we studied the coronary autoregulation of the isolated beating pig heart in response to brief occlusions of the coronary artery (Olivecrona, 2007), to step-wise changes in loading conditions and contractile states (Hoffman *et al.*, 1990), and to pharmacologic vasodilating stimuli. The absence of reactive hyperemia, the linear relation between coronary blood flow and coronary driving pressure, and the fact that intracoronary administration of papaverine did not yield a transient

increase in blood flow, strongly indicate that the coronary circulation in the isolated beating pig heart is in a permanent state of maximum hyperemia.

The constant (minimal) resistance of the coronary vascular bed might be a result of the non-physiologic shear stresses applied to the coronary endothelial cells during isolation, transportation, and preparation of the heart, thereby triggering the endothelium cells lining the arterioles and small arteries to synthesize nitric oxide (Kelm *et al.*, 1990; Kostic *et al.*, 1992) or other substances that regulate the vasomotor tone of arterioles (Furchgott *et al.*, 1980). In addition, the coronary vascular injury by cardioplegia and reperfusion (Hearse *et al.*, 1993) may explain the fall of coronary resistance, in analogy to the situation during cardiac surgery (Hiratzka *et al.*, 1987; Digerness *et al.*, 1988). Also the slaughtering process itself may influence the endothelial function of the coronary circulation. Known from heart transplantation, brain death, here caused by electrocution, induces a cytokine storm release (Takada *et al.*, 1998), which is associated with myocardial depression and accompanied by pronounced vasodilation (Deng, 2002). After death was achieved by exsanguination, the heart was immediately isolated, cooled, and cannulated for administration of 1 L of cold cardioplegic solution to the coronary arteries. Consequently, warm ischemic time never exceeded 5 minutes, thereby limiting ischemia-reperfusion injury.

Although not all physiologic feedback mechanisms are still intact, the isolated beating pig heart is, in combination with a compliant preload system and a standard four-element windkessel model as afterload, capable of generating flow patterns and pressure curves that closely mimic hyperemic human coronary flow and pressure. Besides the fact that its use is beneficial from a time, cost and ethical perspective (Modersohn *et al.*, 2011), it therefore also allows testing and validating of cardiovascular devices (i.e., heart valves, stent grafts, and ventricular assist devices) under well-controlled circumstances. Moreover, it enables study of intracoronary diagnostic techniques, and to perform coronary interventions similar to that in humans in a clinical setting where persistent hyperemia is required. The permanent state of maximum hyperemia makes the model excellently suitable for coronary physiology research in which steady-state hyperemia is paramount i.e., index of myocardial resistance (Fearon *et al.*, 2003) and fractional flow reserve (Tonino *et al.*, 2009; Pijls *et al.*, 1993), important intracoronary diagnostic techniques in the human catheterization laboratory (European Society of Cardiology guidelines (Wijns *et al.*, 2010)). In addition, it provides a research tool that allows other biochemical, physiologic, morphologic and pharmacologic indices to be studied without the confounding effects of other organs, the systemic circulation, and circulating neurohumoral substances.

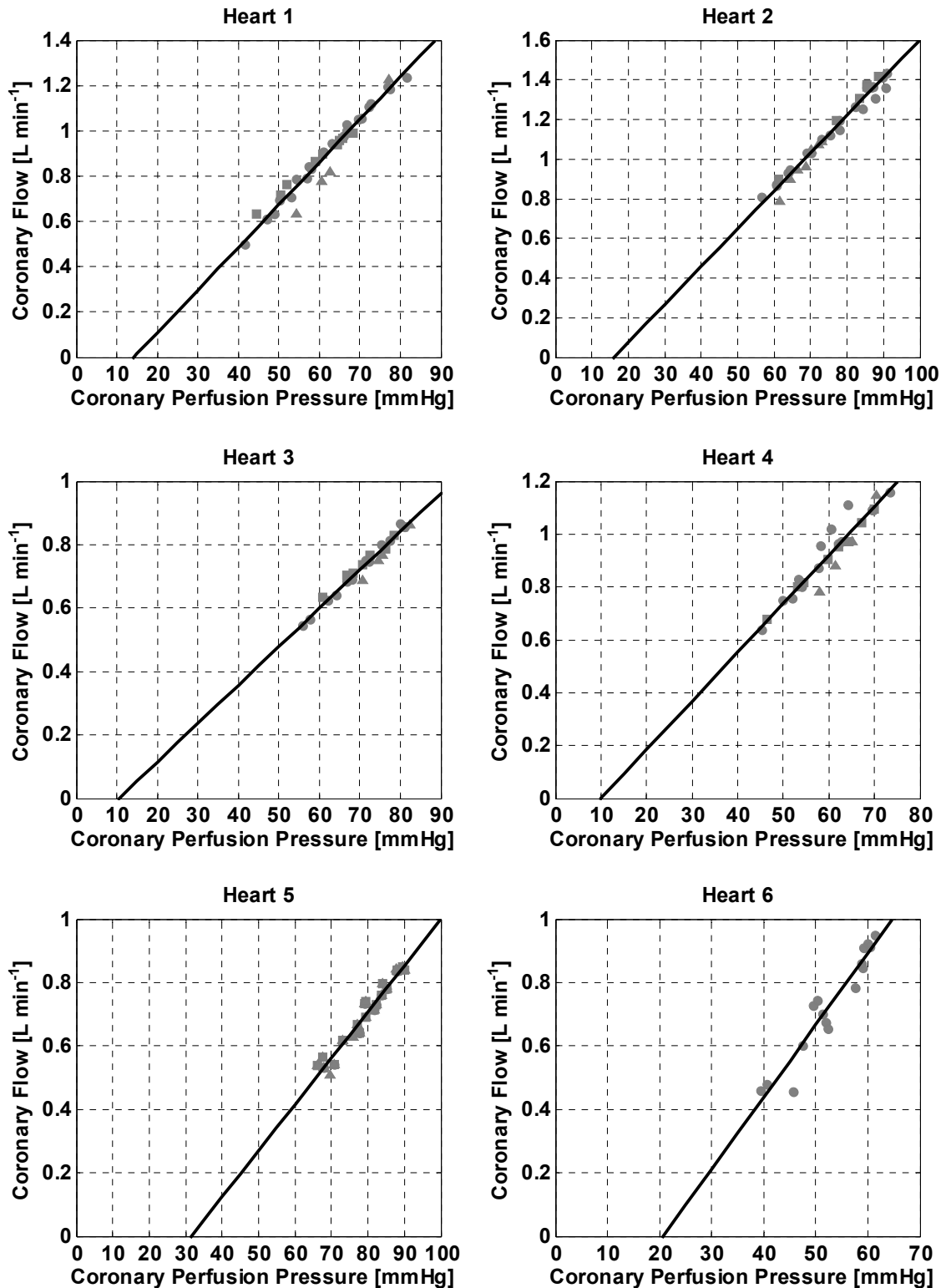


Figure 5.3: Relationship between coronary driving pressure and coronary blood flow. In the physiologic pressure range, a linear relationship ($R^2 = 0.94 \pm 0.03$, $p < 0.001$) with a positive non-zero intercept (10 - 32 mmHg) exists between coronary driving pressure and coronary blood flow for a wide variation of preload (squares), afterload (circles) and contractility (triangles). This relation was consistently observed for all individual slaughterhouse pig hearts and illustrates that the resistance of the coronary vascular bed is nearly constant.

5.5 Conclusion

The absence of reactive hyperemia, the linear relation between coronary blood flow and coronary driving pressure, and the fact that intracoronary administration of papaverine did not yield a transient increase in blood flow, strongly indicate that the coronary circulation in the isolated beating pig heart is in a permanent state of maximum hyperemia. Therefore, it is a suitable platform for testing and validating of cardiovascular devices (i.e., heart valves, stent grafts, and ventricular assist devices) under well-controlled circumstances.

Chapter 6

Intra-aortic balloon pump support in the isolated beating pig heart in non-ischemic and ischemic pump failure

The contents of this chapter are based on:

Schampaert S., Van Nunen L.X., Pijls N.H.J., Rutten M.C.M., Van Tuijl S., Van de Vosse F.N., Van 't Veer M.; Intra-aortic balloon pump support in the isolated beating pig heart in non-ischemic and ischemic pump failure; -, (-): -, submitted.

Abstract

The blood pressure changes induced by the intra-aortic balloon pump (IABP) are expected to create clinical improvement in terms of coronary perfusion and myocardial oxygen consumption. However, the measured effects reported in literature are inconsistent and ambiguous in human and experimental studies. Aim of this study was to investigate the influence of persisting ischemia on IABP efficacy in healthy hearts and in shock. Twelve slaughterhouse pig hearts (hearts 1 - 12) were isolated, prepared, and connected to an external circulatory system. Through coronary reperfusion and controlled cardiac loading, physiologic cardiac performance was achieved. Different clinical scenarios, ranging from normal contractile state to cardiogenic shock, were simulated by step-wise administration of negative inotropic drugs, while adapting systemic vascular resistance accordingly. In hearts 7 - 12, the clinical condition of a large myocardial infarction with different degrees of pump failure was mimicked by gradually creating severe global myocardial ischemia superimposed upon the decreased contractile states. IABP support was applied in all hearts under all conditions and evaluated. Without ischemia, the IABP induced a significant (but mild) increase in coronary blood flow and cardiac output. These effects were strongly augmented in the presence of persisting ischemia, where coronary blood flow increased by $49 \pm 24 \%$ ($p < 0.01$) and cardiac output by $17 \pm 6 \%$ ($p < 0.01$), in case of ischemia and severe pump failure. As expected, myocardial oxygen consumption increased in case of ischemia ($21 \pm 17 \%$; $p < 0.01$), while it slightly decreased without ischemia ($-3 \pm 6 \%$; $p < 0.01$). In case of progressive pump failure due to persistent myocardial ischemia, the IABP increased hyperemic coronary blood flow and cardiac output significantly, and reversed the progressive hemodynamic deterioration within minutes. This suggests that IABP therapy in acute myocardial infarction is most effective in patients with viable myocardium, suffering from persistent myocardial ischemia despite adequate epicardial reperfusion.

6.1 Introduction

By rapid inflation and deflation of the catheter-mounted polyurethane balloon, synchronous with the cardiac cycle, the intra-aortic balloon pump (IABP) has proven to induce a diastolic blood pressure augmentation as well as a systolic reduction in afterload (Weber *et al.*, 1974; Urschel *et al.*, 1970; Powell *et al.*, 1970; Gill *et al.*, 1973). The induced diastolic blood pressure augmentation is believed to be an increased driving force for coronary perfusion, and thus to increase coronary blood flow. However, although some experimental animal studies indeed demonstrate that the IABP augments coronary blood flow (Gill *et al.*, 1973; Hirsch *et al.*, 1966; Feola *et al.*, 1971; Watson *et al.*, 1974; Willerson *et al.*, 1976; Saini *et al.*, 1975; Swank *et al.*, 1978), others report unchanged flow during IABP support (Lefemine *et al.*, 1962; Shaw *et al.*, 1974; Watson *et al.*, 1976; Gewirtz *et al.*, 1982). Data in humans also show considerable variability, ranging from 30 % increase (Mueller *et al.*, 1971), to no change (Leinbach *et al.*, 1971) or even 10 % decrease (Williams *et al.*, 1982) in coronary blood flow with the IABP *in situ*. In addition to the diastolic blood pressure augmentation, the IABP also induces a systolic reduction in afterload, which theoretically reduces the energy consumption of the heart. However, also in this respect the measured effects reported in literature are inconsistent and ambiguous in human and experimental studies (Hirsch *et al.*, 1966; Mueller *et al.*, 1971; Kern *et al.*, 1999; Santa-Cruz *et al.*, 2006).

It has been suggested that the variable degree of IABP efficiency depends on patient's baseline hemodynamics (Powell *et al.*, 1970; Zehetgruber *et al.*, 1997; Kern *et al.*, 1993). Both Zehetgruber *et al.* (1997) and Kern *et al.* (1993) measured the change in coronary blood flow velocity in patients undergoing IABP therapy, and showed that the increase in coronary blood flow velocity was considerably larger in patients with a compromised hemodynamic status compared to those with normal baseline hemodynamics. In addition, an animal study of Powell *et al.* (1970) showed a decrease in myocardial oxygen consumption during support when myocardial performance and coronary blood flow were normal, while an increase was observed in case of severely impaired myocardial performance.

The findings mentioned above might be attributed to the presence of coronary autoregulation in healthy situations, and its absence in pathologic states. It is illusionary to presume that the augmented diastolic pressure translates into increased coronary blood flow as long as autoregulation is intact (De Silva *et al.*, 2014). Only when coronary autoregulation is absent, blood flow is directly related to the diastolic perfusion pressure, allowing the IABP to be effective. One of the common clinical conditions where coronary autoregulation is exhausted is large myocardial infarction with successful epicardial stenting, but persistent

microvascular obstruction i.e., with no-reflow. Furthermore, in a case of (persistent) myocardial ischemia with still viable myocardium, myocardial oxygen consumption will naturally increase when more blood is offered to the ischemic tissue, in contrast to the consumption of oxygen in myocardial tissue that is already adequately perfused.

Consequently, the aim of this study was to investigate the effects of IABP support in different clinical scenarios, ranging from normal contractile state to cardiogenic shock, whether or not accompanied by global myocardial ischemia. These scenarios were simulated in the isolated beating pig heart model (De Hart *et al.*, 2011), a platform in which the hemodynamic condition can be controlled very accurately. As the isolated beating pig heart is in a permanent state of exhausted autoregulation (**chapter 5**; Schampaert *et al.*, 2013), it allows evaluation of the IABP without the confounding effect of autoregulatory responses in different states of pump failure, whether or not complicated by superimposed ischemia.

6.2 Materials and methods

6.2.1 Isolated beating pig heart model

Twelve slaughterhouse pig hearts ($n = 2 \times 6$) (heart weight 520 ± 55 g) were isolated, prepared, and connected to an external circulatory system. Through coronary reperfusion and controlled cardiac loading, physiologic cardiac performance was achieved. This process is extensively described in **chapter 5**.

For this study, heart rate was fixed by means of ventricular pacing. The systemic circulation was divided into an upper and a lower part by extending the aorta by a proximal side branch, mimicking the brachycephalic arteries. Distal to the brachycephalic side branch, a standard four-element windkessel model was positioned. A 50 cc polyurethane balloon with a 7 Fr catheter (Maquet Getinge Group, Rastatt, Germany) was positioned in the aorta and connected to a CS300 IABP System (Maquet Getinge Group, Rastatt, Germany). Arterial and venous blood gas values, temperature, and electrolytes were measured using a CDI 500 blood parameter monitoring system (Terumo Cardiovascular Systems Corporation, Tokyo, Japan), which was calibrated using a VetScan i-STAT 1 (Abaxis, Union City, California, U.S.A.) The model of Kelman (1966) was subsequently used to transform the measured blood gas values into actual saturation levels. Hemodynamic parameters were continuously monitored and after performing the hemodynamic interventions, the heart was arrested with a potassium chloride injection into the aortic cannula after cross clamping the aorta.

6.2.2 Hemodynamic interventions

In this model, different clinical scenarios, ranging from normal contractile state to cardiogenic shock, were defined (Figure 6.1). A healthy state was defined as a non-ischemic cardiac output larger than 4.75 L min^{-1} and a mean aortic pressure larger than 77.5 mmHg , pre-shock as a cardiac output between 3.75 and 4.75 L min^{-1} and a mean aortic pressure between 67.5 and 77.5 mmHg , and cardiogenic shock as a cardiac output of less than 3.75 L min^{-1} and a mean aortic pressure of less than 67.5 mmHg . When neglecting venous pressure, these clinical scenarios were all associated with a fixed systemic vascular resistance (ratio of mean aortic pressure and cardiac output), which increases in case of more impaired hemodynamic conditions. With the heart beating in periodic continuous working left heart mode, systemic vascular resistance was adapted in order to achieve the best clinical scenario feasible, given the specific contractility of the heart. Subsequently, the transition between the different hemodynamic states was accomplished by step-wise administration of negative inotropic agents (1 mg metoprolol or 10 mg esmolol per step), while systemic vascular resistance was adapted accordingly. Next, in the second series of six hearts (hearts 7 - 12), the clinical scenario of a large myocardial infarction in conjunction with the pump failure was mimicked. Because occlusion of a large coronary artery in the pig heart could induce severe arrhythmias and even ventricular fibrillation, we chose to create global severe ischemia by decreasing the arterial oxygen supply in the extra-corporeal circulation. In all simulated scenarios, measurements were performed with and without IABP support. The support capabilities of the pump were evaluated in terms of coronary blood flow, cardiac output, and myocardial oxygen consumption, as the mutual relation between these three parameters determines the efficacy of the IABP. To test reproducibility of the observations, the sequence of all measurements was repeated without and with IABP support, leaving all other parameters unchanged.

6.3 Results

6.3.1 Clinical Scenarios of pump failure and ischemia

The isolated beating pig heart was capable of generating flow patterns and pressure curves that closely mimicked aortic and coronary *in vivo* flow and pressure. In all hearts, heart rate could be fixed within a physiologic range ($94 - 125 \text{ min}^{-1}$).

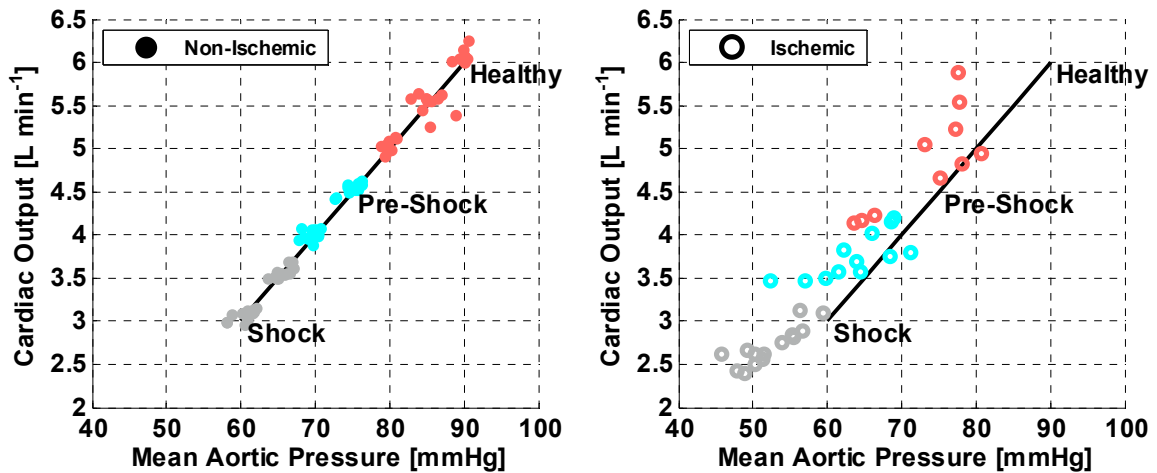


Figure 6.1: Clinical scenarios at baseline, ranging from healthy (red) to pre-shock (cyan) to shock (grey). On the left side (solid dots), no ischemia is present. On the right side (open dots), extensive myocardial ischemia is superimposed upon the different (hypo) contractile states.

Step-wise administration of negative inotropic drugs (1 mg metoprolol or 10 mg esmolol per step), while manually adapting systemic vascular resistance accordingly, enabled the transition towards clinical states of progressively impaired pump failure precisely (Figure 6.1, Table 6.1). Deterioration of myocardial performance was reflected by a decrease in the maximum rate of left ventricular pressure change (dp/dt_{\max}) from 1093 ± 162 in healthy state to 818 ± 212 mmHg s⁻¹ in cardiogenic shock without ischemia. The corresponding decreased aortic pressure, which functioned as driving pressure for coronary perfusion, resulted in a proportional decrease in coronary blood flow and oxygen consumption of the heart, as the external mechanical work the heart had to perform also decreased. In the end, the simulated clinical scenarios, whether or not superimposed by myocardial ischemia, covered the complete range from healthy to pathologic (Figure 6.1).

In the non-ischemic hearts (hearts 1 - 12), myocardial perfusion was considered to be adequate. Beating in a healthy scenario (Figure 6.1, Table 6.1), hyperemic coronary blood flow amounted to 1.2 ± 0.2 L min⁻¹, myocardial oxygen consumption, corrected for the heart's weight, was found to be in the same range as the oxygen consumption of an *in vivo* human heart at rest (5.5 ± 1.7 mL O₂ min⁻¹ 100 g⁻¹), and the blood oxygen saturation level reduced from 97 ± 1 % (arterial) to 84 ± 6 % (venous) on passing through the cardiac tissue. In the hearts where myocardial ischemia was introduced (hearts 7 - 12) (Figure 6.1, Table 6.1), however, the lowered arterial oxygen saturation (56 ± 22 %), despite similar coronary blood flow levels (1.2 ± 0.4 L min⁻¹), induced a (sub)critical oxygen insufficiency. Venous oxygen saturation was depressed accordingly (43 ± 17 %) and went along with a progressive hemodynamic

deterioration over time (Figure 6.2). At the same time, contractility, as reflected by dp/dt_{\max} , further decreased and preload, as reflected by left atrial pressure, further increased (Table 6.1).

Table 6.1: Heart specific baseline hemodynamic parameters (mean \pm SD) recorded with the hearts beating in the different clinical scenarios (ranging from healthy to shock). In hearts 7 - 12, myocardial ischemia was superimposed upon the initially tuned non-ischemic reference state.

	Non-Ischemic (hearts 1 - 12)			Ischemic (hearts 7 - 12)		
	Healthy	Pre-Shock	Shock	Healthy	Pre-Shock	Shock
Q_{cor}	1.2 \pm 0.2	1.0 \pm 0.2	0.8 \pm 0.2	1.2 \pm 0.4	1.0 \pm 0.3	0.7 \pm 0.4
CO	5.5 \pm 0.4	4.3 \pm 0.3	3.3 \pm 0.3	4.9 \pm 0.6	3.7 \pm 0.3	2.7 \pm 0.2
$M\dot{V}O_2$	5.5 \pm 1.7	4.2 \pm 1.7	3.7 \pm 1.6	4.2 \pm 1.4	4.7 \pm 2.0	3.9 \pm 1.4
p_{ao}	84 \pm 4	72 \pm 3	63 \pm 3	73 \pm 6	64 \pm 6	52 \pm 4
p_{la}	14 \pm 3	14 \pm 2	14 \pm 2	29 \pm 4	26 \pm 3	26 \pm 5
dp/dt_{\max}	1093 \pm 162	1077 \pm 367	818 \pm 212	1017 \pm 182	947 \pm 373	668 \pm 156
SVR	1234 \pm 44	1356 \pm 37	1532 \pm 58	1214 \pm 83	1360 \pm 82	1547 \pm 66

Q_{cor} , coronary flow [$L \text{ min}^{-1}$]; CO , cardiac output [$L \text{ min}^{-1}$]; $M\dot{V}O_2$, myocardial oxygen consumption [$mL \text{ O}_2 \text{ min}^{-1} 100 \text{ g}^{-1}$]; p_{ao} , aortic pressure [mmHg]; p_{la} , left atrial pressure [mmHg]; dp/dt_{\max} , maximum rate of left ventricular pressure change [mmHg s^{-1}]; SVR , systemic vascular resistance [dyn s cm^{-5}].

6.3.2 Intra-aortic balloon pump support

A representative example of the effects of IABP support is shown in figure 6.2. When switching on IABP support, rapid inflation and deflation of the catheter-mounted polyurethane balloon, synchronous with the cardiac cycle, induced a diastolic blood pressure augmentation as well as a systolic reduction in afterload. Without ischemia, these blood pressure changes resulted in a significant (but only mild) increase in coronary blood flow and cardiac output, with increases of $10 \pm 6 \%$ ($p < 0.01$) and $3 \pm 2 \%$ ($p < 0.01$), respectively in cardiogenic shock (Figure 6.3A and 6.3B, solid bars; Table 6.2). Furthermore, the IABP induced a limited decrease in myocardial oxygen consumption when the (non-ischemic) heart was perfused adequately ($-3 \pm 6 \%$; $p < 0.01$) (Figure 6.3C, solid bars; Table 6.2). With superimposed ischemia, however, the increase in coronary blood flow and cardiac output (and decrease of left atrial pressure) became largely augmented and the more with increasing degree of pump

failure. In case of severe heart failure with superimposed ischemia, coronary blood flow and cardiac output were able to increase by $49 \pm 24 \%$ ($p < 0.01$) and $17 \pm 6 \%$ ($p < 0.01$) respectively (Figure 6.3A and 6.3B, hatched bars; Table 6.2), while left atrial pressure decreased by $42 \pm 14 \%$ ($p < 0.01$). As expected, myocardial oxygen consumption increased ($21 \pm 17 \%$; $p < 0.01$) when more blood was offered to the ischemic tissue (Figure 6.3C, hatched bars; Table 6.2). All these effects occurred within several minutes and were very reproducible (Figure 6.2).

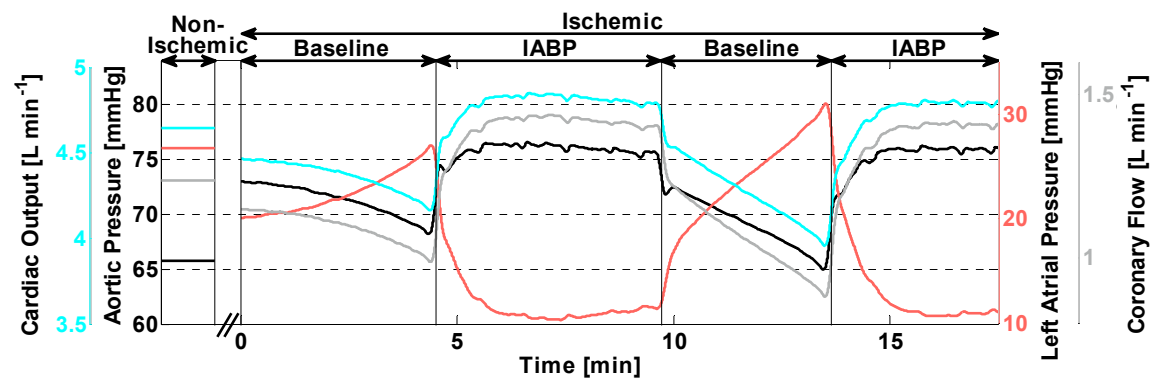


Figure 6.2: Example of the effect of IABP on hemodynamic parameters in one of the hearts, starting in the pre-shock mode. Without ischemia (left part of the figure), cardiac output equals 4.6 L min^{-1} (cyan line), blood pressure equals 76 mmHg (black line), left atrial pressure equals 16 mmHg (red line), and coronary blood flow equals 1.2 L min^{-1} (grey line). Next, additional global ischemia is slowly created by decreasing arterial oxygen saturation in the extracorporeal circulation. This is accompanied by a slow decrease of cardiac output, coronary blood flow, and blood pressure and an increase in left atrial pressure. At a particular point in time (called $t = 0$ min), the downward spiral is accelerated and progressive deterioration occurs. Next, without any change in external oxygen supply or any of the other controllable parameters, the IABP is switched on ($t \approx 5$ min) and within two minutes, a significant improvement of cardiac output, coronary blood flow, and blood pressure occurs, while left atrial pressure decreases dramatically. All parameters stabilize within a few minutes. At $t \approx 10$ min, the IABP is switched off again without any change in any of the controllable parameters, whereafter the heart rapidly deteriorates and enters the negative vicious circle again. By switching on the IABP ($t \approx 15$ min), significant improvement and stabilization occurs again.

6.4 Discussion

In this study, we studied the effects of IABP support on both cardiac and coronary hemodynamics in the isolated beating pig heart under controllable physiologic and pathologic conditions. Although the magnitude of induced effects slightly varied

between the individual hearts, these were generally limited with pump failure alone, but largely augmented with increasing myocardial ischemia. In case of severe pump failure with superimposed myocardial ischemia, the IABP was capable to effectively support the circulation by increasing hyperemic coronary blood flow, blood pressure, and cardiac output by $49 \pm 24 \%$, $13 \pm 5 \%$, and $17 \pm 6 \%$, respectively. At the same time, left atrial pressure decreased by $42 \pm 14 \%$ and myocardial oxygen consumption increased by $23 \pm 10 \%$, reflecting that not only more oxygen was delivered to the ischemic heart but also utilized.

In contrast to former studies to the pathophysiologic mechanism of IABP support, our results were very consistent and reproducible. Those earlier studies reported a wide divergence of changes, e.g., changes in coronary blood flow range from a 100 % increase (Zehetgruber *et al.*, 1997), to no change (Leinbach *et al.*, 1971) or even a 10 % decrease (Williams *et al.*, 1982). We were able to reduce the variability within the same clinical conditions considerably by better classifying the different clinical scenarios, based on their hemodynamic characteristics of pump failure and the presence or absence of myocardial ischemia. This allowed us to evaluate the hemodynamic state dependency of IABP support more accurately.

Table 6.2: Percent changes of hemodynamic parameters (mean [interval]) after starting IABP support (compared to the status without IABP) in the different hemodynamic scenarios, whether or not with superimposed persisting myocardial ischemia (hearts 1 - 12: without ischemia; hearts 7 - 12: with ischemia).

	Non-Ischemic (hearts 1 - 12)			Ischemic (hearts 7 - 12)		
	Healthy	Pre-Shock	Shock	Healthy	Pre-Shock	Shock
Q_{cor}	6 [0, 12]	8 [0, 14]	10 [-2, 22]	27 [6, 53]	31 [4, 56]	49 [26, 105]
CO	1 [-2, 3]	1 [-1, 4]	3 [0, 9]	8 [1, 16]	11 [3, 19]	17 [10, 32]
$M\dot{V}O_2$	-4 [-15, 4]	-4 [-16, 6]	0 [-12, 14]	25 [-5, 66]	14 [-1, 38]	23 [13, 40]
p_{ao}	1 [-2, 10]	1 [-2, 4]	2 [-2, 7]	6 [-1, 11]	8 [-2, 17]	13 [5, 26]
p_{la}	-14 [-33, 6]	-14 [-36, 5]	-15 [-36, -1]	-30 [-52, -1]	-39 [-62, -16]	-42 [-64, -21]
dp/dt_{max}	11 [-18, 43]	3 [-21, 43]	16 [-18, 68]	13 [-18, 43]	9 [-18, 43]	26 [-4, 68]
SVR	0 [-2, 6]	0 [-5, 3]	-1 [-5, 2]	-2 [-5, 0]	-3 [-6, -1]	-3 [-7, 2]

Q_{cor} , coronary flow [% Δ]; CO , cardiac output [% Δ]; $M\dot{V}O_2$, myocardial oxygen consumption [% Δ]; p_{ao} , aortic pressure [% Δ]; p_{la} , left atrial pressure [% Δ]; dp/dt_{max} , maximum rate of left ventricular pressure change [% Δ]; SVR , systemic vascular resistance [% Δ].

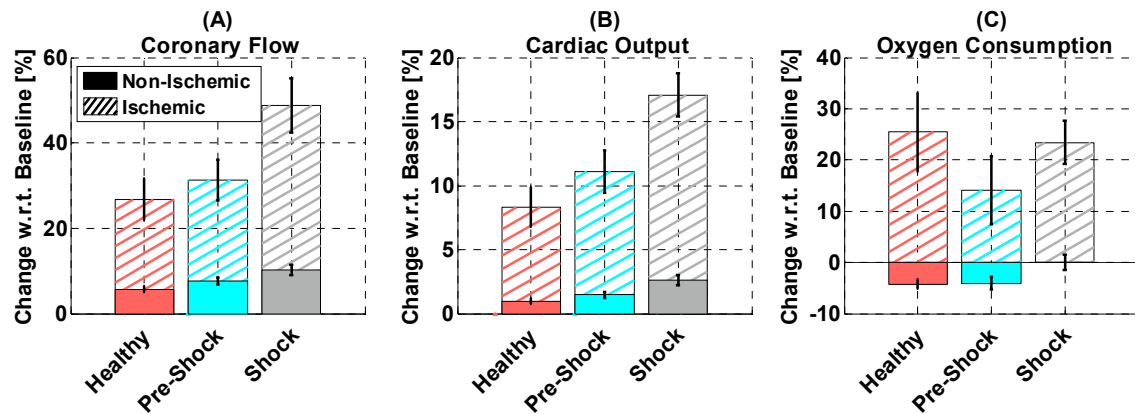


Figure 6.3: Change (mean \pm SEM) by IABP support compared to the status without IABP of coronary blood flow (left), cardiac output (center), and myocardial oxygen consumption (right) for different clinical scenarios, ranging from healthy to cardiogenic shock, whether (hatched) or not (solid) in the presence of global myocardial ischemia.

Former studies in this field consistently overlooked the effect of coronary autoregulation, which counteracts any increase of coronary blood flow by increased diastolic aortic pressure in non-ischemic pump failure (De Silva *et al.*, 2014). Neither did they sufficiently recognize the difference between pump failure due to (irreversible) damage of myocytes (necrosis), as encountered in many clinical conditions of (pre-)shock, and pump failure as a result of temporarily depressed function of still viable myocytes caused by severe ischemia due to no-reflow after acute myocardial infarction or cardiac surgery.

From the data obtained in this study, one can conclude that in case of pump failure alone without myocardial ischemia, the IABP induces only small effects. That is in congruence with earlier negative studies to the effects of the IABP in shock without concomitant ischemia (Thiele *et al.*, 2012; Patel *et al.*, 2011; Perera *et al.*, 2010). With intact autoregulation (which is the case with isolated pump failure outside the setting of acute myocardial infarction or cardiac surgery), it cannot be expected that coronary blood flow will increase and the only effect to be expected is the change of cardiac output by afterload reduction, which is limited as shown in this study. In contrast, in case of pump failure with viable ischemic myocardium and exhausted autoregulation, a direct relation between coronary blood flow and diastolic aortic pressure is present and higher diastolic pressure is linearly related to higher coronary blood flow, as we have shown in **chapter 5** (Schampaert *et al.*, 2013). In such situations, improved perfusion of the ischemic myocardium will in turn relieve ischemia of the myocytes, enhance oxygen utilization, and (partly) restore contractile function and cardiac output, thereby further improving coronary perfusion and reversing a negative spiral. A corresponding clinical condition where autoregulation

is exhausted exists inside the patient with a large myocardial infarction and successful epicardial reperfusion by stenting, but so-called no-reflow and persistent ischemia of still viable myocardium (Bolli *et al.*, 1990). Another clinical scenario resembling these conditions exists inside the patient after coronary bypass surgery with good bypasses but transient myocardial stunning due to (prolonged) extracorporeal circulation (Hiratzka *et al.*, 1987; Digerness *et al.*, 1988).

It has been hypothesized that during IABP support myocardial oxygen consumption should decrease because of the extended work by the IABP due to afterload reduction. In the non-ischemic states, we indeed found a limited decrease in myocardial oxygen consumption despite a small increase of cardiac output, suggesting that external energy was delivered to the circulation indeed, in agreement with findings of Powell *et al.* (1970). However, in the ischemic states, myocardial oxygen consumption increased, which can be explained by the fact that the increased coronary blood flow in this situation effectively increased myocardial oxygen supply, leading to utilization of oxygen by the ischemic myocytes, reduction of myocardial ischemia, and increase of cardiac output.

Based upon the findings of this study, one can also hypothesize that in case of pump failure without ischemia, left ventricular assist devices and transvalvular assist devices, like Impella (Abiomed Cardiovascular Inc., Danvers, Massachusetts, U.S.A.), are more effective than IABP because the action of these devices is based upon direct increase of cardiac output without interacting primarily with coronary blood flow or myocardial oxygen utilization. In contrast, when pump failure is due to (reversible) ischemia of the myocardium, the IABP is effective by relieving ischemia, supporting temporarily depressed contractile function, salvage of myocardium, and therefore beneficial in the long term.

6.4.1 Strengths and limitations of this study

Although the isolated beating pig heart was capable of generating flow patterns and pressure curves that closely mimicked aortic and coronary *in vivo* flow and pressure, *ex vivo* testing is not the equivalent of *in vivo* testing. Not all physiologic feedback mechanisms are still intact in the isolated beating pig heart as proven in earlier: coronary autoregulation is absent (an advantageous in this particular *ex vivo* model to investigate IABP effects) (**chapter 5**; Schampaert *et al.*, 2013), heart rate was fixed within a physiologic range by means of pacing (assuring no interference with the required time for complete inflation and deflation of the balloon), and systemic vascular resistance was only tuned initially to render the prescribed clinical scenarios and not changed thereafter. Furthermore, the effects of IABP support would probably be even more pronounced when the preload reduction following institution

of IABP support would be compensated by increased filling as would have been the case *in vivo*. The reduced preload by the IABP in this model lowered the end diastolic left ventricular filling pressure and volume, and consequently ventricular contractility (Frank-Starling mechanism). So, in the *in vivo* situation where the preload reduction by the IABP would have been compensated, the increase in cardiac output would most likely have been even more pronounced than in our *ex vivo* model.

Because occlusion of a large coronary artery in the pig heart could induce severe arrhythmias and even ventricular fibrillation, we had to create global severe ischemia by step-wise decreasing the arterial oxygen supply in the extra-corporeal circulation, thereby simulating the scenario of a large myocardial infarction with viable myocardium. Another limitation of this method was that the accuracy of measuring blood gasses of the CDI 500 blood parameter monitoring system (Terumo Cardiovascular Systems Corporation, Tokyo, Japan) is reduced when blood oxygen levels are low.

One of the strengths of this isolated beating pig heart model is that a larger number of interacting physiologic parameters involved *in vivo* are excluded, allowing good control of the hemodynamic condition. Measurements can be performed far more accurately than *in vivo*. Another specific strength is that the isolated beating pig hearts are no animal experiments as these organs are slaughterhouse by-products. This *ex vivo* testing is therefore time and cost efficient, while ethical objections are reduced, because sacrificing large animals for experimental research is avoided. Therefore, the isolated beating pig heart forms an accessible platform to investigate the heart and the coronary circulation in its truly morphologic and physiologic way, including studying changes in cardiac output, coronary blood flow, and oxygen metabolism in response to IABP support.

6.5 Conclusion

In this *ex vivo* beating heart study, the IABP significantly improved coronary blood flow, blood pressure, and cardiac output, enhanced oxygen utilization, and within minutes reversed the progressive hemodynamic deterioration in case of severe pump failure with superimposed myocardial ischemia. Consequently, in clinical practice, IABP support can be expected to be most effective in patients with viable myocardium, suffering from persistent myocardial ischemia, despite adequate epicardial reperfusion. This is the case in acute myocardial infarction patients after successful stenting but accompanied by no-reflow or after bypass surgery with stunning and ischemic but viable myocardium. Large randomized clinical trials are mandatory to support these views.

Chapter 7

General discussion

The IABP has a long record of supporting patients after myocardial infarction or cardiac surgery. Although every interventional cardiologist has witnessed cases of patients with acute myocardial infarction with prompt relief of chest pain, ST-segment resolution, and hemodynamic improvement after IABP insertion, this goes along with cases where the IABP had no or only minimal effect. As reasons for these varying observations are unclear, the main objective of the research described in this thesis is to provide medical specialists with a better understanding of the indications for IABP use. The different projects were carried out at the department of Biomedical Engineering at Eindhoven University of Technology and at the department of Cardiology at Catharina Hospital Eindhoven. Using a combination of computational modeling, *in vitro* and *ex vivo* testing, and performing clinical measurements, a complete overview of the physiologic effects of the IABP on both cardiac and coronary hemodynamics was constructed together with clinical settings in which its use would be most effective. In this chapter, the main findings described in this thesis are discussed and recommendations for use are given.

7.1 Research methods

To address the need for advanced models that function in a physiologic manner for testing the interaction between the IABP and the cardiovascular system, different research models were developed and used: a lumped parameter computational model (**chapter 2**), a model-controlled mock circulation system (**chapter 3**), and an isolated beating pig heart platform (**chapter 5**). For validation purposes, *in vivo* data were collected from literature and clinical measurements were performed on patients undergoing IABP therapy. Each of these separate models has its drawbacks and limitations, but when combined, it offers an integrated research strategy, providing the possibility to study different parameters and processes in both an isolated and combined manner.

7.1.1 Computational modeling

In **chapter 2**, a numerical model is presented and validated that couples a 0-dimensional lumped parameter model to the single fiber heart contraction model of Arts *et al.* (1991) and Bovendeerd *et al.* (2006), describing ventricular wall mechanics, myocardial constitutive properties, and intramyocardial pressure. The main advantage of combining these models is the rather simple implementation, which renders stable solutions. Also the computational cost of these simulations is relatively low, making future real-time computation in the catheterization laboratory feasible. Furthermore, the heart contraction model, compared to more

phenomenologic models, is based on microstructural material and macrostructural geometric properties. This enables the simulation of cardiac disease with physiology-based parameter changes. It features the Frank-Starling mechanism and thereby includes cardiac function control, but mechanisms to regulate blood pressure are lacking. A baroreflex mechanism to regulate heart rate, however, can be included easily as was already incorporated into a similar heart contraction model by Cox *et al.* (2009). The circulatory system was subdivided into a large number of small segments and translated into electrical passive components (resistances, inertances, and compliances), based on the following physiologic parameters: radius and segment length, density and viscosity of blood, and vessel wall elasticity and thickness (Westerhof *et al.*, 1969). Final values (resembling the estimation closely) were determined iteratively and resulted in representative pressure and flow signals. Although these windkessel models have proven to be very useful in describing the behavior of the entire vascular tree, detail on local flow and pressure phenomena is lacking and simulated results can therefore only be compared qualitatively to literature values. Distributed electrical transmission line and 1-dimensional wave propagation models are more suitable to describe pressure and flow waves in the individual arteries. The intramyocardial pressure (Bovendeerd *et al.*, 2006), which relates the mechanics of the myofibers to global left ventricular mechanics, made the connection between the model of the left ventricular mechanics and the coronary circulation model of Geven *et al.* (2004), comprising a coronary epicardial artery, an intramyocardial pressure dependent myocardial perfusion resistance, and a venous outlet. By including coronary autoregulation, the differences between resting and hyperemic flow (and its response to blood pressure configuration changes) can be simulated. This autoregulatory mechanism can be incorporated in the coronary circulation model of Geven *et al.* (2004) by extending the coronary artery segment by a modulated arteriolar sphincter, which can be assumed to be the only parameter determining coronary autoregulation (Jayaweera *et al.*, 1999). Within the autoregulation range, the sphincter maintains a balance between myocardial oxygen supply and myocardial oxygen consumption, based on coronary blood flow and the work the heart has to perform, respectively, thereby creating a connection between the coronary autoregulation model and the heart contraction model. Including cardiac metabolism should additionally account for stunned or hibernating myocardium, cell death and ultimately contractile dysfunction in response to a mismatch between myocardial oxygen delivery and energy requirements for a given workload.

7.1.2 Experimental testing

Model-controlled mock circulation

The computational model developed in **chapter 2** was subsequently translated into a hydraulic circuit. The resulting model-controlled mock circulation (**chapter 3**) was implemented in a servo-motor driven system and controlled by an elaborate heart contraction model and a realistic frequency control model. The model, together with a relatively simple lead-lag controller, was shown to be stable and a good tracking performance was realized. The highest tracking errors occurred when the cardiac valves in the model opened or closed, inducing steep left ventricular pressure rises or drops. Nevertheless, the model-controlled mock circulation was capable of generating pressure and flow curves that closely mimicked systemic and pulmonary flow and pressure. The model was able to create identical hemodynamic circumstances, while providing the possibility to study different parameters in an isolated manner. This allowed the model to compare different cardiac assist devices, as we did for the intra-aortic balloon pump and the Impella 2.5 left percutaneous (LP) (Abiomed Cardiovascular Inc., Danvers, Massachusetts, U.S.A.) in **chapter 4** with water as circulating fluid. The use of other fluids, mimicking a more physiologic viscosity, is feasible as well. Nevertheless, the mock circulatory system lacks specific anatomical structures and features. In concordance to the numerical lumped parameter model, autoregulation was limited to heart function and frequency. Coronary autoregulation was not included and blood volume was not regulated. Furthermore, due to the absence of an active atrium, ventricular filling was completely passive, and consequently strongly coupled to ventricular preload (especially in combination with a high frequency, and thus a relatively short ventricular filling time). However, as the preload level is difficult to tune, the potential energy (as a measure for the non-work related oxygen consumption) is hard to evaluate qualitatively in the model-controlled mock circulation.

Isolated beating pig heart

As an intermediate between *in vitro* and *in vivo* testing, the isolated beating pig heart (LifeTec Group, Eindhoven, The Netherlands) forms an accessible platform to investigate the coronary circulation in its truly morphologic and physiologic state, while allowing excellent control of the individual hemodynamic parameters over a large pressure range (De Hart *et al.*, 2011). Moreover, the isolated pig hearts are not categorized as animal experiments as these organs are obtained from a local slaughterhouse and thus categorized as slaughterhouse by-products. This so-called *ex vivo* testing is therefore less demanding in management, and reduces ethical objections, because sacrificing large animals for experimental research is avoided. In

analogy to a denervated transplant heart in its early days, it might be expected that autoregulation is absent in this *ex vivo* beating heart model. The absence of reactive hyperemia, the linear relation between coronary blood flow and coronary driving pressure, and the fact that intracoronary administration of papaverine did not yield a transient increase in blood flow, indicate that the isolated beating pig heart is indeed in a permanent state of exhausted autoregulation (**chapter 5**; Schampaert *et al.*, 2013). This is an advantage in this particular research, as it is illusionary to believe that coronary blood flow will increase with the IABP *in situ* when coronary autoregulation is present (De Silva *et al.*, 2014). In contrast to the developed numerical and *in vitro* models, the energy metabolism of the isolated beating pig heart accounts for stunned or hibernating myocardium, cell death and ultimately contractile dysfunction in response to a mismatch between myocardial oxygen delivery and energy requirements for a given workload. This makes the isolated beating pig heart an accessible platform to investigate the influence of persisting ischemia on IABP efficacy in healthy hearts and in shock, as we did in **chapter 6**. The results of these exceptionally elucidatory experiments corroborated the conclusions at the end of this chapter.

7.1.3 Clinical validation and future perspectives

For validation purposes, blood pressure recordings were collected from ten patients (65 ± 13 years) undergoing IABP therapy (**chapter 2**). The clinical indications covered the wide range of typical indications for IABP use, including cardiogenic shock, coronary artery bypass grafting, out-of-hospital cardiac arrest, persistent ischemia, anterior myocardial infarction, and spontaneous coronary artery dissection. It should be noted that only hemodynamically stable patients were included (mean aortic pressure was 85 ± 9 mmHg), as the hemodynamic condition had to permit switching off the pump for a short period of time (± 30 s) and varying the moments of balloon inflation and deflation around their conventional timing settings, thereby not reflecting the critically ill patient population. Furthermore, the large number of interacting physiologic parameters involved lead to results that show considerable variability and are difficult to interpret. Nevertheless, together with a retrospective evaluation of our own clinical experience with IABP support (Van Nunen *et al.*, 2013) and a sub-analysis of the Counterpulsation Reduces Infarct Size Pre-percutaneous coronary intervention Acute Myocardial Infarction (CRISP-AMI) study (Van Nunen *et al.*, 2014; Patel *et al.*, 2011), the results of the previous chapters have led to the initiation of a large randomized trial in patients with large myocardial infarction to further streamline the use of the IABP.

7.2 Intra-aortic balloon pump support

By rapid inflation and deflation of the catheter-mounted polyurethane balloon, the IABP induced a diastolic blood pressure augmentation as well as a systolic reduction in afterload. In all research models (numerical, *in vitro*, and *ex vivo*), these blood pressure changes resulted in an increase in coronary blood flow and cardiac output. Although the magnitude of coronary blood flow enhancement was limited, it was slightly larger in the numerical and *in vitro* model compared to the *ex vivo* model (in the absence of persistent ischemia). This might be addressed to the lower heart rate in combination with the relatively small shape of the active fiber stress curve in the one fiber model (implemented in the numerical and *in vitro* model). Consequently, a relatively long diastolic phase was prescribed, in which aortic pressure was augmented by the IABP and coronary perfusion enhanced. Secondary, this resulted in a larger decline in afterload, and thus in a larger increase in ventricular stroke volume.

We also showed experimentally (*in vitro* and *ex vivo*) that the coronary blood flow and cardiac output enhancement became the more with increasing degree of pump failure. Although this suggests that IABP support would be most effective in critically ill patients, it is illusionary to presume that the support capabilities of the pump would be sufficient in reversing the progressive hemodynamic deterioration in so-called 'back-against-the-wall' patients, in which IABP support is applied as a last resort. Furthermore, controversy exists whether the augmented pressure is accompanied by an increased coronary blood flow in the presence of coronary artery obstruction and coronary autoregulation (Kern *et al.*, 1993; Kimura *et al.*, 1996; Takeuchi *et al.*, 2004; Yoshitani *et al.*, 2007). A severe coronary artery stenosis might prevent adequate transmission of the augmented diastolic aortic pressure through the stenosis, failing to increase the diastolic inflow to the myocardium and time-averaged blood flow rate (Powell *et al.*, 1970), while in the presence of coronary autoregulation, coronary blood flow is not proportional to aortic pressure anymore, but regulated by a flow regulatory mechanism.

In the non-ischemic isolated beating pig heart, the mild increase in coronary blood flow and cardiac output during IABP support went along with a small decrease in myocardial oxygen consumption. As cardiac energy metabolism was not included in the one fiber model, the changes in myocardial oxygen consumption could not be evaluated in the numerical and *in vitro* model. As an alternative, we evaluated the area within the pressure-volume loop, which is a measure for the delivered cardiac stroke work, but only accounts for the work-related myocardial oxygen consumption (Suga *et al.*, 1990). However, as ventricular filling (and thus the non-work-related oxygen consumption: potential energy) is strongly coupled to ventricular preload,

which is especially hard to tune in the model-controlled mock circulation, this parameter is hard to evaluate qualitatively. In contrast to the total oxygen consumption of the *ex vivo* heart, the work-related myocardial oxygen consumption increased secondary to the increase in stroke volume during IABP support in our numerical and *in vitro* model.

Only in the isolated beating pig heart model, where cardiac metabolism was present, we were able to investigate the effect of IABP support on stunned or hibernating myocardium, cell death, and ultimately contractile dysfunction due to a mismatch between myocardial oxygen supply and myocardial energy requirements for a given workload. When pump failure with superimposed persisting myocardial ischemia was simulated in the isolated beating pig heart, the magnitude of effects induced by the IABP were strongly augmented: coronary blood flow and cardiac output increased up to $49 \pm 24 \%$ and $17 \pm 6 \%$, respectively in case of severe heart failure. This is probably caused by the fact that the increase in coronary blood flow resulted in a decrease of the amount of myocardial ischemia, thereby partly restoring the pump function of the heart. This resulted in a secondary increase in arterial blood pressure and ongoing improvement of coronary perfusion and cardiac function. This upward spiral, however, can only be induced when myocardial tissue is viable. Once myocardial tissue has become necrotic, the IABP will not be able to restore cardiac function, resulting in only a limited coronary blood flow increase. The finding that the presence of myocardial ischemia is a major determinant of IABP efficacy is supported by our own retrospective clinical experience with IABP support (Van Nunen *et al.*, 2013), where the survival rate in patients undergoing IABP support with persisting ischemia (30-day and 1-year survival: 93 % and 89 %, respectively) was considerable larger compared to patients in cardiogenic shock alone (30-day survival: 64 %). Also a sub-analysis of the CRISP-AMI study (Van Nunen *et al.*, 2014; Patel *et al.*, 2011), in which survival in patients with large myocardial infarction and persistent ischemia treated with the IABP were compared, suggested that IABP support decreases mortality in large ST-elevation myocardial infarction complicated by persistent ischemia after successful percutaneous coronary intervention. However, as this sub-analysis was non-powered and non-prespecified, the results should be perceived mainly hypothesis-generating and further prospective randomized trials are mandatory.

Based upon the findings of this research, one can also hypothesize that in case of pump failure without ischemia, transvalvular assist devices, such as the Impella 2.5 left percutaneous (LP) (Abiomed Cardiovascular Inc., Danvers, Massachusetts, U.S.A.), are more effective than the IABP because the action of this rotary blood pump are based upon direct increase of cardiac output without interacting primarily with coronary blood flow or myocardial oxygen utilization. In contrast, when pump failure

is due to (reversible) ischemia of the myocardium, the IABP is effective by relieving ischemia, supporting temporarily depressed contractile function, salvage of myocardium, and is therefore beneficial in the long term.

7.3 Conclusion

The integrated research strategy of computational modeling, *in vitro* and *ex vivo* testing, and clinical validation, exposed the interaction between the IABP and the cardiovascular system, while enabling to predict clinical conditions and pump settings in which IABP therapy would be most effective. The IABP considerably improved hyperemic coronary blood flow, blood pressure, and cardiac output, enhanced oxygen utilization, and within minutes reversed the progressive hemodynamic deterioration in case of severe pump failure with superimposed myocardial ischemia. Consequently, in clinical practice, IABP support can be expected to be most effective in patients with viable myocardium, suffering from persistent myocardial ischemia despite adequate epicardial reperfusion. This is the case in acute myocardial infarction after successful stenting but accompanied by no-reflow (reflected by persistent chest pain or ST-elevation) or after bypass surgery with stunning and ischemic but viable myocardium. Large randomized clinical trials are mandatory to support these views (and have been started in the meantime).

References

- Abdolrazaghi M., Navidbakhsh M., Hassani K.; Mathematical modelling of intra-aortic balloon pump; *Computer Methods in Biomechanics and Biomedical Engineering*, 13(5): 567-576, 2010.
- Abe H., Ito Y., Tada M., Opie L.H.; Regulation of cardiac function: molecular, cellular and pathophysiological aspects; *Japan Scientific Societies Press*, Tokyo, 1984.
- Alpert J., Bhaktan E.K., Gielchinsky I., Gilbert L., Brener B.J., Brief D.K., Parsonnet V.; Vascular complications of intra-aortic balloon pumping; *Archives of Surgery*, 111: 1190-1195, 1976.
- Arts T., Bovendeerd P.H., Prinzen F.W., Reneman R.S.; Relation between left ventricular cavity pressure and volume and systolic fiber stress and strain in the wall; *Biophysical Journal*, 59: 93-102, 1991.
- Azevedo C.F., Amado L.C., Kraitchman D.L., Gerber B.L., Edvardsen T., Osman N.F.; The effect of intra-aortic balloon counterpulsation on left ventricular functional recovery early after acute myocardial infarction: a randomized experimental magnetic resonance imaging study; *European Heart Journal*, 26: 1235-1241, 2005.
- Balao L.A., Boston J.R., Antaki J.F.; Elastance-based control of a mock circulatory system; *Annals of Biomedical Engineering*, 29: 244-251, 2001.
- Bellamy R.F.; Diastolic coronary artery pressure-flow relations in dog; *Circulation Research*, 43: 92-101, 1978.
- Biglino G., Verschueren P., Zegels R., Taylor A.M., Schievano S.; Rapid prototyping compliant arterial phantoms for in-vitro studies and device testing; *Journal of Cardiovascular magnetic Resonance*, 15: 2, 2013.
- Birks E.J., Tansley P.D., Hardy J., George R.S., Bowles C.T., Burke M., Banner N.R., Khaghani A., Yacoub M.H.; Left ventricular assist device and drug therapy for the reversal of heart failure; *The New England Journal of Medicine*, 355: 1873-1884, 2006.
- Bolli R., Triana J.F., Jeroudi M.O.; Prolonged impairment of coronary vasodilation after reversible ischemia. Evidence for microvascular "stunning"; *Circulation Research*, 67: 332-343, 1990.
- Botman C.J., Schonberger J., Koolen S., Penn O., Botman H., Dib N., Eeckhout E., Pijls N.H.J.; Does stenosis severity of native vessels influence bypass graft patency? A prospective fractional flow reserve guided study; *The Annals of Thoracic Surgery*, 83: 2093-2097, 2007.
- Bovendeerd P.H.M., Borsje P., Arts T., Van de Vosse F.N.; Dependence of intramyocardial pressure and coronary flow on ventricular loading and contractility: a model study; *Annals of Biomedical Engineering*, 34(12): 1833-1845, 2006.

- Bregman D., Goetz R.H.; Clinical experience with a new cardiac assist device: the dual-chambered intra-aortic balloon assist; *The Journal of Thoracic Cardiovascular surgery*; 62: 577-591, 1971.
- Bregman D., Nichols B., Weiss M.B., Powers E.R., Martin E.C., Casarella W.J.; Percutaneous intraaortic balloon insertion; *American Journal of Cardiology*, 46: 261-264, 1980.
- De Bruyne B., Pijls N.H.J., Barbato E., Bartunek J., Bech J.W., Wijns W., Heyndrickx G.R.; Intracoronary and intravenous adenosine 5'-triphosphate, adenosine, papaverine, and contrast medium to assess fractional flow reserve in humans; *Circulation*, 107: 1877-1883, 2003.
- Bünger R., Haddy F.J., Querengässer A., Gerlach E.; An isolated guinea pig heart preparation with *in vivo* like features; *Pfluegers Archive European Journal of Physiology*, 353: 317-326, 1975.
- Cheng J.M., Den Uil C.A., Hoeks S.E., Van der Ent M., Jewbali L.S.D., Van Domburg R.T., Serruys P.W.; Percutaneous left ventricular assist devices vs. intra-aortic balloon pump counterpulsation for treatment of cardiogenic shock: a meta-analysis of controlled trials; *European Heart Journal*, 30: 2102-2108, 2009.
- Colacino F.M., Arabia M., Moscato F., Danieli G.A.; Modeling analysis, and validation of a pneumatically driven left ventricle for use in mock circulatory systems; *Medical Engineering and Physics*, 29: 829-839, 2007.
- Colacino F.M., Moscato F., Piedimonte F., Danieli G., Nicosia S., Arabia M.; A modified elastance model to control mock ventricles in real-time: Numerical and experimental validation; *American Society for Artificial Internal Organs Journal*, 54: 563-573, 2008.
- Cornhill J.F.; An aortic-left ventricular pulse duplicator used in testing prosthetic aortic heart valves; *The Journal of Thoracic Cardiovascular Surgery*, 73: 550-558, 1977.
- Cox L.G.E., Loerakker S., Rutten M.C.M., De Mol B.A.J.M., Van de Vosse F.N.; A mathematical model to evaluate control strategies for mechanical circulatory support; *Artificial Organs*, 33(8): 593-603, 2009.
- Deng M.C.; Cardiac transplantation; *Heart*, 87: 177-184, 2002.
- Digerness S.B., Kirklin J.W., Naftel D.C., Blackstone E.H., Kirklin J.K., Samuelson P.N.; Coronary and systemic vascular resistance during reperfusion and global myocardial ischaemia; *The Annals of Thoracic Surgery*, 46: 447-454, 1988.
- Erasmí A., Sievers H.H., Scharfshwerdt M., Eckel T., Misfeld M.; *In vitro* hydrodynamics, cusp-bending deformation, and root distensibility for different types of aortic valve-sparing operations: remodeling, sinus prosthesis, and reimplantation; *Journal of Thoracic Cardiovascular Surgery*, 130: 1044-1049, 2005.

- Fearon W.F., Balsam L.B., Farougue H.M., Caffarelli A.D., Robbins R.C., Fitzgerald P.J., Yock P.G., Yeung A.C.; Novel index for invasively assessing the coronary microcirculation; *Circulation*, 107: 3129-3132, 2003.
- Feola M., Haiderer O., Kennedy J.H.; Intra-aortic balloon pumping (IABP) at different levels of experimental acute left ventricular failure; *Chest*, 59: 68-76, 1971.
- Ferrari G., De Lazzari C., Kozarski M., Clemente F., Gorczyńska K., Mimmo R., Monnanni E., Tosti G., Guaragno M.; A hybrid mock circulatory system: testing a prototype under physiologic and pathological conditions; *American Society of Artificial Internal Organs*, 48: 487-494, 2002.
- Franklin G.F., Powell J.D., Emami-Naeini A.; Feedback control of dynamic systems; *Prentice Hall*, Upper Saddle River, 2002.
- Fresiello L., Khir A.W., Molfetta A.D., Kozarski M., Ferrari G.; Effects of intra-aortic balloon pump timing on baroreflex activities in a closed-loop cardiovascular hybrid model; *Artificial Organs*, 37: 237-247, 2013.
- Furchgott R.F., Zawadzki J.V.; The obligatory role of endothelial cells in the relaxing of arterial smooth muscle by acetylcholine; *Nature*, 288: 373-376, 1980.
- Fuster V., Alexander R.W., O'Rourke R.A.; Hurst's The Heart; *McGraw-Hill*, New York, 2001.
- George R.S., Birks E.J., Cheetham A., Webb C., Smolenski R.T., Khaghani A., Yacoub M.H., Kelion A.; The effect of long-term left ventricular assist device support on myocardial sympathetic activity in patients with non-ischaemic dilated cardiomyopathy; *European Journal of Heart Failure*, 15: 1035-1043, 2013.
- Geven M.C.F., Bohté V.N., Aarnoudse W.H., Van den Berg P.M.J., Rutten, M.C.M., Pijls N.H.J., Van de Vosse F.N.; A physiologically representative *in vitro* model of the coronary circulation; *Physiological Measurement*, 25: 891-904, 2004.
- Gewirtz H., Ohley W., Williams D.O., Sun Y., Most A.S.; Effect of intraaortic balloon counterpulsation on regional, myocardial blood flow and oxygen consumption in the presence of coronary artery stenosis: observations in an awake animal model; *American Journal of Cardiology*, 50: 829-837, 1982.
- Gill C.C., Wechsler A.S., Newman G.E., Oldham H.N.; Augmentation and redistribution of myocardial blood flow during acute ischemia by intraaortic balloon pumping; *The Annals of Thoracic Surgery*, 16: 445-453, 1973.
- Griffith G.C., Wallace W.B., Cochran B., Nerlich W.E., Frasher W.G.; The treatment of shock associated with myocardial infarction; *Circulation*, 9: 527-532, 1954.
- Guyton A.C., Hall J.E.; Textbook of medical physiology; *Elsevier Saunders*, Philadelphia, 2006.
- De Hart J., De Weger A., Van Tuijl S., Stijnen J.M.A., Van den Broek C.N., Rutten M.C.M., De Mol B.A.; An *ex vivo* platform to simulate cardiac physiology: a new

- dimension for therapy development and assessment; *International Journal of Artificial Organs*, 34: 495-505, 2011.
- Haston H.H., McNamara J.J.; The effects of intraaortic balloon counterpulsation on myocardial infarct size; *The Annals of Thoracic Surgery*, 28: 335-341, 1979.
- Hearse D.J., Maxwell L., Saldanha C., Gavin J.B.; The myocardial vasculature during ischaemia and reperfusion: a target for injury and protection; *Journal of Molecular and Cellular Cardiology*, 25: 759-800, 1993.
- Henriques J.P.; Rimmelink M., Baan J.; Safety and feasibility of elective high-risk percutaneous coronary intervention procedures with left ventricular support of the Impella Recover LP 2.5; *American Journal of Cardiology*, 97: 990-992, 2006.
- Hill A.; The heat of shortening and the dynamic constants in muscle; *Proceedings of the Royal Society London*, 126: 136-165, 1938.
- Hiratzka L.F., Eastham C.L., Carter J.G.; The effects of cardiopulmonary bypass and cold cardioplegia on coronary flow velocity and the reactive hyperaemic response in patients and dogs; *The Annals of Thoracic Surgery*, 45: 474-481, 1987.
- Hirsch L.J., Lluch S., Katz L.N.; Counterpulsation effects of coronary blood flow and cardiac oxygen utilization; *Circulation Research*, 19: 1031-1040, 1966.
- Van 't Hof A.W., Liem A.L., De Boer M.J., Hoorntje J.C., Suryapranata H., Zijlstra F.; A randomized comparison of intra-aortic balloon pumping after primary coronary angioplasty in high risk patients with acute myocardial infarction; *European Heart Journal*, 20: 659-665, 1999.
- Hoffman J.I.E., Spaan J.A.E.; Pressure-flow relations in coronary circulation; *Physiological Reviews*, 70: 331-390, 1990.
- Iaizzo P.A.; Handbook of Cardiac Anatomy, Physiology, and Devices; *Humana Press*, Totowa, 2005.
- Jayaweera A.R., Wei K., Coggins M., Bin J.P., Goodman C., Kaul S.; Role of capillaries in determining CBF reserve: new insights using myocardial contrast echocardiography; *The American Journal of Physiology Heart and Circulatory Physiology*, 227: 2363-2372, 1999.
- Jimenez J.H., Forbess J., Croft L.R., Small L., He Z.M., Yoganathan A.P.; Effects of annular size, transmitral pressure, and mitral flow rate on the edge-to-edge repair: an *in vitro* study; *The Annals of Thoracic Surgery*, 82: 1362-1368, 2006.
- Jung C., Lauten A., Rödiger C., Krizanac F., Figulla H.R., Ferrari M.; Effect of intra-aortic balloon pump support on microcirculation during high-risk percutaneous intervention; *Perfusion*, 24(6): 417-421, 2009.
- Kantrowitz A., Kantrowitz A.; Experimental augmentation of coronary blood flow by retardation of the arterial pressure pulse; *Surgery*, 34: 678-687, 1953.

- Kantrowitz A., McKinnon W.M.P.; The experimental use of the diaphragm as an auxiliary myocardium; *Surgical Forum*, 9: 266-268, 1958.
- Kantrowitz A., Tjonneland S., Freed P.S., Philips S.J., Butner A.N., Sherman J.L.; Initial clinical experience with intra-aortic balloon pumping in cardiogenic shock; *The Journal of the American Medical Association*, 203(2): 113-118, 1968.
- Kantrowitz A., Cardona R.R., Freed P.S.; Percutaneous intra-aortic balloon counterpulsation; *Critical Care Clinics*, 8: 819-837, 1992.
- Kelm M., Schrader J.; Control of coronary vascular tone by nitric oxide; *Circulation Research*, 66: 1561-1575, 1990.
- Kelman G.R.; Digital computer subroutine for the conversion of oxygen tension into saturation; *Journal of Applied Physiology*, 21: 1375-1376, 1966.
- Kentish J.C., Ter Keurs H.E., Ricciardi L., Bucx J.J., Noble M.I.; Comparison between the sarcomere length-force relations of intact and skinned trabeculae from rat right ventricle. Influence of calcium concentrations on these relations; *Circulation Research*, 58: 755-768, 1986.
- Kern M.J., Aguirre F., Bach R., Donohue T., Siegel R., Segal J.; Augmentation of coronary blood flow by intra-aortic balloon pumping in patients after coronary angioplasty; *Circulation*, 87: 500-511, 1993.
- Kern M.J., Aguirre F.V., Tatineni S., Penick D., Serota H., Donohue T.; Enhanced coronary blood flow velocity during intraaortic balloon counterpulsation in critical ill patients; *Journal of the American College of Cardiology*, 21: 359-368, 1993.
- Kern M.J., Aguirre F.V., Caracciolo E.A., Bach R.G., Donohue T.J., Lasorda D., Ohman E.M., Schnitzler R.N., King D.L., Qhley W.J., Grayzel J.; Hemodynamic effects of new intra-aortic balloon counterpulsation timing methods in patients: a multicenter evaluation; *American Heart Journal*, 137(6): 1129-1136, 1999.
- Khalid L., Dhakam S.H.; A review of cardiogenic shock in acute myocardial infarction; *Current Cardiology Reviews*, 4(1): 34-40, 2008.
- Khair A.W., Price S., Hale C., Young D.A., Parker K.H., Pepper J.R.; Intra-aortic balloon pumping: Does posture matter?; *Artificial Organs*, 29(1): 36-40, 2005.
- Kimura A., Toyota E., Lu S., Masami G., Toyotaka Y., Yoko C., Jun E., Hiroyuki T., Yasuo O., Katsuhiko T., Fumihiko K.; Effects of intraaortic balloon pumping on septal arterial blood flow velocity waveform during severe left main coronary artery; *Journal of the American College of Cardiology*, 27: 810-816, 1996.
- Kolyva C., Pantalos G.M., Pepper J.R., Khair A.W.; How much of the intraaortic balloon volume is displaced toward the coronary circulation?; *Journal of Thoracic and Cardiovascular Surgery*, 140(1): 110-116, 2010.

- Kolyva C., Biglino G., Pepper J.R., Khir A.W.; A mock circulatory system with physiological distribution of terminal resistance and compliance: application for testing the intra-aortic balloon pump; *Artificial Organs*, 36(3): E62-E70, 2012.
- Korakianitis T., Shi Y.; A concentrated parameter model for the human cardiovascular system including heart valve dynamics and atrioventricular interaction; *Medical Engineering and Physics*, 28: 613-628, 2006.
- Kostic M.M., Schrader J.; Role of nitric oxide in reactive hyperemia of the guinea pig heart; *Circulation Research*, 70: 208-212, 1992.
- Krishna M., Zacharowski K.; Principles of intra-aortic balloon pump counterpulsation; *Continuing Education in Anaesthesia, Critical Care & Pain*, 9: 24-28, 2009.
- Kuklinski W.S., Jaron D., Ohley W.J., Greenall R.K.; The intraaortic balloon pump: a nonlinear digital computer model; *Journal of Biomechanical Engineering*, 106: 220-228, 1984.
- Lefemine A.A., Low H.B.C., Cohen M.L., Lunzer S., Harken D.E.; Assisted circulation. III. The effect of synchronized arterial counterpulsation on myocardial oxygen consumption and coronary flow; *American Heart Journal*, 64: 789-795, 1962.
- Leinbach R.C., Buckley M.J., Austen W.G., Petschek H.E., Kantrowitz A.R., Sanders C.A.; Effects of intra-aortic balloon pumping on coronary flow and metabolism in man; *Circulation*, 43: 77-81, 1971.
- Leopaldi A.M., Vismara R., Lemma M., Valerio L., Cervo M., Mangini A., Contino M., Redaelli A., Antona C., Fiore G.B.; *In vitro* hemodynamics and valve imaging in passive beating hearts; *Journal of Biomechanics*, 45: 1133-1139, 2012.
- Leopaldi A.M., Vismara R., Gelpi G., Romagnoni C., Fiore G., Redaelli A., Lemma M., Antona C.; Intracardiac visualization of transcatheter aortic valve and valve-in-valve implantation in an *in vitro* passive beating heart; *Journal of the American College of Cardiology*, 6: 92-93, 2013.
- Matthys K., Carlier S., Segers P., Ligthart J., Sianos G., Serrano P., Verdonck P.R., Serruys P.W.; *In vitro* study of FFR, QCA, and IVUS for the assessment of optimal stent deployment; *Catheterization and Cardiovascular Intervention*, 54: 363-375, 2001.
- McGeoch R.J., Oldroyd K.G.; Pharmacological options for inducing maximal hyperaemia during studies of coronary physiology; *Catheterization and Cardiovascular Intervention*, 71: 198-204, 2008.
- McGinn A.L., White C.W., Wilson R.F.; Interstudy variability of coronary flow reserve. Influence of heart rate, arterial pressure, and ventricular preload; *Circulation*, 81: 1319-1330, 1990.

- Meyns B., Dens J., Sergeant P.; Initial experiences with the Impella device in patients with cardiogenic shock – Impella support for cardiogenic shock; *The Thoracic and Cardiac Surgeon*, 51(6): 312-317, 2003.
- Modersohn D., Eddicks S., Grosse-Siestrup C., Ast I., Holinski S., Konertz W.; Isolated hemoperfused heart model of slaughterhouse pigs; *International Journal of Artificial Organs*, 24: 215-221, 2011.
- Van de Molengraft M.J.G., Veldpaus F.E., Kok J.J.; An optimal estimation method for nonlinear models of mechanical systems; *Journal of Dynamic Systems Measurement and Control*, 116: 805-810, 1994.
- Moulopoulos S.D., Topaz S., Kolff W.J.; Diastolic balloon pumping (with carbon dioxide) in the aorta: A mechanical assistance to the failing circulation; *American Heart Journal*, 63: 669-675, 1962.
- Mueller H., Ayres S.M., Conklin E.J., Giannelli S., Mazzara J.T., Grace W.T., Nealon T.F.; The effects of intra-aortic counterpulsation on cardiac performance and metabolism in shock associated with acute myocardial infarction; *Journal of Clinical Investigation*, 50: 1885-1900, 1971.
- Ntalianis A.S., Drakos S.G., Charitos C., Dolou P., Pierrakos C.N., Terrovitis J.V., Papaioannou T., Charitos E., Nanas J.N.; Effects of intra-aortic balloon pump versus centrifugal pump on myocardial energetics and systemic circulation in a porcine model of rapidly worsening acute heart failure; *American Society of Artificial Internal Organs Journal*, 54: 600-605, 2008.
- Van Nunen L.X., Van 't Veer M., Schampaert S., Steerneman B.J.E.M., Rutten M.C.M., Van de Vosse F.N., Pijls N.H.J.; Intra-aortic balloon counterpulsation in acute myocardial infarction: old and emerging indications; *Netherlands Heart Journal*, 21(12): 554-560, 2013.
- Van Nunen L.X., Van 't Veer M., Schampaert S., Rutten M.C.M., Van de Vosse F.N., Patel M.R., Pijls N.H.J.; Intra-aortic balloon counterpulsation reduces mortality in large anterior myocardial infarction complicated by persistent ischemia; a CRISP AMI substudy; *EuroIntervention*, (-):-, accepted.
- Ochsner G., Amacher R., Amstutz A., Plass A., Schmid Daners M., Tevaearai H., Vandenberghe S., Wilhelm M.J., Guzzella L.; A novel interface for hybrid mock circulations to evaluate ventricular assist devices; *IEEE Transactions on Biomedical Engineering*, 60: 507-516, 2013.
- O'Gara P.T., Kushner F.G., Ascheim D.D., Casey D.E., Chung M.K., De Lemos J.A., Ettinger S.M., Fang J.C., Fesmire F.M., Franklin B.A., Granger C.B., Krumholz H.M., Linderbaum J.A., Morrow D.A., Newby L.K., Ornato J.P., Ou N., Radford M.J., Tamis-Holland J.E., Tommaso C.L., Tracy C.M., Woo Y.J. Zhao D.X.; 2013 ACCF/AHA Guideline for the management of ST-elevation myocardial infarction: a report of

- the American College of Cardiology Foundation/American Heart Association task force on practice guidelines; *Journal of the American College of Cardiology*, 61(4): e78-e140, 2013.
- Olivecrona G.; Coronary reactive hyperemia; *KFS AB*, Lund, 2007.
- Pantalos G.M., Koenig S.C., Gillars K.J., Giridharan G.A., Ewert D.L.; Characterization of an adult mock circulation for testing cardiac support devices; *American Society of Artificial Internal Organs Journal*, 50: 37-46, 2004.
- Papaioannou T.G., Mathioulakis D.S., Nanas J.N., Tsangaris S.G., Stamatelopoulos S.F., Mouloupoulos S.D.; Arterial compliance is a main variable determining the effectiveness of intra-aortic balloon counterpulsation: quantitative data from an *in vitro* study; *Medical Engineering & Physics*, 24: 279-284, 2002.
- Patel M.R., Smalling R.W., Thiele H., Barnhart H.X., Zhou Y., Chandra P., Chew D., Cohen M., French J., Perera D., Ohman E.M.; Intra-aortic balloon counterpulsation and infarct size in patients with acute anterior myocardial infarction without shock: the CRISP AMI randomized trial; *Journal of the American Medicine Association*, 306: 1329-1337, 2011.
- Perera D., Stables R., Thomas M., Booth J., Pitt M., Blackman D., De Belder A., Redwood S.; Elective intra-aortic balloon counterpulsation during high-risk percutaneous coronary intervention: a randomized controlled trial; *Journal of the American Medicine Association*, 304: 867-874, 2010.
- Pijls N.H.J., Van Son J.A., Kirkeeide R.L., De Bruyne B., Gould K.L.; Experimental basis of determining maximum coronary, myocardial, and collateral blood flow by pressure measurements for assessing functional stenosis severity before and after percutaneous transluminal coronary angioplasty; *Circulation*, 87: 1354-1367, 1993.
- Pohl U., Lamontagne D., Bassenge E., Busse R.; Attenuation of coronary autoregulation in the isolated rabbit heart by endothelium derived nitric oxide; *Cardiovascular Research*, 28: 414-419, 1994.
- Powell W.J., Dagget W.M., Magro A.E., Bianco J.A., Buckley M.J., Sanders C.A., Kantrowitz A.R., Austen W.G.; The effects of intra-aortic balloon counterpulsation on cardiac performance, oxygen consumption, and coronary blood flow in dogs; *Circulation Research*, 26: 753-764, 1970.
- Raess D.H., Weber D.M.; Impella 2.5; *Journal of Cardiovascular Translational Research*, 2: 168-172, 2009.
- Reimer K.A., Murry C.E., Yamasawa I., Hill M.L., Jennings R.B.; Four brief periods of myocardial ischemia cause no cumulative ATP loss or necrosis; *American Journal of Physiology*, 25: 1306-1315, 1986.

- Remmelink M., Sjauw K.D., Henriques J.P.S., Vis M.M., Koch K.T., Tijssen J.G.; Effects of left ventricular unloading by Impella Recover LP2.5 on coronary hemodynamics; *Catheterization and Cardiovascular Intervention*, 70: 532-537, 2007.
- Remmelink M., Sjauw K.D., Henriques J.P.S., De Winter R.J., Vis M.M., Koch K.T., Paulus W.J., De Mol B.A.J.M., Tijssen J.G.P., Piek J.J., Baan J.; Effects of mechanical left ventricular unloading by Impella on left ventricular dynamics in high-risk and primary percutaneous coronary intervention patients; *Catheterization and Cardiovascular Intervention*, 75: 187-194, 2010.
- Reul H., Minamitani H., Runge J.; A hydraulic analog of the systemic and pulmonary circulation for testing the artificial hearts; *Proceedings of European Society of Artificial Organs*, 2: 120-127, 1975.
- Reynolds H.R., Hochman J.S.; Cardiogenic shock. Current concepts and improving outcomes; *Circulation*, 117: 686-697, 2008.
- Richards A.L., Cook R.C., Bolotin G., Buckner G.D.; A dynamic heart system to facilitate the development of mitral valve repair techniques; *Annals of Biomedical Engineering*, 37: 651-660, 2009.
- Van Roon A.M., Mulder L.J., Althaus M., Mulder G. Introducing a baroreflex model for studying cardiovascular effects of mental workload; *Psychophysiology*, 41: 961-981, 2004.
- Saini V.K., Hood W.B., Hechtman H.B., Berger R.L.; Nutrient myocardial blood flow in experimental myocardial ischemia; *Circulation*, 52: 1086-1090, 1975.
- Santa-Cruz R.A., Cohen M.G., Ohman E.M.; Aortic counterpulsation: a review of the hemodynamic effects and indications for use; *Catheterization and Cardiovascular Interventions*, 67: 68-77, 2006.
- Sato H., Hori M., Ozaki H., Yokoyama H., Imai K., Morikawa M., Takeda H., Inoue M., Kamada T.; Exercise-induced upward shift of diastolic left ventricular pressure-volume relation in patients with dilated cardiomyopathy. Effects of beta-adrenoceptor blockade; *Circulation*, 88: 2215-2223, 1993.
- Schampaert S., Pennings K.A.M.A., Van de Molengraft M.J.G., Pijls N.H.J., Van de Vosse F.N., Rutten M.C.M.; A mock circulation model for cardiovascular device evaluation; *Physiological Measurement*, 35: 687-702, 2014.
- Schampaert S., Van 't Veer M., Rutten M.C.M., Van Tuijl S., De Hart J., Van de Vosse F.N., Pijls N.H.J.; Autoregulation of coronary blood flow in the isolated beating pig heart; *Artificial Organs*, 37: 724-730, 2013.
- Scheidt S., Wilner G., Mueller H., Summers D., Lesch M., Wolff G., Krakauer J., Rubenfire M., Fleming P., Noon G., Oldham N., Killip T., Kantrowitz A.; Intra-aortic balloon counterpulsation in cardiogenic shock. Report of a co-operative clinical trial; *New England Journal of Medicine*, 228: 979-984, 1973.

- Schreurs P.J.G.; Discrete System Computation; *Eindhoven University of Technology*, Eindhoven, 2012.
- Segers P., Fostier G., Neckebroeck J., Verdonck P.; Assessing coronary artery stenosis severity: *in vitro* validation of the concept of fractional flow reserve; *Catheterization and Cardiovascular Intervention*, 46: 375-379, 1999.
- Seyfarth M., Sibbing D., Bauer I., Fröhlich G., Bott-Flügel L., Byrne R., Dirschinger J., Kastrati A., Schömig A.; A randomized clinical trial to evaluate the safety and efficacy of a percutaneous left ventricular assist device versus intra-aortic balloon pumping for treatment of cardiogenic shock caused by myocardial infarction; *Journal of the American College of Cardiology*, 52(19): 1584-1588, 2008.
- Shaw J., Taymor D.R., Pitt B.; Effects of intraaortic balloon counterpulsation on regional coronary blood flow in experimental myocardial infarction; *American Journal of Cardiology*, 34: 552-556, 1974.
- De Silva K., Lumley M., Kailey B., Alastruey J., Guilcher A., Asrress K.N., Plein S., Marber M., Redwood S., Perera D.; Coronary and microvascular physiology during intra-aortic balloon counterpulsation; *Journal of the American College of Cardiovascular Interventions*, -():-, 2014
- Sjauw K.D., Engstrom A.E., Henriques J.P.S.; Percutaneous mechanical cardiac assist in myocardial infarction. Where are we now, where are we going?; *Acute Cardiac Care*, 9: 222-230, 2007.
- Smith B., Barnea O., Moore T.W.; Optimal control system for the intra-aortic balloon pump; *Medical and Biological Engineering and Computing*, 29: 180-184, 1991.
- Spaan J.A.E., Piek J.J., Hoffman J.I.E., Siebes M.; Physiological basis of clinically used coronary hemodynamic indices; *Circulation*, 113: 446-455, 2006.
- Steg P.G., James S.K., Atar D., Badano L.P., Blömstrom-Lundqvist C., Borger M.A., Di Mario C., Dickstein K., Ducrocq G., Fernandez-Aviles F., Gershlick A.H., Giannuzzi P., Halvorsen S., Huber K., Juni P., Kastrati A., Knuuti J., Lenzen M.J., Mahaffey K.W., Valgimigli M., Van 't Hof A., Widimsky P., Zahger D.; ESC guidelines for the management of acute myocardial infarction in patients presenting with ST-segment elevation: the task force on the management of ST-segment elevation acute myocardial infarction of the European Society of Cardiology (ESC); *European Heart Journal*, 33: 2569-2619, 2012.
- Stone G.W., Marsalese D., Brodie B.R., Griffin J.J., Donohue B., Costantini C.; A prospective, randomized evaluation of prophylactic intraaortic balloon counterpulsation in high risk patients with acute myocardial infarction treated with primary angioplasty. Second primary angioplasty in myocardial infarction (PAMI-II) trial investigators; *Journal of American College of Cardiology*, 29: 1459-1467, 1997.

- Subramanian V.A., Goldstein J.E., Sos T.A., McCabe J.C., Hoover E.A., Gay W.A.; Preliminary clinical experience with percutaneous intraaortic balloon pumping; *Circulation*, 62(suppl I): 123-129, 1980.
- Suga H.; Ventricular energetic; *The American Physiological Society*, 70: 247-277, 1990.
- Suga H., Sagawa K., Shoukas A.A.; Load independence of the instantaneous pressure-volume ratio of the canine left ventricle and effects of epinephrine and heart rate on the ratio; *Circulation Research*, 32: 314-322, 1973.
- Sun Y.; Modeling the dynamic interaction between left ventricle and intra-aortic balloon pump; *American Physiological Society*, 261: 1300-1311, 1991.
- Swank M., Singh H.M., Flemma R.J., Mullen D.C., Lepley D.; Effect of intra-aortic balloon pumping on nutrient coronary flow in normal and ischemic myocardium; *The Journal of Thoracic and Cardiovascular Surgery*, 76: 538-544, 1978.
- Takada M., Nadeau K., Hancock W.W., Mackenzie H.S., Shaw G.D., Waaga A.M., Chandraker A., Sayegh M.H., Tilney N.L.; Effects of explosive brain death on cytokine activation of peripheral organs in the rat; *Transplantation*, 65: 1533-1542, 1998.
- Takeuchi M., Nohtomi Y., Yoshitani H., Miyazaki C., Sakamoto K., Yoshikawa J.; Enhanced coronary flow velocity during intra-aortic balloon pumping assessed by transthoracic Doppler echocardiography; *Journal of the American College of Cardiology*, 43(3): 368-376, 2004.
- Thiele H., Zeymer U., Neumann F.J., Ferenc M., Olbrich H.G., Hausleiter J., Richardt G., Hennersdorf M., Empen K., Fuernau G., Desch S., Eitel I., Hambrecht R., Fuhrmann J., Böhm M., Ebel H., Schneider S., Schuler G., Werdan K.; Intraaortic balloon support for myocardial infarction with cardiogenic shock; *The New England Journal of Medicine*, 367: 1287-1296, 2012.
- Timms D., Hayne M., McNeil K., Galbraith A.; A complete mock circulation loop for the evaluation of left, right, and biventricular assist device; *Artificial Organs*, 29(7): 564-572, 2005.
- Timms D., Gregory S., Greatrex N., Percy M., Fraser J., Steinseifer U.; A compact mock circulation loop for *in vitro* testing of cardiovascular devices; *Artificial Organs*, 35: 384-391, 2010.
- Tonino P.A.L., De Bruyne B., Pijls N.H.J., Siebert U., Ikeno F., Van 't Veer M., Klauss V., Manoharan G., Engstrøm T., Oldroyd K.G., Ver Lee P.N., MacCarthy P.A., Fearon W.F.; Fractional flow reserve versus angiography for guiding percutaneous coronary intervention; *New England Journal of Medicine*, 360: 213-224, 2009.
- Urschel C.W., Eber L., Forrester J., Matloff J., Carpenter R., Sonnenblick E.; Alteration of mechanical performance of the ventricle by intra-aortic balloon counterpulsation; *American Journal of Cardiology*, 25: 546-551, 1970.

- Vaes M., Rutten M., Van de Molengraft R., Van de Vosse F.; Left ventricular assist device evaluation with a model-controlled mock circulation; *Proceedings of the American Society of Mechanical Engineers Summer Bioengineering Conference (Keystone, Colorado, 20-24 June)*, 2007.
- Vandenberghe S., Segers P., Josemans H., Van Loon J.P., Rakhorst G., Verdonck P.R.; *In vitro* assessment of the unloading and perfusion capacities of the PUCA II and the IABP; *Perfusion*, 19(1): 25-32, 2004.
- Vandenberghe S., Segers P., Steendijk P., Meyns B., Dion R.A.E., Antaki J.F., Verdonck P.; Modeling ventricular function during cardiac assist: Does time-varying elastance work?; *American Society of Artificial Internal Organs Journal*, 52(1): 4-8, 2006.
- Warnock J.N., Konduri S., He Z., Yoganathan A.P.; Design of a sterile organ culture system for the ex vivo study of aortic heart valves; *Journal of Biomechanical Engineering*, 127: 857-861, 2005.
- Watson J.T., Willerson J.T., Fixler D.E., Sugg W.L.; Temporal changes in collateral coronary blood flow in ischemic myocardium during intra-aortic balloon pumping; *Circulation*, 50: 249-254, 1974.
- Watson J.T., Fixler D.E., Plat M.R., Nall B.B., Jet G.K., Willerson J.T.; The influence of combined intra-aortic balloon counterpulsation and hyperosmotic mannitol on regional myocardial blood flow in ischemic myocardium in the dog; *Circulation*, 38: 506-513, 1976.
- Weber K.T., Janicki J.S.; Intra-aortic balloon counterpulsation: a review of physiological principles, clinical results, and device safety; *The Annals of Thoracic Surgery*, 17: 602-636, 1974.
- De Weger A., Van Tuijl S., Stijnen J.M.A., Steendijk P., De Hart J.; Direct endoscopic visual assessment of a transcatheter aortic valve implantation and performance in the PhysioHeart, an isolated working heart platform; *Circulation*, 121: 261-262, 2010.
- Weisfeldt M.L., Shock N.W.; Effect of perfusion pressure on coronary flow and oxygen usage of nonworking heart; *American Journal of Physiology*, 218: 95-101, 1970.
- Westerhof N., Bosman F., De Vries C.J., Noordergraaf A.; Analog studies of the human systemic arterial tree; *Journal of Biomechanics*, 2: 121-143, 1969.
- Westerhof N.; Cardiac work and efficiency; *Cardiovascular Research*, 48: 4-7, 2000.
- Wijns W., Kolh P., Danchin N., Di Mario C., Falk V., Folliguet T., Garg S., Huber K., James S., Knuuti J., Lopez-Sendon J., Marco J., Menicanti L., Ostojic M., Piepoli M.F., Pirlet C., Pomar J.L., Reifart N., Ribichini F.L., Schalij M.J., Sergeant P., Serruys

- P.W., Silber S., Sousa Uva M., Taggart D.; Guidelines on myocardial revascularization; *European Heart Journal*, 31: 2501-2555, 2010.
- Willerson J.T., Watson J.T., Plat M.R.; Effect of hypertonic mannitol and intraaortic counterpulsation on regional myocardial blood flow and ventricular performance in dogs during myocardial ischemia; *American Journal of Cardiology*, 37: 514-519, 1976.
- Williams D.O., Korr K.S., Gewirtz H., Most A.S.; The effect of intraaortic balloon counterpulsation on regional myocardial blood flow and oxygen consumption in the presence of coronary artery stenosis in patients with unstable angina; *Circulation*, 66: 593-597, 1982.
- Wolvek S.; The evolution of the intra-aortic balloon: The Datascope contribution; *Journal of Biomaterials Applications*, 3(4): 527-534, 1989.
- Yoshitani H., Akasaka T., Kaji S., Kawamoto T., Kume T., Neishi Y., Koyama Y., Yoshida K.; Effects of intra-aortic balloon counterpulsation on coronary pressure in patients with stenotic coronary arteries; *American Heart Journal*, 154(4): 725-731, 2007.
- Zehetgruber M., Mundigler G., Christ G., Merhaut C., Klaar U., Kratochwill C., Neunteufl T., Hofmann S., Heinz G., Maurer G., Siostrzonek P.; Relation of hemodynamic variables to augmentation of left anterior descending coronary flow by intraaortic balloon pulsation in coronary artery disease; *The American Journal of Cardiology*, 80: 951-955, 1997.

Summary

Computational and experimental characterization of intra-aortic balloon pump support

The intra-aortic balloon pump (IABP) is a minimally invasive cardiac assist device. By rapid inflation and deflation of the catheter-mounted polyurethane balloon, synchronous with the cardiac cycle, it induces a diastolic blood pressure augmentation as well as a systolic reduction in afterload. Although these blood pressure changes are expected to create clinical improvement in terms of coronary perfusion and myocardial oxygen consumption, the measured effects reported in literature are inconsistent and ambiguous in human and experimental studies. Therefore, the research described in this thesis focusses on using an integrated method of computational, *in vitro*, *ex vivo*, and *in vivo* models to characterize the IABP and its impact on cardiac and coronary hemodynamics, in order to predict clinical settings in which its use would be most effective.

In **chapter 2**, a computational model was presented and validated that couples a 0-dimensional lumped parameter model to an elaborate heart contraction model, which was based on microstructural material and macrostructural geometrical properties. The IABP was modeled as a cylinder-shaped collapsible tube with a cross-sectional area concentric with the vessel at any moment in time. In this system, the interaction between the IABP and the cardiovascular system, and how alterations of specific IABP parameters (i.e., timing) affect this coupling, was tested. For validation purposes, data were collected from ten patients undergoing IABP therapy. In both model and patients, the support capabilities of the IABP benefitted the most when the balloon was deflated simultaneously with ventricular contraction, whereas inflation before onset of diastole unconditionally interfered with ejection.

To address the need for a hydraulic circuit that function in a physiologic manner for testing cardiovascular devices under well-controlled circumstances, an integrated mock circulation system was developed in **chapter 3**. The model featured an elaborate heart contraction model, a realistic frequency control model, and a relatively simple lead-lag controller. The behavior of the system was tested in response to changes in left ventricular contractile states, loading conditions, and heart rate. The physiologic response indicates a proper implementation of the incorporated feedback mechanisms and allows the presented set-up for *in vitro* testing of cardiovascular devices.

In that regard, the laboratory model was used in **chapter 4** to compare the support capabilities of the IABP and the Impella 2.5 left percutaneous (LP), a relatively new transvalvular assist device that challenge the position of the IABP. Different clinical

scenarios were simulated, while the IABP and the Impella 2.5 LP supported the (endangered) circulation in turn. The hemodynamic differences between both support devices were small. Both systems approximately yielded a 10 % coronary blood flow increase and a 10 % cardiac output increase. However, as the transvalvular assist device provided significantly better left ventricular unloading, the support capabilities were slightly in favor of the Impella 2.5 LP.

When using the isolated beating pig heart model for further testing of cardiovascular devices, knowledge about the state of physiologic regulatory processes is mandatory. In **chapter 5**, six slaughterhouse pig hearts were isolated, prepared, and connected to an external circulatory system. Through coronary reperfusion and controlled cardiac loading, physiologic cardiac performance was achieved. The autoregulation of coronary blood flow in the working isolated beating pig heart was studied in response to brief occlusions of the coronary artery, to step-wise changes in left ventricular loading conditions and contractile states, and to pharmacologic vasodilating stimuli. The absence of reactive hyperemia, the linear relation between coronary blood flow and coronary driving pressure, and the fact that intracoronary administration of papaverine did not yield a transient increase in blood flow, strongly indicate that the coronary circulation in the isolated beating pig heart is in a permanent state of maximum hyperemia.

Informed on the state of coronary autoregulation in the isolated beating pig heart, the influence of persisting ischemia on IABP efficacy was investigated in 'healthy' hearts and in shock in **chapter 6**. In twelve slaughterhouse pig hearts, different clinical scenarios were simulated, whether or not accompanied by myocardial ischemia, whereupon IABP support was applied. Without ischemia, the IABP induced a mild increase in coronary blood flow and cardiac output, which was strongly augmented in the presence of persisting ischemia. Myocardial oxygen consumption increased in case of ischemia, while it slightly decreased without. Consequently, the IABP reversed and stabilized the progressive hemodynamic deterioration due to myocardial ischemia within minutes.

The integrated research strategy of computational modeling, *in vitro* and *ex vivo* testing, and clinical validation enabled to predict clinical conditions and pump settings in which IABP use would be most effective. Consequently, in clinical practice, IABP support can be expected to be most effective in patients with viable myocardium, suffering from persistent myocardial ischemia, despite adequate epicardial reperfusion.

Samenvatting

Numerieke en experimentele karakterisering van intra-aortale ballonpomp ondersteuning

De intra-aortale ballon pomp (IABP) is een minimaal invasief ondersteuningssysteem voor de pompfunctie van het hart. Door het intermitterend opblazen en leegzuigen van de ballon, synchroon met de hartcyclus, induceert deze zowel een diastolische bloeddrukaugmentatie als een systolische bloeddrukreductie. Hoewel deze bloeddrukveranderingen klinische verbetering beogen in termen van coronaire perfusie en myocardiaal zuurstofgebruik, zijn de gemeten effecten bij patiënten en dierproeven inconsistent. Daarom richt het onderzoek beschreven in dit proefschrift zich op het gebruik van een geïntegreerde methode van numerieke, *in vitro*, *ex vivo* en *in vivo* modellen om de IABP en de invloed ervan op de cardiale en coronaire hemodynamica te karakteriseren. Doel is om beter te kunnen voorspellen in welke klinische situaties het gebruik van de pomp het meest effectief zal zijn.

In **hoofdstuk 2** werd een numeriek model ontwikkeld waarin een 0-dimensionaal discreet model gekoppeld werd aan een gedetailleerd hartcontractie model. Dit hartcontractie model was gebaseerd op microstructurele materiaaleigenschappen en macrostructurele geometrie-eigenschappen. De IABP werd beschreven als een concentrische cilindervormige buis in het bloedvat. In dit systeem werd de interactie tussen de IABP en het cardiovasculaire stelsel getest, alsmede hoe deze koppeling beïnvloed werd door specifieke parameters (zoals timing). Voor validatie doeleinden zijn data verzameld bij tien patiënten die behandeld werden met de IABP. In zowel het model als de patiënten was het ondersteunende effect van de IABP maximaal wanneer de ballon tegelijkertijd met ventriculaire contractie werd leeggezogen. Balloninflatie voor de start van diastole verhinderde te allen tijde optimale ejectie.

Om in de behoefte aan een fysiologisch hydraulisch model voor het testen van cardiovasculaire systemen te voldoen, werd in **hoofdstuk 3** een geïntegreerd hydraulisch simulatiemodel ontwikkeld. Dit model werd gereguleerd door een gedetailleerd hartcontractie model, een realistisch frequentiemodel en een relatief simpele regelaar. Het gedrag van het systeem werd getest in reactie op contractiliteit, belasting, en frequentieveranderingen van het linker ventrikel. Het fysiologische gedrag van het model pleitte voor een goede implementatie van de ingebouwde terugkoppelingsmechanismen. Dit maakt de *in vitro* opstelling uitermate geschikt voor het testen van cardiovasculaire systemen.

In dat perspectief werd het laboratorium model in **hoofdstuk 4** gebruikt om de ondersteunende werking van de IABP en de Impella 2.5 left percutaneous (LP) met elkaar te vergelijken. Dit omdat de Impella 2.5 LP, een relatief nieuw transvalvulair

ondersteuningssysteem, concurreert met de huidige positie van de IABP. Verschillende klinische scenario's werden gesimuleerd terwijl de IABP en de Impella 2.5 LP de circulatie om beurten ondersteunden. De hemodynamische verschillen tussen beide systemen waren klein. Zowel de IABP als de Impella 2.5 LP induceerde een toename in coronaire bloedstroom en hartminuutvolume van ongeveer 10 %. Omdat het transvalvulaire systeem het linker ventrikel aanzienlijk beter ontlastte, is de ondersteuning van de pompfunctie licht in het voordeel van de Impella 2.5 LP.

Bij het gebruik van het geïsoleerde kloppende varkenshart voor het testen van cardiovasculaire systemen is kennis over de toestand van fysiologische regelmechanismen noodzakelijk. In **hoofdstuk 5** werden zes varkensharten, verkregen direct na het doden van het dier in het slachthuis, geïsoleerd, geprepareerd en gekoppeld aan een extern circulatiesysteem. Door coronaire reperfusie en gecontroleerde cardiale belasting werd de fysiologische functie van het hart hersteld. De autoregulatie van de coronaire bloedstroom werd bestudeerd in reactie op kortstondige oclusies van de kransslagaderen, op stapsgewijze veranderingen in belasting en contractiliteit van het linker ventrikel, en op farmacologische vasodilaterende stimuli. De afwezigheid van reactieve hyperemie, de lineaire relatie tussen coronaire bloedstroom en aortadruk, en het feit dat intra-coronaire toediening van papaverine niet leidde tot een toename in bloedstroom, doen sterk vermoeden dat de coronaire circulatie in het geïsoleerde kloppende varkenshart zich in een permanente staat van maximale hyperemie bevindt.

Geïnformeerd over de toestand van het coronair autoregulatie-systeem, werd de invloed van persisterende ischemie op de effectiviteit van de IABP onderzocht in **hoofdstuk 6**. In twaalf *ex vivo* varkensharten werden verschillende klinische situaties gesimuleerd, al dan niet gecombineerd met myocardiaal zuurstofgebrek. Al deze situaties werden ondersteund met de IABP. Zonder ischemie induceerde de IABP een geringe toename in coronaire bloedstroom en hartminuutvolume. Deze effecten namen sterk toe wanneer sprake was van persisterend zuurstofgebrek. Myocardiaal zuurstofgebruik nam toe in de aanwezigheid van ischemie, terwijl een lichte afname werd geobserveerd in de afwezigheid hiervan. Zodoende was de IABP in staat de progressieve hemodynamische achteruitgang, veroorzaakt door het myocardiale zuurstofgebrek, binnen enkele minuten om te keren en te stabiliseren.

De geïntegreerde onderzoeksstrategie van numeriek modelleren, *in vitro* en *ex vivo* testen en klinische validatie, stelden ons in staat klinische condities en pomp instellingen te definiëren waarin het gebruik van de IABP het meest effectief lijkt te zijn. In de klinische praktijk wordt verwacht dat IABP therapie het meest effectief zal zijn wanneer deze wordt toegepast bij patiënten met vitaal myocardweefsel, lijdend aan persisterende ischemie, ondanks adequate epicardiale reperfusie.

Gedicht

Geschreven door Mathieu van Kelle ter gelegenheid van Sinterklaasavond 2013

Waarde hooggeleerde opposenten, hier draait het allemaal om.
De aorta is waar hij ingaat, die intra-aortale ballon.
Maar over die ballon vertel ik pas aan het eind.
Eerst zal ik uitleggen waarom het hart zo op en neer deint.

Het bloed komt binnen in het rechter atrium.
Dat is het aller eerste stadium.
Het komt hier van overal uit het lichaam naar toe stromen,
het kan vanuit je hersenen of uit je tenen komen.
Vervolgens gaat het bloed via de tricuspidalisklep naar het rechter ventrikel.

Voor wie de draad al kwijt is, lees het maar terug in mijn artikel!

Na het samentrekken van het rechter ventrikel stroomt het bloed naar de longen,
waar zuurstofmoleculen in het bloed sprongen.
Het komt vervolgens het linker atrium ingelopen,
waarna een lang verhaal volgt, iets met sinus- en AV-knopen.
Via de mitralisklep stroomt het bloed het linker ventrikel in.

*- By the way- wat zijn die hartkleppen toch fantastische weefsels niettemin!
Als je die nou toch eens in een lab zou kunnen maken,
dan zou je zeker hoog op de wetenschappelijke ladder geraken!*

Nadat het linker ventrikel helemaal is vol gegaan,
komen we bij de isovolumetrische contractiefase aan.
Er wordt dan door de cardiomyocyten hard getrokken,
zodat ze samentrekking van de hartspier uitlokken.
Doordat de kleppen gesloten zijn gebleven,
zal de druk in het ventrikel opleven.
In de druk-volume curve gaat de druk nu lijnrecht omhoog,
terwijl het volume geen milliliter afboog.
Als echter de ventrikeldruk hoger is dan de aortadruk,
gaat de aortaklep open in een ruk.
Bloed stroomt via de aorta naar de rest van het lichaam,
en dan begint het hele riedeltje weer van voor af aan.

Waarde hooggeleerde opposenten, het kan echter zo zijn,
dat het hart werkt niet zo fijn.
Als een persoon een hartinfarct heeft gekregen,
kan het hart niet meer zo goed bewegen.
Het kan dan wel een steuntje in de rug gebruiken,
en dan komt de intra-aortale ballonpomp opduiken.

Een ballon wordt dan in de aorta gestoken,
zonder dat de bloedstroom wordt onderbroken.
Tijdens diastole krijgt het een belangrijke functie toegewezen,
waardoor de patiënt sneller kan genezen.
Tijdens die fase zal de ballon namelijk opzwellen,
wat de perfusie van de kransslagaderen doet herstellen.
Vervolgens krimpt de ballon tijdens systole ineen.
Een soort vacuüm-effect maakt dat de *afterload* afneemt meteen.
Door deze lagere druk in het aorta vat,
hoeft het hart een minder hoge druk op te bouwen, dan wanneer die ballon er niet zat.
Het hart hoeft dus minder hard te werken,
waardoor het hopelijk sneller kan aansterken.

Althans, dat is allemaal theorie.
Ik ben uit gaan zoeken of dit allemaal wel klopt of niet.
Ik zette de tering naar de nering.

Al is dit onderwerp natuurlijk niet zo geraffineerd als tissue engineering.

Verschillende klinische scenario's passeerden de revue,
en zie in dit proefschrift de resultaten nu.
De verhelderde indicaties voor gebruik zullen voor artsen nuttig zijn,
en bijdragen aan gegronde besluitvorming, dat is wel zo fijn!
Zo heb ik een brug geslagen tussen de geneeskunde en techniek,
wat mijns inziens de meerwaarde bewijst van een medisch ingenieur in de kliniek.

Hopelijk was dit een heldere uiteenzetting, ik deed in ieder geval mijn best.
Gelukkig is daar de pedel al: Hora Est!

Dankwoord

Traditioneel wordt in het dankwoord onderstreept wat voor een beproeving en lijdensweg de conceptie van het proefschrift is geweest. Omdat dit bij mij niet aan de orde was, zal ik alle wanhoop buiten beschouwing laten en wil ik gewoon een aantal mensen met nadruk bedanken voor hun bijdrage aan dit werk.

In het bijzonder gaat mijn dank uit naar mijn (co-)promotoren. Ik heb jullie begeleiding uit verschillende invalshoeken altijd zeer gewaardeerd. Nico, jij hebt in mijn ontwikkeling als wetenschapper een essentiële rol gespeeld. Ik dank je voor je oprechtheid en kritische blik, maar bovenal voor het vertrouwen dat je me gaf. Ik prijs mezelf zeer gelukkig met een promotor zoals jij. Frans, ondanks dat je officieel niet mijn promotor bent, beschouw ik je wel als zodanig. Ik heb een enorme bewondering voor jouw scherpzinnigheid. Een speciaal bedankje gaat uit naar het feit dat ik je mocht vergezellen tijdens de studiereis naar Singapore en Maleisië. Ik vond het geweldig! Marcel R., ik heb genoten van jouw onuitputtelijke enthousiasme en positieve instelling. Zonder jouw oneindige stroom aan ideeën was dit proefschrift niet zo geworden als het nu is. Marcel van 't V., na een afspraak met jou had ik altijd het gevoel weer met sprongen vooruit te kunnen. Jouw nuchtere en relativerende blik heeft me altijd aangenaam verrast.

De leden van de beoordelingscommissie, Peter Hilbers, Divaka Perera, Bart Meyns en Frank Baaijens, dank ik voor het beoordelen van het proefschrift op zijn wetenschappelijke waarde en de deelname aan de oppositie.

Ontzettend veel dank ben ik verschuldigd aan de mannen van LifeTec Group, in het bijzonder Sjoerd. Bedankt voor jullie (veelal belangeloze) inzet en ondersteuning bij de talloze kloppende hart experimenten. Lokien, door onze verschillende achtergronden vulden wij elkaar perfect aan. Ik hoop dat we nog lang van elkaars expertises gebruik kunnen maken. Verder dank ik graag mijn collega's en kamergenoten voor de leerzame bijeenkomsten op de vakgroep, de informele praatjes in de wandelgangen en de prettige werksfeer. Ik heb de laagdrempelige communicatie en open-deur mentaliteit altijd zeer gewaardeerd.

Daarnaast wil ik graag nog enkele personen bedanken die niet direct een bijdrage hebben geleverd aan de wetenschappelijke inhoud van dit proefschrift, maar wel heel belangrijk zijn geweest in het leven buiten de universiteit; want wetenschap is geweldig, maar tijd met familie en vrienden het dierbaarst!

Allereerst mijn paranimfen: Jaap en Rieneke. Wat ben ik blij dat jullie naast me staan op de bijzondere dag van mijn promotie. Jaap, of het nu op een borrel is of bij een promotiefeest: gezelligheid gegarandeerd. Ik ben ervan overtuigd dat vanavond niet de laatste keer is dat we 'studentikoos' een biertje drinken! Rieneke, tijdens onze

studie waren wij onafscheidelijk en hebben we samen de geneugten van het studentenleven geproefd. Je bent en blijft een vriendin voor het leven!

Dat brengt mij tevens bij de overige leden van damesdispuut $\Delta\gamma\phi\delta$. Anne, Inge, Sophie en Ariane, bedankt voor de heerlijke etentjes en de altijd goede gesprekken. Inmiddels zijn jullie allen jullie eigen promotieonderzoek aan het afronden, dus we hebben nog heel wat feestjes voor de boeg! Verder wil ik Dames 1 van PSV Handbal bedanken voor het plezier dat jullie mij geven in deze sport. Ik prijs jullie gedrevenheid en doorzettingsvermogen op het veld, maar zeker ook de gezelligheid en betrokkenheid erbuiten.

Roosendaal is inmiddels toch wel een beetje mijn tweede 'thuis' geworden. Ad, Elly en Evelyn, bedankt voor de heerlijke carpaccio en het kennismaken met het Tullepetaonse Pattelulle. Opa en oma, bedankt voor jullie oprechte interesse en aanmoediging gedurende mijn academische en sportieve carrière. Jullie zijn mijn grootste fans! Rachel, soms elkaars tegenpolen, soms twee handen op één buik. Ik had me geen leukere zus kunnen wensen. Pap en mam, bedankt voor jullie liefde, steun en rotsvaste vertrouwen in mijn kunnen. Het feit dat mijn onderzoek voor jullie vaak best een beetje een mysterie was, is altijd heerlijk verfrissend en relativerend voor mij geweest. Tot slot, lieve Mathieu, er is niemand die beter bij mij past dan jij. Met jouw levenslust, relativeringsvermogen en lach is elke dag een feest. Ik hou van jou!

Stéphanie Schampaert

Curriculum vitae

Stéphanie Schampaert was born in Eindhoven on July 9th 1987. She attended secondary education at Lyceum Bisschop Bekkers in Eindhoven, where she graduated in 2005 (*cum laude*). In the same year she started studying Biomedical Engineering at Eindhoven University of Technology (TU/e), and obtained a Master's degree in Medical Engineering in 2010 (*cum laude*). During her Master's training, she spent four months in the Cardiovascular Research Laboratory at Texas Heart Institute (Houston, U.S.A.), where she measured static and dynamic characteristics of an axial flow pump. For her Master's thesis, she performed research at the department of Cardiology at Catharina Hospital Eindhoven, where she studied the interaction between the intra-aortic balloon pump (IABP) and the cardiovascular system using a combined computational-experimental approach. This work was later nominated for a TU/e Academic Award as best final project of the department Biomedical Engineering. Due to the promising clinical impact of this work, she continued her research activities as a PhD candidate in the Cardiovascular Biomechanics group after graduation, which resulted in this thesis. In collaboration with LifeTec Group, she studied the (an)aerobic metabolic effects of IABP support in an isolated beating pig heart model. For validation purposes, she was closely involved in retro- and prospective clinical studies at Catharina Hospital Eindhoven. Parallel to her research activities, she played competitive handball at Dutch national level.

List of publications

Schampaert S., Van Nunen L.X., Pijls N.H.J., Rutten M.C.M., Van Tuijl S., Van de Vosse F.N., Van 't Veer M.; Intra-aortic balloon pump support in the isolated beating pig heart in non-ischemic and ischemic pump failure; -, -(-):-, submitted.

Van Nunen L.X., Van 't Veer M., **Schampaert S.**, Rutten M.C.M., Van de Vosse F.N., Patel M.R., Pijls N.H.J.; Intra-aortic balloon counterpulsation reduces mortality in large anterior myocardial infarction complicated by persistent ischemia; a CRISP AMI substudy; *EuroIntervention*, -(-):-, accepted.

Van Nunen L.X., Lenders G., **Schampaert S.**, Van 't Veer M., Wijnbergen I., Brueren G.R.G., Tonino P.A.L., Pijls N.H.J.; Single bolus intravenous regadenoson injection versus central venous infusion of adenosine for maximum coronary hyperaemia in fractional flow reserve measurement; *EuroIntervention*, -(-):-, e-published ahead of print.

Bozkurt S., Van Tuijl S., **Schampaert S.**, Van de Vosse F.N., Rutten M.C.M.; Arterial pulsatility improvement in a feedback-controlled continuous flow left ventricular assist device: An ex-vivo experimental study; *Medical Engineering & Physics*, -(-):-, e-published ahead of print.

Schampaert S., Pennings K.A.M.A., Van de Molengraft M.J.G., Pijls N.H.J., Van de Vosse F.N., Rutten M.C.M.; A mock circulation model for cardiovascular device evaluation; *Physiological Measurement*, 35: 687-702, 2014.

Van Nunen L.X., Van 't Veer M., **Schampaert S.**, Steerneman B.J.E.M., Rutten M.C.M., Van de Vosse F.N., Pijls N.H.J.; Intra-aortic balloon counterpulsation in acute myocardial infarction: old and emerging indications; *Netherlands Heart Journal*, 21(12): 554-560, 2013.

Schampaert S., Van 't Veer M., Rutten M.C.M., Van Tuijl S., De Hart J., Van de Vosse F.N., Pijls N.H.J.; Autoregulation of coronary blood flow in the isolated beating pig heart; *Artificial Organs*, 37(8): 724-730, 2013.

Schampaert S., Rutten M.C.M., Van 't Veer M., Van Nunen L.X., Tonino P.A.L., Pijls N.H.J., Van de Vosse F.N.; Modeling the interaction between the intra-aortic balloon pump and the cardiovascular system: the effect of timing; *American Society of Artificial Internal Organs Journal*, 59(1): 30-36, 2013.

Schampaert S., Van 't Veer M., Van de Vosse F.N., Pijls N.H.J., De Mol B.A.J.M., Rutten M.C.M.; *In vitro* comparison of support capabilities of intra-aortic balloon pump and Impella 2.5 left percutaneous; *Artificial Organs*, 35(9): 983-901, 2011.

Bozkurt S., Pennings K.A.M.A., **Schampaert S.**, Van de Vosse F.N., Rutten M.C.M.; A method to increase the pulsatility in hemodynamic variables in a left ventricular assist device supported human circulation system; *The International Federation for Medical and Biological Engineering Proceedings*, 36: 328-331, 2011.